MIGRATORY CUES FOR ENCEPHALITOGENIC EFFECTOR T CELLS WITHIN THE CNS DURING THE DIFFERENT PHASES OF EAE

DOCTORAL THESIS

In partial fulfillment of the requirements for the degree
"Doctor rerum naturalium (Dr. rer. nat.)"
in the Molecular Medicine Study Program
at the Georg-August University Göttingen

submitted by

Christian Schläger

born in Bad Kissingen

Göttingen, 01.02.2013

Members of the Thesis Committee

Supervisor

Prof. Dr. med. Alexander Flügel
Institute for Multiple Sclerosis Research,
Department of Neuroimmunology,
Waldweg 33, 37073 Göttingen, Germany.
Tel.: +49-(0)551-39 13332
e-mail: fluegel@med.uni-goettingen.de

2nd member of the thesis committee

Prof. Dr. rer. nat. Holger Reichardt
Göttingen University Medical School,
Department of Cellular and Molecular Immunology,
Humboldtallee 34, 37073 Göttingen, Germany.
Tel.: +49-(0)551-393365
e-mail: hreichardt@med.uni-goettingen.de

3rd member of the thesis committee

Prof. Dr. med. Mikael Simons
Max-Planck-Institute of Experimental Medicine,
Department of Neurology,
Hermann-Rein-Str. 3, 37075 Göttingen, Germany.
Tel.: +49-(0)551-3899 533
e-mail: msimons@gwdg.de

AFFIDAVIT

Here I declare that my doctoral thesis entitled

"Migratory cues for encephalitogenic effector T cells within the CNS during the different phases of EAE"

has been written independently with no other sources and aids than quoted.

_____

Christian Schläger

Göttingen, February 2013

Publications

Publications in scientific journals

1. Schläger C, Odoardi F, Kitz A, Haberl M, Schlosser C, Lodygin D, Fischer H, Reichardt HM, Nelson P, Issekutz T, Flügel A.
   Live tracking of chemokine effects on effector T cell invasion into the central nervous system.
   in preparation

2. Lodygin D, Odoardi F, Schläger C, Körner H, Kitz A, Nosov M, van den Brandt J, Reichardt HM, Haberl M, Flügel A.
   A combination of fluorescent NFAT and H2B sensors uncovers dynamics of T cell activation in real time during CNS autoimmunity.
   Nat Med., in press

3. Odoardi F, Sie C, Streyl K, Ulaganathan VK, Schläger C, Lodygin D, Heckelsmiller K, Nietfeld W, Ellwart J, Klinkert WE, Lottaz C, Nosov M, Brinkmann V, Spang R, Lehrach H, Vingron M, Wekerle H, Flügel-Koch C, Flügel A.
   T cells become licensed in the lung to enter the central nervous system. .
   Nature. 2012; 488(7413):675-9.

4. Flügel A, Schläger C, Lühder F, Odoardi F.
   Autoimmune disease in the brain – how to spot the culprits and how to keep them in check.
   J Neurolo Sci. 2011; 311 S1 S3–S11. (Review)

5. Bartholomäus I *, Kawakami N *, Odoardi F, Schläger C, Miljkovic D, Ellwart JW, Klinkert WE, Flügel-Koch C, Issekutz TB, Wekerle H, Flügel A. (*equal contribution)
   Effector T cell interactions with meningeal vascular structures in nascent autoimmune CNS lesions.
   Nature. 2009; 462(7269):94-8.

Table of Contents

List of Figures ..... **v**

Acknowledgements ..... **vii**

Abstract ..... **viii**

Abbreviations ..... **ix**

1. Introduction **10**

1.1. Immunological Background 10

1.1.1. Immune privilege and the central nervous system (CNS) 10
1.1.2. Overcoming CNS barriers during T cell-mediated autoimmunity 11
1.1.3. Immune cell interactions with the vessel endothelium 12
1.1.4. Leukocyte migration within the tissue – putative role for chemokines as migratory cues 14

1.2. Experimental/Technical Background 15

1.2.1. Experimental Autoimmune Encephalomyelitis- Insights into T cell-mediated CNS autoimmunity 15
1.2.2. Tools for visualizing autoimmune responses in the CNS 18

1.3. Aims of this work 20

2. Material and Methods **21**

2.1. Material 21

2.2. Methods 22

2.2.1. Generation of GFP^+ T cell cultures 22
2.2.2. Adoptive T cell transfer 24
2.2.3. Intrathecal injection procedure 24
2.2.4. Flow cytometric cell quantification 24
2.2.5. Cell Sorting 25
2.2.6. Re-transfer of migratory T cells 26
2.2.7. Interference with integrin signaling 26
2.2.8. Interference with chemokine signaling 26
2.2.9. Intravital TPLSM: surgical procedure 27
2.2.10. Intravital TPLSM: Technical equipment 28
2.2.11. Intravital TPLSM: Processing of raw data 29
2.2.12. Intravital TPLSM: Analysis of T cell motility 29
2.2.13. Intravital TPLSM: Labeling of phagocytic cells and blood vessels 30
2.2.14. Intravital TPLSM: Analysis of T cell interactions with meningeal phagocytes/ Analysis of early T cell activation 30
2.2.15. Quantitative PCR 31
2.2.16. Chemotaxis assay 32
2.2.17. Histology 32

3. Results 33

3.1. Infiltration of myelin-reactive T cells into the CNS during *t*EAE 33

3.2. Motility of encephalitogenic effector T cells during the different EAE phases 35

3.2.1. Motility of encephalitogenic T cells within the leptomeningeal vessel lumen during the preclinical phase of EAE 35

3.2.2. Locomotive behavior of encephalitogenic T cells within the meningeal environment during the different phases of EAE 37

3.3. Impact of chemokines on T cell locomotion *in vivo* during EAE 39

3.3.1. Impact of chemokines on T cell locomotion within the lumen of leptomeningeal blood vessels during the preclinical phase of EAE 39

3.3.2. Chemokines influence intraluminal T cell migration under inflammatory and non-inflammatory conditions 45

3.4. Impact of chemokines on T cell migration within the extravascular space during the different phases of EAE 51

3.4.1. Role of chemokines on the motility of extravasated T cells 51

3.5. Impact of chemokines in stabilizing T cells during their migration in the extravascular space 56

3.5.1. Role of chemokines on the interaction between T cells and meningeal phagocytes 58

3.5.2. Role of chemokines during the re-activation of encephalitogenic T cells within the living CNS tissue 62

4. Discussion 65

4.1. Migratory behavior of effector T cells within the lumen of leptomeningeal blood vessels 65

4.1.1. Intraluminal crawling of effector T cells 65

4.1.2. Intraluminal crawling of effector T cells is dependent on chemokine signaling 66

4.2. Effects of chemokines on extravasated T cells 69

4.2.1. Role of chemokines as chemoattractants for encephalitogenic T cells 69

4.2.2. Chemokines stabilize T cell migration within the meningeal environment 70

4.2.3. Chemokines stabilize interactions between T cells and meningeal phagocytes but do not affect T cell activation 71

5. Summary and Conclusion 73

6. References 74

7. Curriculum vitae 88

List of Figures

Figure 1 | Multistep paradigm of leukocyte transmigration. 13

Figure 2 | Monophasic disease course of adoptive transfer EAE in LEWIS rats. 16

Figure 3 | Encephalitogenic effector T cells are licensed in the periphery to enter the CNS tissue. 17

Figure 4 | Migratory T cells have a dissimilar mRNA expression profile compared to T cell blasts. 17

Figure 5 | 3D reconstruction of nuclear NFAT-translocation. 18

Figure 6 | $T_{MBP\text{-}GFP}$ cells do not enter the CNS directly after transfer. 34

Figure 7 | Autoaggressive $T_{MBP\text{-}GFP}$ cells infiltrate the spinal cord during EAE. 34

Figure 8 | Intraluminal locomotive behavior of $T_{MBP\text{-}GFP}$ cells in different organs during the preclinical phase of EAE. 35

Figure 9 | Direction of the blood flow has no influence on intravascular T cell crawling. 36

Figure 10 | Motility of encephalitogenic effector T cells within leptomeningeal blood vessels. 36

Figure 11 | Migration pattern of extravasated $T_{MBP\text{-}GFP}$ cells during the different phases of EAE. 37

Figure 12 | Migration pattern and motility characteristics of extravasated $T_{MBP\text{-}GFP}$ cells during the different phases of EAE. 38

Figure 13 | Motility of extravasated $T_{MBP\text{-}GFP}$ cells within the meningeal environment during the different phases of EAE. 38

Figure 14 | Chemokine receptor expression pattern in $T_{MBP\text{-}GFP}$ cells during the preclinical phase of EAE. 39

Figure 15 | Migratory $T_{MBP\text{-}GFP}$ cells respond foremost to the inflammatory chemokine CXCL11. 40

Figure 16 | Interference with chemokine signaling disturbs intraluminal T cell crawling. 41

Figure 17 | Interference with chemokine signaling does not inhibit T cell rolling. 42

Figure 18 | Chemokine signaling is essential for the duration of T cell crawling *in vivo*. 42

Figure 19 | Interference with chemokine signaling influences the crawling velocity. 42

Figure 20 | PTx pre-treated migratory T cells are incapable of intravascular crawling. 43

Figure 21 | Chemokines influence the orientation of intravascular crawling. 43

Figure 22 | α4 integrins contribute to intravascular T cell locomotion but do not influence the orientation of crawling. 44

Figure 23 | Expression pattern of chemokine ligands in endothelial cells during the different phases of EAE. 46

Figure 24 | Integrity of meningeal blood vessels is disrupted in the preclinical phase of EAE. 47

Figure 25 | Chemokine receptor expression pattern and chemotaxis of *ex vivo* isolated migratory $T_{OVA\text{-}GFP}$ cells. 48

Figure 26 | Chemokine signaling contributes to crawling of T lymphocytes under non-inflammatory conditions. 49

Figure 27 | Chemokines influence intravascular locomotion pattern of T cells under non-inflammatory conditions. 49

Figure 28 | Influence of chemokines on intravascular crawling is more pronounced under inflammatory conditions. 51

Figure 29 | Inflammatory cytokines and chemokines are up-regulated during the preclinical and acute phases of EAE. 52

Figure 30 | Chemokine receptor expression pattern within $T_{MBP\text{-}GFP}$ cells during the course of EAE. 53

Figure 31 | Encephalitogenic effector T cells respond mainly to inflammatory chemokines. 53

Figure 32 | Role of chemokines on the motility of extravasated $T_{MBP\text{-}GFP}$ cells during the course of EAE..... 54

Figure 33 | Role of chemokines on the motility of extravasated $T_{OVA\text{-}GFP}$ cells during the course of EAE. Analyses 55

Figure 34 | Administration of PTx reduces T cell adhesion to the meningeal surface. 56

Figure 35 | Inflammatory chemokines stabilize T cell adhesion to the meningeal surface during EAE. 57

Figure 36 | PTx pre-treated migratory T cells fail to adhere to the leptomeningeal surface after i.th. transfer.. 57

Figure 37 | Extravasated T cells interact with meningeal phagocytes that are embedded in fibrillar ECM structures. 58

Figure 38 | Inflammatory chemokines are up-regulated in meningeal phagocytes during the preclinical and acute phases of EAE. 59

Figure 39 | Interference with chemokine signaling influences short-lasting contacts between $T_{MBP\text{-}GFP}$ cells and resident meningeal phagocytes. 60

Figure 40 | Interference with chemokine signaling does not influence long-lasting contacts between $T_{MBP\text{-}GFP}$ cells and resident meningeal phagocytes. 61

Figure 41 | Interference with chemokine signaling has no impact on interactions between motile $T_{OVA\text{-}GFP}$ cells and meningeal phagocytes. 62

Figure 42 | Short-lasting contacts with resident phagocytes prompt *de novo* NFAT-translocations in T_{MBP} cells. 63

Figure 43 | Interference with chemokine signaling has no influence on early T cell activation. 64

Figure 44 | Inhibition of chemokine signaling does not interfere with T cell activation. 64

Acknowledgements

I would like to express gratitude to a number of people for their unstinting contribution to the present work. My greatest thanks go to my mentor and supervisor *Prof. Alexander Flügel* for giving me the opportunity to work in his department at the IMSF in Göttingen and for introducing me to the Department of Neuroimmunology at the Max-Planck Institute in Martinsried. Further, I owe him a great debt for his support and for erudite and encouraging discussions during the years of my practical work. Secondly, my extreme gratitude goes to *Dr. Francesca Odoardi,* for her support in theoretical and practical issues, for encouraging dialogues and discussions, her outstanding mentorship and mental assistance. I am also very grateful to numerous colleagues at the Max-Planck Institute for Neurobiology in Martinsried and at the IMSF in Göttingen. Foremost, I would like to thank *Christopher Sie,* a former colleague at the IMSF for providing excellent help in computing questions, for his moral support and scientific discussions. Second, I am very grateful to *Dr. Ingo Bartholomäus* for his sophisticated training in surgical procedures and animal monitoring and his introduction to the two-photon technique. Further, I would like to thank him and *Dr. Vijay Ulaganathan* for their mental and personal support. I owe a great debt to *Adriane Stas, Simone Hamann, Corinna Schlosser* and *Michael Haberl* for their practical and moral support during my time at the IMSF. Further I am grateful to *Dr. Dimitri Lodygin* for sharing his scientific expertise and the opportunity to support him with his excellent project. Moreover, I would like to thank *Cathy Ludwig* for innumerous organizational matters as well as her irreplaceable proofreading. Further, great thanks goes to *Omar Diaz* for IT support. Last but not least I would like to thank *my family*, my girlfriend *Judith* and all close *friends* that strongly supported me over the years.

Abstract

In multiple sclerosis (MS), encephalitogenic T cells are considered to breach distinct cerebral barriers in order to gain access to their target tissue, the CNS. However, it remains poorly understood exactly *how* auto-reactive T cells overcome these boundaries and *which* migratory cues guide them on their journey. In the present work, intravital two-photon laser scanning microscopy (TPLSM) was employed to examine in detail the migratory behavior of adoptively transferred GFP^+ $CD4^+$ MBP-reactive T cells under the influence of chemokine signaling during different disease phases of experimental autoimmune encephalomyelitis (EAE), an animal model for MS.

During preclinical EAE, encephalitogenic effector T cells were crawling along the intraluminal surface of leptomeningeal blood vessels preferentially against the direction of the blood stream. Intravenous administration of pertussis toxin (PTx) or a neutralizing anti-CXCR3mAb revealed that chemokines play an essential role for this intravascular crawling behavior. (1) Intraluminal crawling was almost completely abolished; (2) the remaining fraction of cells profoundly changed their motility characteristics, i.e. they crawled for a shorter time with increased velocity and reversed their orientation to go with instead of against the flow.

Once myelin-reactive T cells had transgressed the vascular barriers they continued their migration throughout the meningeal surface. Interference with chemokine signaling at this stage had only a moderate impact on the basal T cell motility. However, chemokines were important for stabilizing the contacts between T cells and resident phagocytes and furthermore prevented the detachment of T cells from the meningeal surface into the cerebrospinal fluid (CSF).

In sum, the data indicate that encephalitogenic T cells invade the CNS through a well-coordinated sequence of distinct steps, in which chemokines play a major role. Chemokines regulate effector T cell infiltration by controlling adhesion-dependent migratory steps and intercellular interactions during CNS inflammation.

Abbreviations

APC	**A**ntigen-**P**resenting **C**ell
BBB	**B**lood-**B**rain **B**arrier
CNS	**C**entral **N**ervous **S**ystem
CSF	**C**erebro**s**pinal **F**luid
DC	**D**endritic **C**ell
EAE	**E**xperimental **A**utoimmune **E**ncephalomyelitis
ECM	**E**xtra**c**ellular **M**atrix
FCS	**F**etal **C**alf **S**erum
GAG	**G**lycos**a**mino**g**lycan
GFP	**G**reen **F**luorescent **P**rotein
HEV	**H**igh **E**ndothelial **V**enule
i.p.	**i**ntra**p**eritoneal / **i**ntra**p**eritoneally
i.th.	**i**ntra**th**ecal / **i**ntra**th**ecally
i.v.	**i**ntra**v**enous / **i**ntra**v**enously
LFA-1	**L**ymphocyte **F**unction-associated **A**ntigen-**1**
LPAM-1	**L**ymphocyte **P**eyer's patch **A**dhesion **M**olecule-**1**
LPS	**L**ipo**p**oly**s**accharid
MadCAM-1	**M**ucosal **ad**dressin **C**ell **A**dhesion **M**olecule-**1**
MBP	**M**yelin **B**asic **P**rotein
Met-	**Met**hionin-
MHC	**M**ajor **H**istocompatibility **C**omplex
MS	**M**ultiple **S**clerosis
NFAT	**N**uclear **F**actor Of **A**ctivated **T** cells
OVA	**Ova**lbumin
p.t.	**p**ost **t**ransfer
PTx	**P**ertussis **T**o**x**in
RANTES	**R**egulated on **A**ctivation, **N**ormal **T** cell **E**xpressed and **S**ecreted
TCR	**T C**ell **R**eceptor
*t*EAE	**t**ransfer **EAE**
TPLSM	**T**wo-**P**hoton **L**aser **S**canning **M**icroscope/**M**icroscopy
VLA-4	**V**ery **L**ate **A**ntigen-**4**

1. Introduction

1.1. Immunological Background

1.1.1. Immune privilege and the central nervous system (CNS)

The CNS has been traditionally considered as an "immune privileged site", a term which emphasizes its incapability to elicit inflammatory responses towards diverse antigens (ENGELHARDT & RANSOHOFF, 2005). However, immune reactions do take place within the CNS, as demonstrated by viral infections, ischemia and numerous inflammatory diseases of brain and spinal cord including multiple sclerosis (ENGELHARDT & RANSOHOFF, 2005). This obvious paradox reveals that the privileged status of the CNS is not absolute and for several reasons could be described less strictly and more accurately as "immune-specialized" (GALEA et al., 2007; HOLMAN et al., 2011).

(1) The immune privileged status of the CNS is mainly restricted to its parenchyma proper, since professional antigen-presenting cells like dendritic cells (DCs) and macrophages are found within meningeal and choroid plexus tissue (GALEA et al., 2005; ANANDASABAPATHY et al., 2011; RANSOHOFF & ENGELHARDT, 2012). Along with the observation that microglia express low levels of MHC molecules on the cell surface, these studies demonstrate a definite capability of antigen-presentation within the CNS (OUSMAN & KUBES, 2012).
(2) Although the CNS is devoid of classical lymphatic vessels (CSERR & KNOPF, 1992), antigen drainage from the CNS parenchyma to cervical lymphnodes is described and occurs along the olfactory nerves into the deep cervical lymphnodes (BRADBURY et al., 1981; KIDA et al., 1993).
(3) The CNS is shielded from the periphery by various endothelial and epithelial barriers that prevent – to a certain extent - the free exchange of macromolecules, antibodies and the transgression of cells (ABBOTT, 2005; ABBOTT et al., 2010). However, to some extent peripheral immune cells are able to breach these barriers under non-inflammatory conditions, as documented for T lymphocytes (WEKERLE et al., 1986; HICKEY et al., 1991; REBOLDI et al., 2009; BARTHOLOMÄUS et al., 2009).

1.1.2. Overcoming CNS barriers during T cell-mediated autoimmunity

Multiple sclerosis (MS) is a demyelinating disease of the central nervous system, characterized by inflammatory lesions that consist of T cell and macrophage infiltrates. Since these lesions arise within the tissue without any signs of infectious agents MS is considered to be an autoimmune disease (FLÜGEL et al., 2011). The origin of the underlying autoimmune response seems to be classically T cell-mediated due to several reasons.

Firstly, genome-wide association studies have identified links between the susceptibility for MS with genes involved in T cell function (SAWCER et al., 2011). Secondly, brain antigen-reactive T cells can be found within the normal human immune repertoire and these cells are potentially capable of inducing autoimmune responses as demonstrated by studies in transgenic mice expressing human MHC molecules (FUGGER, 2000). Finally, adoptive transfer of T cells reactive against myelin-components is sufficient to induce experimental autoimmune encephalomyelitis (EAE) in rodents that shares pathological similarities to MS (BEN-NUN et al., 1981). Nevertheless, it remains unclear how and where potential self-reactive T cells encounter their cognate antigen and get activated.

According to one possible scenario, autoaggressive T lymphocytes encounter non-self antigens in secondary lymphatic organs that share close similarities to self-antigens of the CNS (molecular mimicry) (WUCHERPFENNIG & STROMINGER, 1995). Alternatively, T cells passing the deep cervical lymph nodes are stimulated by brain-derived antigen that has reached the lymphatics of the nasal mucosa via drainage of interstitial fluid through the cribriform plate (CSERR & KNOPF, 1992; KIDA et al., 1993). Following activation, autoaggressive T cells are thought to leave the periphery, force their way into the CNS and get re-activated by local antigen (GOVERMAN, 2009). Consequently, this cascade of events leads to local tissue inflammation, demyelination and neuronal damage (LASSMANN et al., 2007). But how and in which way are self-reactive T cells thought to infiltrate the CNS? At least three main routes come into consideration (RANSOHOFF et al., 2003).

(1) An obvious access point for immune cells is the epithelial blood cerebrospinal fluid barrier (BCSFB) of the choroid plexus and circumventricular organs, which forms a physical barrier comprised of tight junctions between ependymal cells (ABBOTT et al., 2010). It has been postulated that $CD4^+$ $Th17^+$ cells were able to breach the BCSFB in a CCL20-dependent manner under non-inflammatory conditions (REBOLDI et al., 2009).
(2) The endothelial blood-brain barrier (BBB) of brain and spinal cord parenchymal

microvessels allegorizes a second entry port for circulating immune cells (ENGELHARDT & RANSOHOFF, 2005). It comprises a close-meshed network of adjacent endothelial cells, connected by tight junctions (KNIESEL & WOLBURG, 2000).
(3) Immune cells can enter the CNS meninges via the blood-leptomeningeal barrier (BLMB) which forms a boundary between the blood and the CSF-containing perivascular space (ENGELHARDT & RANSOHOFF, 2012).

1.1.3. Immune cell interactions with the vessel endothelium

Independently of which route leukocytes choose for entering the CNS, they first have to breach an endothelial barrier. Notably, the body of knowledge on leukocyte-endothelial interactions is mostly based on observations within peripheral blood vessels and high endothelial venules (HEVs) within lymphoid organs. According to these studies, interactions between leukocytes and the vessel endothelium follows a cascade of sequential adhesion steps (**Fig.1**). Each of these steps is mediated by different molecules on both leukocytes and endothelial cells (BUTCHER et a., 1991; LEY et al., 2007).

During their passage through different blood vessels, leukocytes are in close proximity to the vessel endothelium. This phenomenon – most evident in post-capillary venules – is promoted by a hemodynamic effect called "margination" (JAIN & MUNN, 2009). Accordingly, erythrocytes occupy the center of the blood stream, thereby squeezing circulating leukocytes to the vascular walls (SCHMID-SCHÖNBEIN et al., 1980). This positioning facilitates the initial step of the interaction cascade, i.e. the capture of circulating leukocytes by the vessel endothelium (LEY, 1996). This initial transient interaction is mediated by P-selectin glycoprotein ligand 1 (PSGL-1) on leukocytes and members of the selectin family that are expressed foremost on endothelial cells (LEY et al., 2007; MCEVER & CUMMINGS., 1997). For instance, activated Th1- but not Th2 cells are captured via PSGL-1 to endothelial cells expressing P- and E-selectin (AUSTRUP et al., 1997).

Once captured, leukocytes roll along the vascular endothelium, a locomotion that is accompanied by a significantly reduced velocity (ENGELHARDT, 2008). Leukocyte rolling has been shown to be dependent on shear stress supporting formation and release of molecular bonds between selectins and respective ligands (LAWRENCE et al., 1997; MARSHALL et al., 2003). Alternatively, capturing and/or rolling can also be mediated by α4β1 (VLA-4), α4β7 (LPAM-1), αLβ2 (LFA-1) integrins and distinct adhesion molecules, VCAM-1, MadCAM-1 and ICAM-1, respectively (BERLIN et al., 1995; LEY et al., 2007; SIGAL et al.,

2000; KERFOOT & KUBES, 2002; VAJKOCZY et al., 2001).

However, during transient interactions, integrins remain in an intermediate/low-affinity conformational mode that prevents a firm interaction between immune cells and the vessel endothelium (CONSTANTIN et al., 2000). The situation changes once leukocytes recognize glycosaminoglycan (GAG)-bound chemokines (PROUDFOOT, 2006) on the vessel endothelium that are either directly produced by endothelial cells or translocated from the basolateral to the apical site of the vessel (MIDDLETON et al., 2002). Thereby, chemokines can act as homing molecules, guiding circulating immune cells to inflammatory sites or into lymphoid organs (KUNKEL & BUTCHER, 2002; MIYASAKA & TANAKA, 2004). Chemokine binding to G protein-coupled receptors (GPCRs) on the surface of leukocytes triggers an inside–out signal to integrins (SHAMRI et al., 2005; KIM et al., 2003). Thereby, integrins undergo conformational changes leading to increased affinity and avidity for their corresponding adhesion molecules (KINASHI, 2005). This sequence of events results in a firm attachment of leukocytes to the inner vascular walls.

Following firm adhesion to the endothelium, leukocytes undergo a phenotypical change from a spherical to a rather flattened cell shape. Subsequently, the attached leukocytes protrude with their leading edges, which results in intraluminal crawling (RIDLEY et al., 2003; SHULMAN et al., 2009). Intraluminal crawling of leukocytes has been previously described as a prerequisite for the final step, the diapedesis (PHILLIPSON et al., 2006). Diapedesis can occur via a paracellular route through endothelial junctions, or via a transcellular pathway through the body of endothelial cells (**Fig.1**) (LEY et al., 2007).

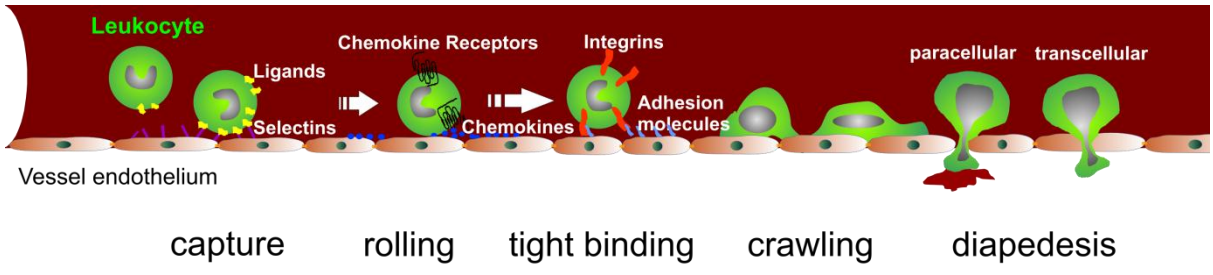

Figure 1 | Multistep paradigm of leukocyte transmigration. Following capture, leukocytes roll along the vessel endothelium until they recognize immobilized chemokines on the vascular wall. Ligand binding to chemokine receptors results in a conformational change in integrins resulting in an immediate arrest of the leukocytes. Thereafter, polarization of the attached immune cells leads to intraluminal crawling, a putative prerequisite for paracellular and/or transcellular diapedesis.

1.1.4. Leukocyte migration within the tissue – putative role for chemokines as migratory cues

Once leukocytes have overcome endothelial barriers, it is poorly understood *how* exactly these cells migrate within extravascular spaces.

It is highly conceivable that the migration pattern of extravasated leukocytes is modulated by components of the extracellular matrix (ECM) (NOURSHARGH et al., 2010). Thereby it remains unclear whether the cells are guided in such 3D environments by fibrillar structures like reticular fibers, since lymphocytes have been reported to migrate along but also independently from their substrates (NOURSHARGH et al., 2010; BAJÉNOFF et al., 2006).

Furthermore, it remains unsolved which cues are necessary for guiding extravasated immune cells within distinct tissues, including the interstitium of the CNS.

Histological analysis of brain samples from MS patients revealed a putative role for chemokines in this respect (SØRENSEN et al., 1999; DOGAN & KARPUS, 2004). Chemokines represent a group of low molecular weight cytokines that are classified according to a common structural characteristic, that is, four highly conserved cysteine residues that compose their three-dimensional structure (ZLOTNIK & YOSHIE, 2000). Based on the number and the position of the first two residues within the amino-terminal region, chemokines can be divided in four subtypes, i.e. C-x-C, C-C, C and C-x3-C (KARPUS & RANSOHOFF, 1998).

It has been shown that chemokine ligands– mainly inflammatory chemokines– are up-regulated in acute MS lesions (e.g. CCL5, CXCL10), and that mononuclear cell infiltrates bear respective chemokine receptors (CCR5, CXCR3) on their surface (TREBST & RANSOHOFF, 2001). Moreover, CSF from MS patients contains elevated levels of inflammatory chemokines including CCL5 and CXCL10 compared to control samples (SØRENSEN et al., 1999). Furthermore, also classical homeostatic chemokines, including CCL19 are found to be up-regulated in brain samples and the CSF from MS patients (KRUMBHOLZ et al., 2007) as well as CCR7-bearing cells within inflammatory cuffs of acute lesions (KIVISÄKK et al., 2004). However, none of these studies provide evidence that chemokines may serve as guidance cues for infiltrating leukocytes.

In general, chemokines are capable of attracting immune cells within tissues by chemotactic gradients (KUNKEL & BUTCHER, 2002). For instance, signaling via CCR7 was shown to be required for dendritic cells (DCs) to reach intranodal T cell zones (BRAUN et al., 2011). Furthermore, chemokines can directly influence the motility of leukocytes within the tissue in

a chemokinetic manner (WORBS et al., 2007).

The induction of chemotaxis and chemokinesis in leukocytes requires a ligand – receptor interplay. Upon chemokine binding, the respective GPCR undergoes a conformational change leading to a realignment of several membrane helices (WESS et al., 2008). This structural rearrangement results in a re-assignation of the α subunit of receptor-associated heterotrimeric G Proteins (ROSENBAUM et al., 2009). Thereby, the receptor acts as a guanine nucleotide exchange factor (GEF) on the associated G protein α-subunit (MARTY & YE, 2010). As a consequence, the newly formed GTP-bound "active" α-subunit dissociates from the βγ dimer (βγ-subunit) (MILLAR & NEWTON, 2010). Unfolding their role as second messengers, both subunits trigger an entire cascade of events including functional inhibition of adenylate cyclase, activation of phosphoinositol 3-kinase (PI3K), phospholipase C, protein kinase C (PKC), and protein kinase A, generation of inositol triphosphate, and a transient elevation of intracellular calcium levels (MARTY & YE, 2010).

1.2. Experimental/Technical Background

1.2.1. Experimental Autoimmune Encephalomyelitis- Insights into T cell-mediated CNS autoimmunity

A big leap forward in exploring the T cell-mediated pathogenesis of multiple sclerosis was achieved by the development of the animal model experimental autoimmune encephalomyelitis (EAE). Originally, rodent EAE was actively induced by immunizing animals with CNS homogenates combined with adjuvants in order to provoke an adaptive immune response against the injected agents (LIPTON & FREUND, 1953). Later it was found that EAE can also be induced by adoptive transfer of *ex vivo* isolated autoaggressive $CD4^+$ T cells into healthy recipient animals (BEN-NUN et al., 1981; HOLDA & SWANBORG, 1982).

In the present work, an adoptive transfer model of EAE (*t*EAE) in LEWIS rats has been used to study the different steps leading to T cell-mediated autoimmunity in the CNS. This model induces a highly reproducible disease with an incidence of nearly 100%. The transferred autoaggressive $CD4^+$ T cells are reactive against myelin basic protein (MBP) and produce both IFN-γ and IL-17 (BARTHOLOMÄUS et al., 2009), leading to a strong inflammation within the CNS followed by a modest demyelination restricted to ventral and dorsal routes of

the spinal cord (MANNIE et al., 2009). The disease is characterized by a monophasic disease course manifested by rapid progressive ascending pareses followed by subsequent spontaneous recovery (**Fig.2**).

A hallmark of LEWIS rat *t*EAE is an obligatory prodromal phase of 3-4 days prior to manifestation of clinical symptoms (preclinical phase) (**Fig.2**). The underlying mechanism for this delay has been extensively investigated over the last years (FLÜGEL et al., 2001; ODOARDI et al., 2012). It turned out, that freshly activated T cell blasts are incapable of infiltrating the CNS tissue directly after transfer. Instead, the transferred T cells immediately disappear from the circulation and accumulate in peripheral organs, mainly within lung and spleen parenchyma. Within the periphery, these T cells undergo profound phenotypical changes during which they gain a "migratory phenotype". Thereby, they get licensed to re-enter the circulation from where they infiltrate the leptomeningeal areas of the dorsal spinal cord between days 2 and 3 days post transfer (**Fig.3**) (FLÜGEL et al., 2001; ODOARDI et al., 2012). The phenotypical changes in migratory T cells comprise a down-regulation of activation markers (e.g. IFN-γ, IL-17) and simultaneously, an up-regulation of cell adhesion molecules (e.g. Ninjurin-1) and chemokine receptors compared to T lymphoblasts (**Fig.4**).

Notably, the migratory phenotype is not antigen-restricted since ovalbumin-specific T cells undergo similar phenotypical changes. As a consequence, T_{OVA} cells are able to enter the CNS meninges with similar kinetics compared to their myelin-reactive counterparts, albeit in substantially lower numbers (ODOARDI et al., 2012).

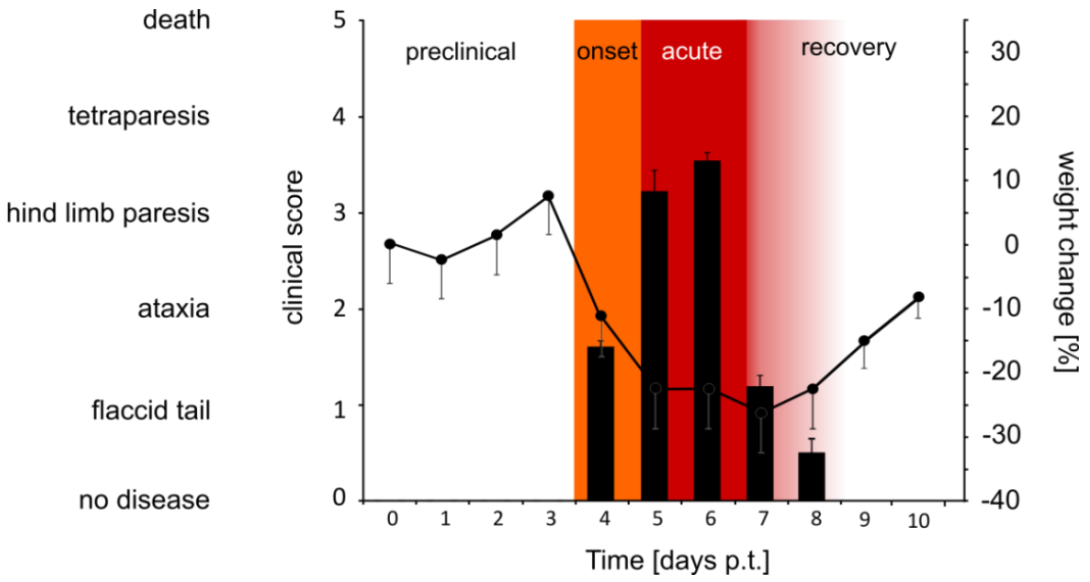

Figure 2 | Monophasic disease course of adoptive transfer EAE in LEWIS rats. Clinical signs appear only after an obligatory delay of approximately 3-4 days post intravenous (i.v.) transfer of MBP-specific T lymphoblasts. Disease symptoms reach their peak 1-2 days after disease onset. Animals start to recover around day 7 p.t. Left and right axis display clinical disease score and relative weight change over time, respectively. Corresponding disease phases are indicated at the top of the graph.

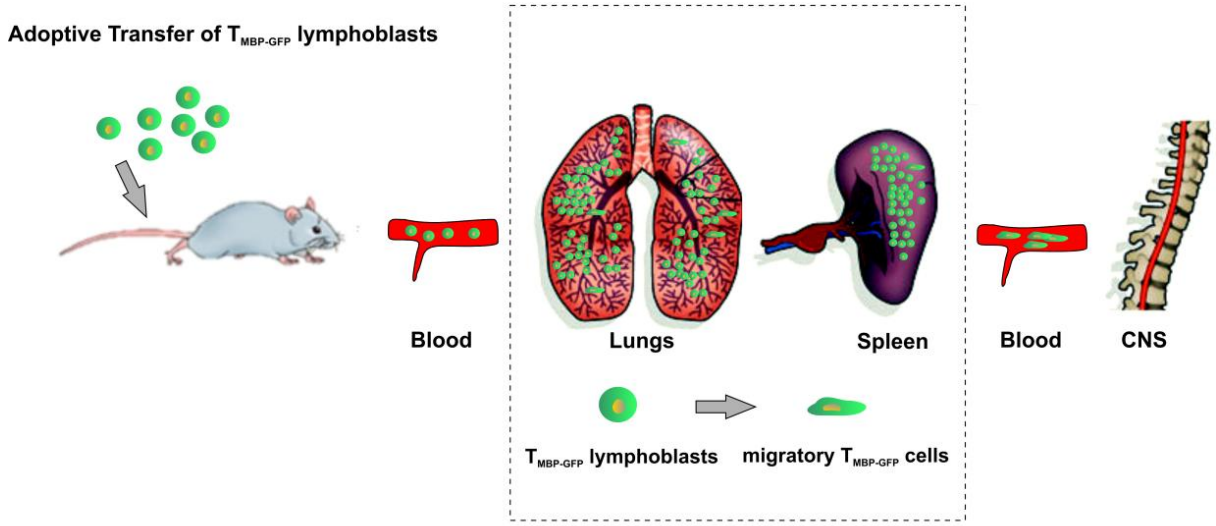

Figure 3 | Encephalitogenic effector T cells are licensed in the periphery to enter the CNS tissue. *In vitro* activated $T_{MBP-GFP}$ blast cells are injected intravenously into healthy LEWIS rats, from where they home to peripheral tissues. There, they undergo profound changes in their phenotype. After acquiring migratory skills, $T_{MBP-GFP}$ cells re-enter the blood 2-3 days post transfer and reach their target organ, the CNS (modified from RANSOHOFF, 2012).

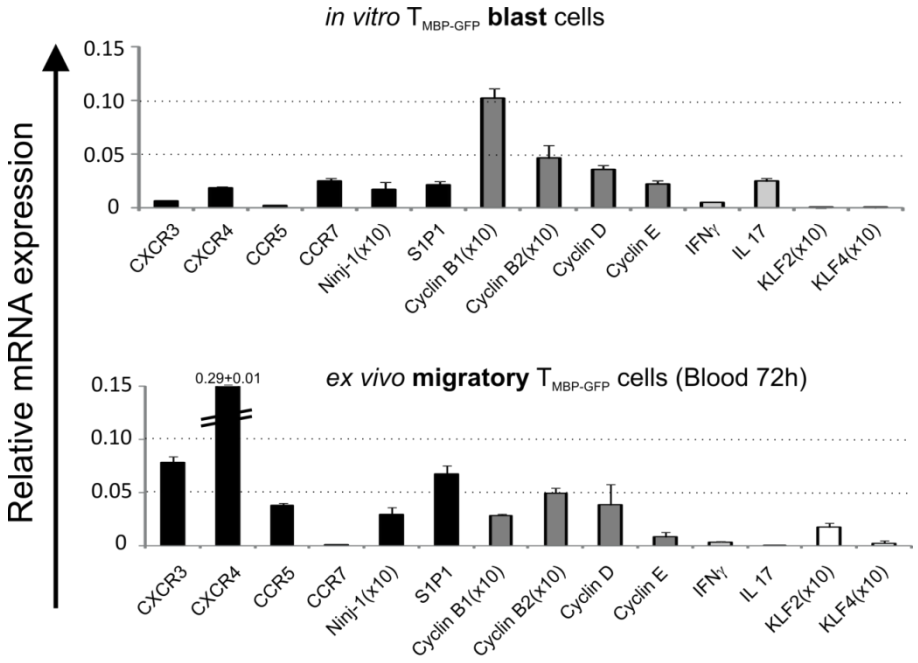

Figure 4 | Migratory T cells have a dissimilar mRNA expression profile compared to T cell blasts. Graphs represent mRNA expression profiles of *in vitro* activated $T_{MBP-GFP}$ blast cells (**top**) compared to *ex vivo* isolated migratory $T_{MBP-GFP}$ cells from blood 72h p.t. (**bottom**). Means and s.d.of replicate measurements are shown. Values refer to specific copies in relation to β-actin copies. Representative results of at least 3 independent experiments are shown (ODOARDI et al., 2012).

1.2.2. Tools for visualizing autoimmune responses in the CNS

An advantage of *t*EAE is its susceptibility to manipulation. For instance, defined effector T cell populations can be labeled prior to transfer. Originally, this was achieved by radioactive tracers (KLINKERT et al., 1987) until the development of genetic transduction approaches to label MBP-specific T cells without interfering with their cellular functions (FLÜGEL et al., 1999). Thus, the coding sequence of green fluorescent protein (GFP) can be retrovirally introduced into the genome of myelin-reactive T cells enabling a stable expression of the fluorescent tag in the cytosol without dilution through mitotic events (FLÜGEL et al., 1999). This technique opened the possibility to trace adoptively transferred GFP^+ T cells *in vivo* and allows a functional characterization of *ex vivo* isolated cells during EAE (FLÜGEL et al., 2001; KAWAKAMI et al., 2004; KAWAKAMI et al., 2005 (1)).

Moreover, retroviral gene transfer can be employed to introduce a variety of molecular reporters into cells, e.g. fluorescently-marked NFAT. Nuclear factor of activated T cells (NFAT) is an early activation marker localized within the cell's cytoplasm in a highly phosphorylated state (CRABTREE & OLSON, 2002; SHAW et al., 1988). After TCR stimulation, calcineurin, a Ca^{2+}-dependent phosphatase dephosphorylates NFAT, which in turn is transported to the nucleus of the cell (CLIPSTONE & CRABTREE, 1992). There, NFAT exhibits its role as transcription factor, promoting the expression of several activation-linked genes, e.g. IL-2 and IFN-γ (CHOW et al., 1999; KIANI et al., 2001).
The expression of a fluorescently-labeled NFAT biosensor (e.g. NFAT-YFP) can be utilized for real-time monitoring of T cell activation within the living CNS tissue (LODYGIN et al., in press). The co-expression of a fluorescently-tagged histone protein (e.g. H2B-mcherry) within the same cell opens the possibility of discriminating between cytosolic and nuclear NFAT (**Fig.5**) (LODYGIN et al., in press).

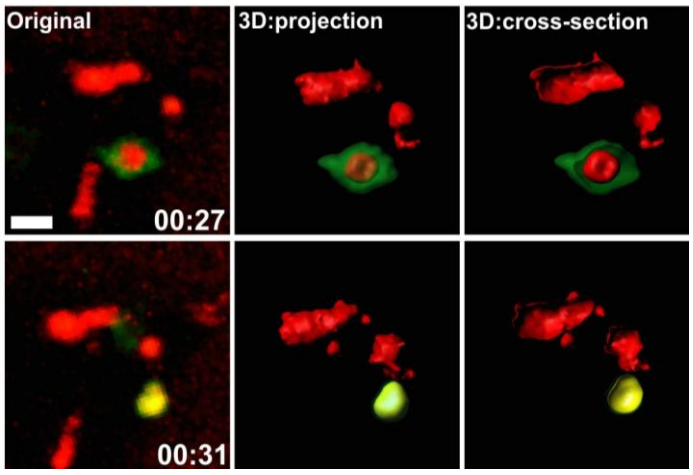

Figure 5 | 3D reconstruction of nuclear NFAT-translocation. Original snapshots, 3D projections and 3D cross-sections of an individual T cell bearing either cytosolic NFAT-YFP (green, upper row) or nuclear NFAT-YFP (yellow, lower row) are depicted. NFAT-translocation was induced upon contact with a resident phagocytic cell, highlighted by Texas-Red®-dextran labeling. Yellow color reflects a co-localization of NFAT-YFP with the red T cell nucleus (H2B-mcherry). Data are published in LODYGIN et al., (in press).

Visualization and temporal tracing of genetically engineered T cells *in vivo* requires a high microscopic standard. Up to now, the state of the art is non-linear optical two-photon laser scanning microscopy (TPLSM). In conventional, linear microscopy, such as confocal microscopy, fluorochromes are excited via single photons with short wavelength, thus high energy (DENK & SVOBODA, 1997). As a consequence, the electrons of the fluorescent dyes are elevated after photon absorption from a non-excited basal state to an activated, higher energy state (HELMCHEN & DENK, 2005). Once they reach this activated level, electrons can drop back to the basal state, a process accompanied by fluorescence emission (DENK et al., 1990). The emitted light of the fluorochromes can be detected and is of longer wavelength than the original excitation wavelength (ZIPFEL et al., 2003). Whenever the density of photons in time and space is high enough, the same fluorochromes can be excited with non-linear light of low energy, usually in the near infrared range (DENK & SVOBODA, 1997).

TPLSM systems are equipped with powerful lasers (i.e. titanium-sapphire lasers; 3-5W) that are capable of providing laser pulses in a femto-second range, a prerequisite for the coincidental photon absorption by the fluorochrome (DIASPRO & ROBELLO, 2000). Two-photon excitation has several advantages for *in vivo* imaging compared to conventional one-photon excitation.

Firstly, due to the high temporospatial density of photons required for the two-photon effect, only tissue in the perifocal plane is excited while avoiding excitation of adjacent tissue outside the focal plane (POTTER, 1996). Secondly, since fluorescent dyes within the specimen are excited with low energy, phototoxic damage to the tissue and bleaching of the dye are reduced to a minimum (KAWAKAMI & FLÜGEL, 2010). Thirdly, light with long wavelength is less scattered in biological tissues, creating the possibility of deeper penetration of the specimen compared to confocal microscopy (RUBART, 2004). Finally, two-photon excitation generates a quantum effect, i.e. the generation of higher harmonics (e.g. 2^{nd} harmonic). The latter makes it possible to visualize non-centrosymmetric structures, like extracellular matrix components (ZIPFEL et al.; 2003).

1.3. Aims of this work

In experimental autoimmune encephalomyelitis (EAE), a model for multiple sclerosis (MS), autoaggressive effector T cells infiltrate the CNS, get re-activated and trigger the initiation of an inflammatory response towards myelin-components. However, up to now it is not completely understood, how these distinct infiltration steps are regulated.

In this study, intravital two-photon microscopy (TPLSM) was employed in order to examine in real-time the invasion process of adoptively transferred GFP^+ $CD4^+$ MBP-reactive T cells during the different phases of EAE. Furthermore, it was to be clarified *which* factors regulate the migration of T cells during the different infiltration steps and *how* they modulate the T cells' locomotive pattern within the living CNS tissue. Thereby, the focus lay on chemokines that had been shown in the past to interfere with the clinical course of EAE.

In detail, the aim was to ascertain if chemokines contribute to T cell locomotion *in vivo* and if yes, which chemokines are of relevance for distinct T cell infiltration steps. In order to achieve this, the plan was to interfere with chemokine signaling at different time points in the autoimmune process by applying several blocking agents during intravital imaging of the preclinical, acute and recovery phases of EAE.

2. Material and Methods

2.1. Material

If not otherwise indicated, the buffers were prepared in Milli-Q purified H_2O (MILLIPORE GmbH, Schwalbach, Germany).

DMEM	66.9g/5l	Gibco DMEM Powder (52100-021), (INVITROGEN, Carlsbad, USA)
	18.59g/5l	$NaHCO_3$ (CARL ROTH GmbH, Karlsruhe, Germany)
T cell medium (TCM)	1l	DMEM
	10ml	Gibco Non essential Amino Acids, (INVITROGEN, Carlsbad, USA)
	10ml	Gibco Penicillin / Streptomycin (INVITROGEN, Carlsbad, USA)
	10ml	Gibco Sodium Pyruvate (INVITROGEN, Carlsbad, USA)
	10ml	L-Glutamine (PAN BIOTECH GmbH, Aidenbach, Germany)
	10ml	L-Asparagine Monohydrate (SIGMA ALDRICH, Munich, Germany)
	4µl	2-β-Mercaptoethanol (13.6mol/l), (INVITROGEN, Carlsbad, USA)
Re-stimulation Medium (RM)	200ml	T cell medium
	2ml	Rat serum
T cell Growth Factor (TCGF)	425ml	T cell medium
	50ml	Horse Serum
	25ml	Conditioned medium from splenocytes treated with the mitogen Concanavalin A (ROSENBERG et al., 1978)
Freezing Medium	40ml 50ml 10ml	TCM Horse Serum DMSO (CARL ROTH GmbH, Karlsruhe, Germany)

EH Medium	375ml	DMEM
ACK buffer	125ml	Gibco HEPES 1M (INVITROGEN Carlsbad, USA)
	0.15mol/l	NH_4Cl (CARL ROTH GmbH, Karlsruhe, Germany)
	1mmol/l	$KHCO_3$ NH_4Cl (CARL ROTH GmbH, Karlsruhe, Germany)
	0.1mmol/l	Na_2·EDTA/Titriplex (CARL ROTH GmbH, Karlsruhe, Germany)
		Adjust to pH 7.2 – 7.4 with 1N HCl
Isotonic percoll	9x Vol.	Percoll (GE HEALTHCARE, Munich, Germany)
	1x Vol.	PBS 10x
Underlay percoll	7ml	Isotonic Percoll
	3.9ml	PBS 1x
Complete Freund´s adjuvant	10ml	Incomplete Freund's adjuvant (DIFCO LABORATORIES, Detroit, USA)
	100mg	Mycobacteria (M.Tuberculosis H37Ra, DIFCO LABORATORIES, Detroit, USA)
MBP		Isolated from guinea pig brains as described (EYLAR et al., 1974).

2.2. Methods

2.2.1. Generation of GFP^+ T cell cultures

Animals were held under standardized conditions and had free access to water and food. All experiments were performed according to local regulations for animal welfare of Bavaria and Lower Saxony federal states.

6-8 week old female LEWIS rats (ANIMAL FACILITY OF THE MEDICAL SCHOOL GÖTTINGEN, Göttingen, Germany; ANIMAL BREEDING FACILITIES OF THE MAX-PLANCK INSTITUTE FOR BIOCHEMISTRY, Martinsried, Germany; JANVIER, Le Genest St Isle, France) were immunized with 100µg Guinea Pig Myelin Basic Protein (MBP) or Ovalbumin (OVA, albumin from chicken egg white Grade V) (A5503, SIGMA ALDRICH, Munich, Germany). Equal volumes of complete Freund´s adjuvant (CFA, 4mg/ml) and

respective antigen (1mg/ml) were mixed using tuberculin glass syringes (POULTEN & GRAF GmbH, Wertheim, Germany). Thereafter, a total volume of 200µl (4 x 50µl) was injected subcutaneously into popliteal cavity and tail base. Animals were sacrificed via CO_2 inhalation 9-10 days after the immunization procedure. Notably, at this time point, animals showed no signs of clinical EAE. Draining lymphnodes, namely inguinal, paraaortic and popliteal lymphnodes were isolated. Afterwards, the tissue was homogenized. The thus obtained lymphocyte suspension was set to $2x10^6$ cells/ml and was immediately co-cultured with $1.5x10^5$/ml retro-viral/GFP-cassette (FLÜGEL et al., 1999) containing packaging cells GPE86 (MARKOWITZ et al., 1988). Thereafter, cells were transferred to U-bottom 96-well plates (THERMOFISHER SCIENTIFIC INC., Braunschweig, Germany) in a total volume of 100µl RM containing 10µg/ml antigen. During primary culture, cells were held under 10% CO_2 in humidified atmosphere (Heraeus Heracell 240 incubator, THERMOFISHER SCIENTIFIC INC., Braunschweig, Germany). Two days following primary culture, 50µl TCGF medium was added to 96-well plates. Thereafter (1-2 days later), 100µl of supernatant were discarded and substituted with TCGF containing either 0.4mg/ml Geneticin/G418 (PAA LABORATORIES GmbH, Pasching, Austria) or 1µg/ml Puromycin (CARL ROTH GmbH, Karlsruhe, Germany). Subsequently, cells were transferred into 96 flat bottom wells (THERMOFISHER SCIENTIFIC INC., Braunschweig, Germany). On day 6 or 7 after primary culture, cells were stimulated by substitution of 100µl supernatant with RM containing $1.4x10^7$ irradiated (30Gy) thymocytes/ml, antigen (10µg/ml) and Geneticin (0.4mg/ml) or Puromycin (1µg/ml). Two days later, 50µl TCGF containing Geneticin/Puromycin was added to the wells. One day later, retroviral transduction efficiency was controlled by using an Axiovert 200M fluorescence microscope (CARL-ZEISS MICROIMAGING, Jena, Germany). Wells with the highest transduction rate were pooled and transferred to 6cm dishes (SARSTEDT AG & CO., Nürnbrecht, Germany) followed by addition of TCGF. 3 days later, GFP^+ lymphocytes were re-stimulated by co-culturing of $3.5x10^6$ T lymphocytes together with $7x10^7$ irradiated lymphocytes in 5ml RM containing antigen and antibiotics as described above. The latter procedure was repeated up to 3 times following a 6-7 day cycle. In the present study, T cells were frozen two days post re-stimulation (from 3rd re-stimulation on) as fully activated lymphoblasts. Alternatively, for expanding T cell cultures, T lymphocytes were frozen on day 6 or 7 after re-stimulation and re-stimulated immediately after thawing.

2.2.2. Adoptive T cell transfer

$CD4^+$ $T_{MBP\text{-not labeled}}$, $T_{MBP–GFP}$, $T_{OVA–GFP}$ and $T_{MBP/NFAT\text{-}YFP/Cherry\text{-}H2b}$ cell lines were generated and tested for phenotype, cytokine profile and antigen specificity as described (FLÜGEL et al., 2001). After thawing, the T lymphoblast suspension was immediately diluted with EH-buffer containing 10% FCS. Thereafter, cells were centrifuged for 8min at 4°C with 300xg (Multifuge Heraeus S 1S-R, THERMOFISHER SCIENTIFIC INC., Braunschweig, Germany) and the pellet was re-suspended in EH buffer. Adoptive transfer EAE was induced by intravenous injection of $5x10^6$ effector T cells in 1ml EH into the tail vein of healthy LEWIS rats that were narcotized with Diethlyether (CARL ROTH GmbH, Karlsruhe, Germany). In some experiments $2.5x10^6$ $T_{OVA–GFP}$ cells were co-injected together with $5x10^6$ $T_{MBP\text{-not labeled}}$ cells. Weight and clinical scores were measured daily (score 0= no disease; 1= flaccid tail; 2= gait disturbance; 3= complete hind limb paralysis; 4= tetraparesis; 5 = death).

2.2.3. Intrathecal injection procedure

Animals were anaesthetized by intra-muscular injection of 10mg kg^{-1} xylazine (ECUPHAR GmbH, Greifswald, Germany) combined with 50mg kg^{-1} ketamine (MEDISTAR ARZNEIMITTELVERTRIEB GmbH, Ascheberg, Germany). Thereafter, animals were fixated within a stereotactic device (NARISHIGE SCIENTIFIC INSTRUMENT LAB., Tokyo, Japan). Subsequently, an injection needle (BD ½ cc Tuberculin Syringe, BECTON DICKINSON GmbH, Heidelberg, Germany) was placed between level C1 and C2 with puncture of the cisterna magna. The syringe was held under negative pressure to ensure inflow of liquor cerebrospinalis. Thereby, a correct positioning of the needle was warranted. A total volume between 60-80µl was injected during a 15min time period. Afterwards, animals were placed on a heating blanket to prevent hypothermia during anesthesia.

2.2.4. Flow cytometric cell quantification

Animals were sacrificed via CO_2 inhalation. Single cell suspensions from spinal cord meninges and parenchyma were obtained by tissue homogenization. After centrifugation (8min, 4°C, 300xg), pellets were re-suspended in a defined volume of EH medium. For quantification of cells from spleen, pellets were re-suspended in ACK-buffer to achieve erythrocyte-lysis. Afterwards, cells were washed in ice-cold PBS (8min, 4°C, 300xg) and the pellet was re-suspended in EH medium.

For evaluation of peripheral blood lymphocyte numbers, animals were sacrificed as described above. Afterwards, blood was taken with an EDTA (CARL ROTH GmbH, Karlsruhe, Germany)-moistened syringe by heart puncture. To isolate lymphocytes from total blood, a density gradient separation was performed as following: Blood was mixed with PBS (1x volume) at room temperature and carefully laid on top of 0.5 volume lymphocyte separation medium (LSM1077, PAA LABORATORIES GmbH, Pasching, Austria). Subsequently the 2 phases were centrifuged at 836xg at room temperature for 30min with minimal acceleration ramp (Multifuge Heraeus 1S-R, THERMOFISHER SCIENTIFIC INC., Braunschweig, Germany). The obtained interphase was collected and washed once with ice-cold PBS. Thereafter, the pellet was re-suspended in a defined volume of EH medium.

For quantification of GFP^+ cells, defined volumes of cell suspension were mixed with a definite number of fluorescence beads (BECTON DICKINSON GmbH, Heidelberg, Germany) and subsequently acquired via flow cytometry (BD FACSCalibur™, BECTON DICKINSON GmbH, Heidelberg, Germany).

2.2.5. Cell Sorting

Animals were sacrificed by CO_2 inhalation. Spleen and blood cell suspensions were prepared as described in **2.2.4**. Samples from spinal cord were processed as following: Meninges were carefully separated from parenchyma and placed in ice-cold EH buffer. After homogenization cell suspensions were washed once with EH buffer (8min at 4°C, 300xg). Thereafter, pellets were re-suspended in 25ml EH medium. For lymphocyte separation, suspensions were mixed with 10.8ml isotonic percoll solution. Thereafter, 10ml underlay percoll were cautiously laid below the mixture. Next, a density gradient was achieved by a 30min centrifuge step with minimal acceleration ramp (1616xg, RT). The interface was separated carefully, washed once with PBS and the obtained pellets were re-suspended in defined volumes of EH medium. For all samples - including spinal cord meninges, parenchyma, blood and spleen - collector tubes were moistened with 1ml RM. Thereafter RM medium was substituted with EH buffer. Cell sorting was performed by using a BD FACSAria™ III (BECTON DICKINSON GmbH, Heidelberg, Germany) with minimum flow speed at 4°C. The obtained fraction of sorted GFP^+ T cells was transferred into E-cups and centrifuged 1min with 800xg at 4°C using a Centrifuge 5415 (EPPENDORF VERTRIEB DEUTSCHLAND GmbH, Wesseling-Berzdorf, Germany). Subsequently, pellets were re-suspended with a defined volume of QIAzol Lysis Reagent (QIAGEN GmbH, Hilden, Germany) and stored at -80°C.

2.2.6. Re-transfer of migratory T cells

$T_{MBP\text{-}GFP}$ cells were isolated from spleens of donor animals 2.5-3 days post transfer as described in **2.2.4.** Cell suspension was depleted from splenic macrophages. In brief, splenic cell suspension was washed once in EH buffer and the pellet was re-suspended in TCM. The obtained suspension was transferred to 10cm cell culture dishes (SARSTEDT AG & CO., Nürnbrecht, Germany) and incubated for 1h in a Heraeus Heracell 240 incubator (THERMOFISHER SCIENTIFIC INC., Braunschweig, Germany) at 37°C in humidified atmosphere under 10% CO_2. Afterwards, macrophages were found attached to the bottom of the cell culture plates. Next, the macrophage-depleted cell suspension was carefully transferred to 50ml Cellstar® tubes (GREINER BIO-ONE GmbH, Frickenhausen, Germany) and washed once with EH medium for 8min at 4°C with 300xg. Finally, cells were re-injected intrathecally (total volume= 60µl) or intravenously (total volume= 1ml) into healthy animals.

2.2.7. Interference with integrin signaling

In order to block α4β1 integrin signaling, a neutralizing mouse anti-rat monoclonal antibody against VLA-4 (anti-CD49d, clone TA-2; HOJO et al., 1998) was injected i.v. The antibody was administered at a single dose of 4mg kg^{-1} during intravital TPLSM recordings. The antibody was kindly provided by Prof. Thomas Issekutz (GRACE HEALTH CENTER, DALHOUSIE UNIVERSITY, Halifax, Canada). After recording, saturated binding of the antibody was controlled as described (BARTHOLOMÄUS et al., 2009).

2.2.8. Interference with chemokine signaling

For intravital studies focusing on *intraluminal* T cell migration, 20µg kg^{-1} pertussis toxin A oligomer (LIST BIOLOGICAL LABORATORIES, INC., Campbell, USA), 2mg kg^{-1} Met-RANTES (courtesy of Dr. Peter Nelson, UNIVERSITY HOSPITAL LMU MUNICH, Munich, Germany), 4mg kg^{-1} Hamster anti-rat CXCR3mAb (clone XR3.2, courtesy of Prof. Thomas Issekutz, GRACE HEALTH CENTER, DALHOUSIE UNIVERSITY, Halifax, Canada), 5mg kg^{-1} Plerixafor/AMD3100 (GENZYME GmbH, Neu-Isenburg, Germany) or PBS were applied before or during intravital imaging intravenously via an OPS 50ml Luerlock infusion set (B.BRAUN MELSUNGEN AG, Melsungen, Germany) with a total volume of 1ml. In some experiments, pertussis toxin oligomer B (Olig.-B) (LIST BIOLOGICAL LABORATORIES, INC., Campbell, USA) and an Armenian hamster IgG Isotype antibody (ABCAM, Cambridge, UK) served as controls. The doses for respective

monoclonal antibodies and blocking agents were used according to their blocking efficiency in *in vitro* chemotaxis assays (see **2.2.16**) and/or were similar to those described in literature (Met-RANTES: GRÖNE et al., 1999, Plerixafor/AMD3100: MATTHYS et al., 2001, anti-CXCR3mAb: SPORICI & ISSEKUTZ, 2010).

For intravital studies on *extravasated* T cells, 1µg kg^{-1} pertussis toxin A oligomer, 1mg kg^{-1} Met-RANTES, 0.5mg kg^{-1} Plerixafor/AMD3100 or PBS were applied before (4h) or during intravital imaging intrathecally (d3 p.t., d8 p.t.) via a micromanipulator into the cisterna magna (total volume 60 µl) after stereotactic fixation of anaesthetized animals (see **2.2.3**). During full inflammation (d5 p.t.), blocking agents were injected intravenously for technical reasons. In some experiments, pertussis toxin oligomer B (Olig.-B) (LIST BIOLOGICAL LABORATORIES, INC., Campbell, USA) and an Armenian hamster IgG Isotype antibody (ABCAM, Cambridge, UK) were used as controls. For re-transfer experiments (see **2.2.6**) *ex vivo* isolated migratory T cells were incubated with either 100ng ml^{-1} pertussis toxin A (PTx) or B-Oligomer (Olig.-B) (LIST BIOLOGICAL LABORATORIES, INC., Campbell, USA) for 1h at 37°C in TCM medium. Afterwards, cells were washed twice with PBS and re-injected into healthy recipient rats as described in **2.2.6**.

In order to confirm successful treatment, cells were isolated from different organs as described. Afterwards, a T cell chemotaxis assay was performed on the respective chemokines namely CCL5, CXCL11 and CXCL12 (see **2.2.16**).

2.2.9. Intravital TPLSM: surgical procedure

Animals were anaesthetized by intra-muscular injection of 10mg kg^{-1} xylazine combined with 50mg kg^{-1} ketamine. Thereafter, animals were intubated via a small incision of the trachea and immediately ventilated with 1.5–2% isoflurane (BAXTER GmbH, Höchstadt a.d. Aisch, Germany) using a custom built ventilation system. This system was driven by an Inspira Advanced single animal pressure-controlled ventilator (HARVARD APPARATUS, Holliston, USA). Medical oxygen (UNIVERSITÄTSMEDIZIN GÖTTINGEN, Göttingen, Germany) and pressurized air were routed through an isoflurane vaporizer (UNO ROESTVASTSTAAL BV, Zevenaar, Netherlands) and several gas reservoirs (DRÄGER MEDICAL DEUTSCHLAND GmbH, Lübeck, Germany). Both inspired and expired air was analyzed via OHMEDA 5250RGM devices (GE HEALTHCARE, Munich, Germany). During imaging, animals were stabilized in a custom-made microscope stage and their body temperature regulated and maintained (37-37.5°C) via a heated pad (TELEMETER

ELECTRONIC GmbH, Donauwörth, Germany) connected to a custom-built thermo-controller (TC-1, TORSTEN NÄGEL, ELEKTRONISCHE WERKSTATT, UNIVERSITÄT GÖTTINGEN, Göttingen, Germany). Fluid supply during imaging sessions was warranted by using a Perfusor® fm device (B.BRAUN MELSUNGEN AG, Melsungen, Germany). Body temperature and heart rate were recorded using Animal Monitor software 7.3x (VOLKER STAIGER, MAX-PLANCK INSTITUTE OF NEUROBIOLOGY, Martinsried, Germany). For intravital TPLSM recordings of the leptomeninges, a spinal cord window was prepared as described previously at level Th12/L1 (BARTHOLOMÄUS et al., 2009). Briefly, a midline skin incision of 2–3cm was performed followed by subsequent detachment of the paravertebral musculature from the spine. Thereafter, a laminectomy on one of the three exposed vertebral bodies was performed. Preparing the dermal blood vessels of the ear required a careful separation into a ventral and a dorsal half. Thereafter, blood vessels of the ventral half were cautiously exposed. For all preparations, tissue was immediately covered with sodium-chloride solution (B.BRAUN MELSUNGEN AG, Melsungen, Germany) after exposure in order to prevent dehydration.

2.2.10. Intravital TPLSM: Technical equipment

Time-lapse two-photon laser-scanning microscopy was performed using a LSM710/Axio Examiner. Z1 confocal microscope (CARL-ZEISS MICROIMAGING, Jena, Germany) combined with a >2.5Watts Ti:Sapphire Chameleon Vision II Laser device (COHERENT GmbH, Dieburg, Germany). The excitation wavelength was tuned to 880nm or 1010nm and routed through a 20x water NA1.0 immersion objective W Plan Apochromat (CARL-ZEISS MICROIMAGING, Jena, Germany). Typically, areas of 424.27 x 424.27µm (512 x 512px) width were scanned and 50–100µm z-stacks were acquired. The acquisition rate during bi-directional scanning was approximately 1.3s per z-plane including 2 times line-averaging. Importantly, for reproducible motility analyses, the interval time was kept exactly to 32sec while varying the numbers of z-sections (usually between 18 and 25) or distances between 2 z-planes (step-size, typically between 2 and 6µm). For quantification of intraluminal crawling T cells, an extended area of 5 adjacent spots of approximately 2121.35 x 424.27µm (2560 x 512px) was analyzed. To this end, a software-controlled motorized stage was used (PRIOR SCIENTIFIC INSTRUMENTS GmbH, Jena, Germany). Typically, extended areas were acquired with a rate of approximately 1.3s per plane and 24s per z-stack with only 1x line-averaging. The resulting interval time varied between ~120 and 170sec depending on the number of z-stacks. Emitted fluorescence was detected using non-descanned detectors

(CARL-ZEISS MICROIMAGING, Jena, Germany) equipped with 442/46nm, 525/50nm, 550/49nm and 624/40nm band-pass filters (SEMROCK INC., New York, USA).

2.2.11. Intravital TPLSM: Processing of raw data

TPLSM time-lapse recordings were acquired and processed by Zen 2009 Software (CARL-ZEISS MICROIMAGING, Jena, Germany) obtaining 2D movies/images by generating maximum intensity projections out of 3D- and 4D stacks. Afterwards, movies and images were exported as .avi or .tif files, respectively without any compression algorithm. Thereafter, 2D data were further processed using ImageJ 1.46i software (NATIONAL INSTITUTE OF HEALTH, Bethesda, USA). Brightness and contrast as well as color balance adjustments of single RGB channels were performed with implemented plugins. In some cases, movies had to be stabilized using the ImageJ StackReg tool. The red channel was set as reference since it contained locally fixed objects (e.g. blood vessels). Annotations were made using ImageJ, Corel Photo Paint X4 and Corel Draw X4 (COREL CORPORATION, Ottawa, Canada).

2.2.12. Intravital TPLSM: Analysis of T cell motility

Imaris 7.1.1 software (BITPLANE, Zurich, Switzerland) was used for 3D reconstructions and 4D analysis of acquired raw data. Analysis of T cell motility required the automated Imaris Track module with subsequent manual revision afterwards. Motility parameters including T cell velocity, crawling duration and meandering index were calculated from the obtained x, y, z-coordinates using Excel 2010 (MICROSOFT CORPORATION, Washington, USA). Average velocities of individual T cells within a 30min recording interval were determined as described previously (BARTHOLOMÄUS et al., 2009). Instantaneous velocities of individual T cells were determined based on coordinates generated with Imaris 7.1.1 software (BITPLANE, Zürich, Switzerland) using a custom-built Excel 2010 script. Afterwards, single displacements were assigned according to the intraluminal crawling direction (up- or downstream). Crawling duration was defined as the average time an individual T cell spent crawling within a 30min time interval. Notably, cells that were visible for less than 2 frames (~1min) were excluded from the analysis. Correlation between intraluminal rolling and crawling T cells in different organs was done by calculating absolute numbers of both rolling and crawling cells within a 30min acquisition period. Notably, rolling T cells appeared as several round shaped dots in the direction of the blood flow as described (BARTHOLOMÄUS et al., 2009). The meandering index is defined as a ratio between total

T cell path length and the sum of the entire single displacements during a 30min time interval. Statistical evaluations were performed with GraphPad 5.0.4 (GRAPHPAD SOFTWARE INC., San Diego, USA). Statistical tests for data analysis are mentioned in the figure legends. Alpha level was set to 0.05, p values are: *p < 0.05, **p < 0.01, ***p < 0.001, ****p < 0.0001.

2.2.13. Intravital TPLSM: Labeling of phagocytic cells and blood vessels

To label meningeal phagocytes, small molecular (3kDa) Texas Red®-conjugated dextran (INVITROGEN, Carlsbad, USA) was injected at doses of 40µg/rat via a stereotactic device into the cisterna magna of anaesthetized animals 48h p.t. Blood vessel lumen was visualized by intravenous infusion of 200µg (2000kDa) Texas Red®-conjugated dextran before or during intravital TPLSM recordings. For testing the endothelial permeability, small molecular (3kDa) Texas Red®-conjugated dextran was used.

2.2.14. Intravital TPLSM: Analysis of T cell interactions with meningeal phagocytes/ Analysis of early T cell activation

Meningeal phagocytes were visualized as described in **2.2.13**. Notably, only spots with similar density of fluorescently labeled phagocytes were considered for analysis. For evaluation of single contact durations and contact frequencies, exclusively motile GFP^+ T cells were used for examination. Cells were considered motile if they moved more than 10µm away from their origin during a 30min acquisition interval. Contact durations were determined by manually counting the frames between initial attachment and detachment of GFP^+ T cells to/from meningeal phagocytes. Since not all T cells were visible during the entire observation period of 30min, contact frequencies (No. of contacts) were calculated as follow: the total number of phagocytes contacted by an individual T cell was divided by the T cell's total number of displacements. The obtained value was extrapolated to 30 minutes. Long-lasting contacts (≥ 30min) were evaluated by counting stationary GFP^+ T cells that were in close vicinity (≤ 1 cell diameter distance) to resident phagocytes. For evaluation of T cell activation *in vivo*, exclusively double fluorescent $T_{MBP/NFAT\text{-}YFP/Cherry\text{-}H2b}$ cells with clear YFP and mCherry signal were considered for 4D analyses. T cells with nuclear (translocated) or cytosolic (not translocated) NFAT were defined by analyzing fluorescent overlap between the green and red channel. Merged (yellow): translocated; not merged: not translocated. Statistical analyses were performed as described in **2.2.12**.

2.2.15. Quantitative PCR

For transcriptome analyses *ex vivo* sorted cells or total tissues were stored in QIAzol Lysis Reagent (QIAGEN GmbH, Hilden, Germany). Preparation of mRNA and reverse transcription were performed according to standard protocols from SIGMA-ALDRICH and INVITROGEN, respectively. For TaqMan® analysis, ABI-Prism 5700 Sequence Detector 'TaqMan®' software (APPLIED BIOSYSTEMS DEUTSCHLAND GmbH, Darmstadt, Germany) was used. β-actin served as housekeeping gene. Rat primers and probes used for detection of activation markers and chemokines receptors/ligands were the following:

Gene (*Symbol*)	**Forward primer 5' - 3'**	**Reverse primer 5' - 3'**	**Probe FAM-5' - 3'-TAMRA**
Beta-actin (*Bact*)	GTACAACCTCCTTGCAGCTCCT	TTGTCGACGACGAGCGC	CGCCACCAGTTCGCCATGGAT
Interferon gamma (*Ifng*)	AACAGTAAAGCAAAAAAGGATGCATT	TTCATTGACAGCTTTGTGCTGG	CGCCAAGTTCGAGGTGAACAACCC
Interleukin-17A (*Il17a*)	GAGTCCCCGGAGAATTCCAT	GAGTACCGCTGCCTTCACTGT	ATGTGCCTGATGCTGTT
Chemokine (C-C motif) ligand 5 (Ccl5)	CAACCTTGCAGTCGTCTTTGTC	GATGTATTCTTGAACCCACTTCTTCTC	AGGAACCGCCAAGTGTGTGCCAAC
Chemokine (C-C motif) ligand 19 (Ccl19)	TAGAGGTGCACAGAGCTGGTA	GCCTTCCGCTACCTTCTTAT	CCTTAGTGTGGTGAACACAACAGCAGG
Chemokine (C-X-C motif) ligand 9 (Cxcl9)	TTGCCCCAAGCCCTAACTG	ACCCTTGCTGAATCTGGGTCTAG	CATCGCTACACTGAAGAACGGAGATC
Chemokine (C-X-C motif) ligand 10 (Cxcl10)	CGTGCTGCTGAGTCTGAGT	GTCTCAGCGGCTGTTCAT	CTCAAGGGATCCCTCTCGGAAGAAC
Chemokine (C-X-C motif) ligand 11 (Cxcl11)	GGTTCCAGGCTTCGTTATGTTC	AACTTCCTTGATTGCTGCCATT	CTGTCTTTGCATCGACCGCGGAGT
Chemokine (C-X-C motif) ligand 12 (Cxcl12)	GTCAAACATCTGAAAATCCTCAACAC	GGTCAATGCACACTTGTCTGTTGT	ACTGTGCCCTTCAGATTGTTGCAAGGCT
Chemokine (C-C motif) receptor 5 (*Ccr5*)	GTTCTCCTGTGGACCGGGTATACG	ATTGTCAAACGCTTCTGCAAAC	AGCTTACACGATCAGGATT
Chemokine (C-C motif) receptor 7 (*Ccr7*)	GTGTAGTCCACGGTGGTGTTCTC	CTGGTCATTTTCCAGGTGTGCT	CCGATGTAGTCGTCTGTGA
Chemokine (C-X-C motif) receptor 3 (*Cxcr3*)	AGCAGCCAAGCCATGTACCTT	TAGGGAGATGTGCTGTTTTCC A	AGGTCAGTGAACGTCAAGTGC TAGATGCCTC
Chemokine (C-X-C motif) receptor 4 (*Cxcr4*)	GAGGTCATCAAGCAAGGATGT	GGGTTCAGGCAACAGTGGA	TTCGAGAGCGTCGTGCACAA

2.2.16. Chemotaxis assay

Transwell chambers (CORNING COSTAR GmbH, Bodenheim, Germany) with 5µm pore size were equilibrated with 235µl TCM medium in the bottom wells over night at 37°C. Afterwards, medium was substituted with TCM (+1%BSA) and 0.1µg CCL19 (PEPROTECH GmbH, Hamburg, Germany), CCL5 (ABD SEROTEC, Düsseldorf, Germany) CXCL10 or CXCL12 (R&D SYSTEMS GmbH, Wiesbaden-Nordenstadt, Germany). TCM (+1% BSA) without chemokine ligands served as control. T lymphocytes from spleen, blood and spinal cord meninges were isolated *ex vivo* as described above, quantified via flow cytometry and adjusted to $1x10^6$ T cells per ml in TCM (+1% BSA) medium. Thereafter, T cells were put in the upper wells and the chamber was kept at 37°C in humidified atmosphere containing 10% CO_2 for 5h. Numbers of GFP^+ T cells in the bottom wells were calculated (see **2.2.4**) relative to the input.

2.2.17. Histology

Animals were sacrificed as described and perfused with 4% PFA in PBS. Following explantation, the entire spinal cord was post-fixated for 2 days at 4°C. In order to decalcify samples, the tissue was transferred into PBS (+14% EDTA) for 10 days and then into 30% sucrose-containing PBS. Thereafter, each spinal cord was embedded in Tissue Tek O.C.T Compound (SAKURA FINETEK GERMANY GmbH, Staufen, Germany) followed by transversal cutting (15µm slices) using a CM305S cryostat (LEICA MICROSYSTEMS GmbH, Wetzlar, Germany) at −20°C. Images of the slices were acquired using an Axio Observer Fluorescence Microscope (CARL-ZEISS MICROIMAGING, Jena, Germany).

3. Results

3.1. Infiltration of myelin-reactive T cells into the CNS during *t*EAE

CNS autoimmune inflammation was induced by intravenous transfer of autoaggressive, activated $CD4^+$ T lymphoblasts in healthy LEWIS rats. These cells were reactive against the main myelin component, myelin basic protein (MBP). Retroviral transduction allowed a stable expression of GFP within these T cells ($T_{MBP\text{-}GFP}$ cells), opening the possibility of tracing them *in vivo* (FLÜGEL et al., 1999). In the present work, histological and flow cytometric examinations of spinal cord tissue during the preclinical (d3 p.t.), acute (d5 p.t.) and recovery (d8 p.t.) phases of EAE were combined with intravital TPLSM analyses.

Flow cytometric quantifications of different organs including blood, spinal cord meninges and parenchyma revealed that $T_{MBP\text{-}GFP}$ cells started to accumulate in the circulation 2 days post transfer, reaching a peak in numbers one day later (d3 p.t.) (**Fig.6**). The increase of T cell numbers within the circulation coincided with an infiltration of cells into the CNS meninges starting 3 days post transfer (**Fig.6**). Notably, until this point, animals did not show any signs of clinical EAE (see **Fig.2**). Histological examinations of spinal cord tissue discovered that early infiltrating $T_{MBP\text{-}GFP}$ cells (d3 p.t.) were restricted mainly to the leptomeninges and to the outer layer of the parenchymal white matter (**Fig.7a**).

Ongoing T cell infiltration of spinal cord meninges and parenchyma coincided with the onset of clinical symptoms around day 4 post transfer (not shown). The peak of clinical symptoms was reached one day after disease onset (d5 p.t.) (see **Fig.2**). In this "acute" phase, $T_{MBP\text{-}GFP}$ cells appeared in maximum numbers within spinal cord meninges and parenchyma whereas they were virtually absent from the circulation (**Fig.6**). Histologically, $T_{MBP\text{-}GFP}$ cells were apparently no longer restricted to meningeal and white matter areas but had spread throughout the entire spinal cord surface including the parenchymal grey matter (**Fig.7b**). The animals started to recover from disease symptoms around day 7 post transfer (see **Fig.2**).The reduction in clinical disease severity was accompanied by a massive decrease in $T_{MBP\text{-}GFP}$ cell numbers in spinal cord meninges and parenchyma. Histological examination of spinal cord tissue on day 8 post transfer revealed a similar distribution pattern of the remaining $T_{MBP\text{-}GFP}$ cells as was seen in the acute disease phase, i.e. T cells were spread throughout the entire spinal cord tissue including meninges and white and grey matter areas of the parenchyma (**Fig.7c**).

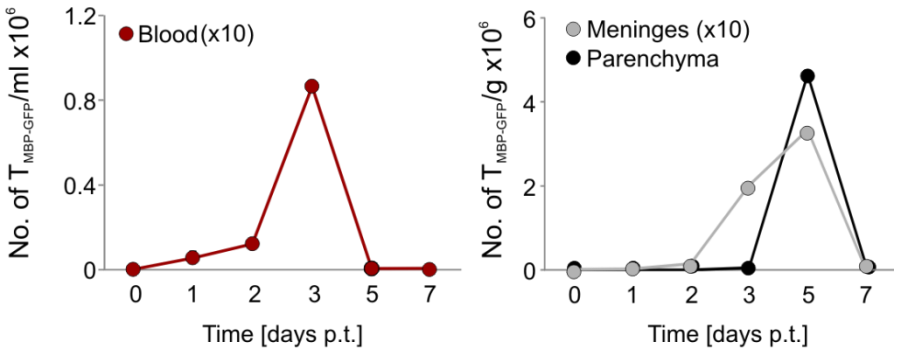

Figure 6 | $T_{MBP-GFP}$ cells do not enter the CNS directly after transfer. Cytofluorometric quantifications of $T_{MBP-GFP}$ cells from blood (left), spinal cord meninges and parenchyma (right) are shown. Dots represent absolute $T_{MBP-GFP}$ cell numbers at the indicated time points after transfer. Representative results from at least 3 independent experiments per time point are depicted.

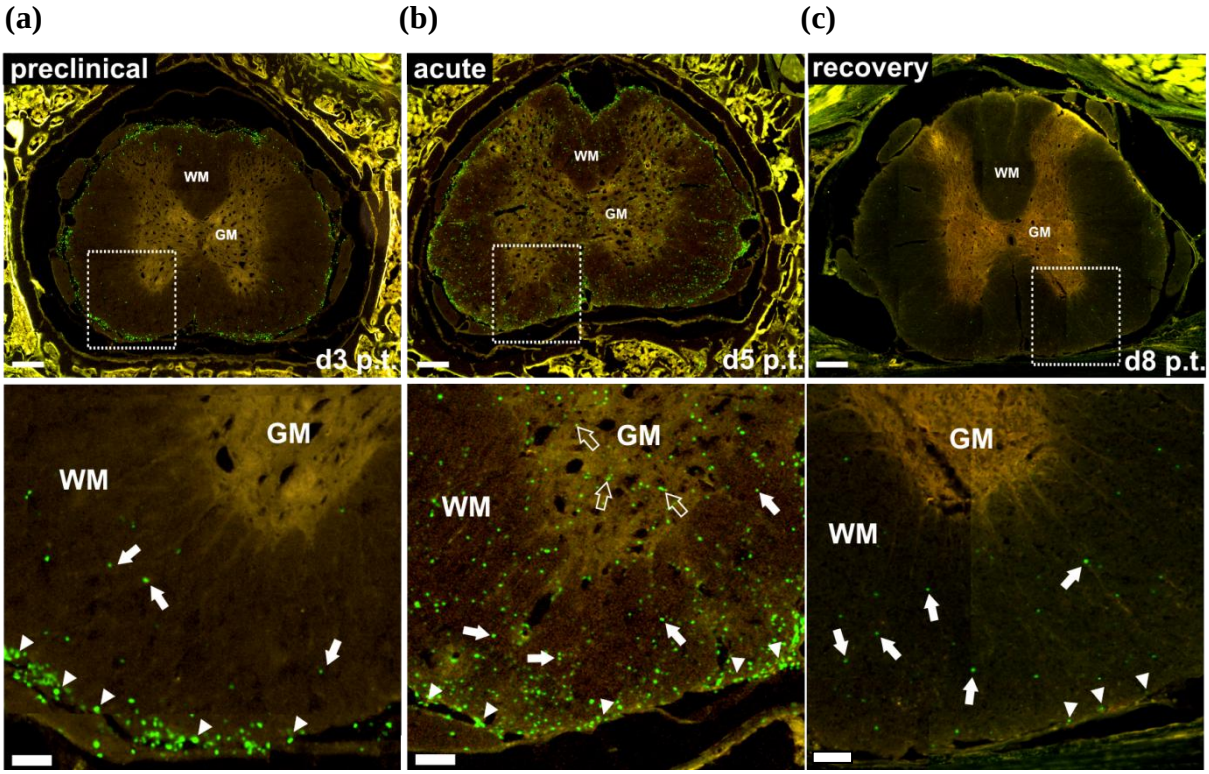

Figure 7 | Autoaggressive $T_{MBP-GFP}$ cells infiltrate the spinal cord during EAE. Histological analysis of spinal cord cross-sections reveals the T cell distribution during **(a)** preclinical (d3 p.t.), **(b)** acute (d5. p.t.) and **(c)** recovery phases (d8 p.t.) of EAE. WM and GM: White matter and grey matter, respectively. Green: $T_{MBP-GFP}$ cells. Arrows: representative $T_{MBP-GFP}$ cells located in the leptomeninges (arrow heads), WM (filled arrows) or GM (open arrows). Scale bars: 500µm. Magnification of individual regions (white dotted rectangles) originated from the overviews. Scale bars: 100µm.

3.2. Motility of encephalitogenic effector T cells during the different EAE phases

3.2.1. Motility of encephalitogenic T cells within the leptomeningeal vessel lumen during the preclinical phase of EAE

Intravital TPLSM was employed to study the migratory behavior of effector T cells within meningeal blood vessels during the preclinical phase of EAE (d3 p.t.). Surprisingly and contrary to findings in peripheral organs including the ear, only a minority of $T_{MBP\text{-}GFP}$ cells (28%) in the meningeal blood vessels rolled along the vascular walls (**Fig.8a,10a**). Instead, the vast majority of encephalitogenic T cells (72%) were crawling on the intraluminal surface of the blood vessels (**Fig.8b,10a**). On average, T cells spent 15min on crawling (**Fig.10b**). This locomotive pattern was independent of the direction of the blood stream since $T_{MBP\text{-}GFP}$ cells were able to alter their migratory route within the vessel lumen (**Fig.9**). Indeed, intraluminal crawling revealed a directional bias since $T_{MBP\text{-}GFP}$ cells tended to travel predominantly against the direction of the blood flow (**Fig.10c**) with an average velocity of 10.4µm/min (**Fig.10d**). The instantaneous velocity of $T_{MBP\text{-}GFP}$ cells was unchanged, independent of the crawling direction (up-or downstream) within the vessel lumen, suggesting a negligible impact of the blood flow on the migration speed (**Fig.10e**).

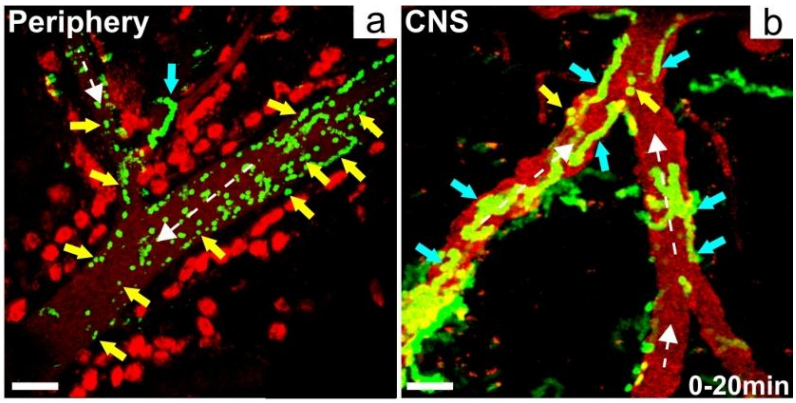

Figure 8 | Intraluminal locomotive behavior of $T_{MBP\text{-}GFP}$ cells in different organs during the preclinical phase of EAE. Intravital TPLSM recordings of **(a)** dermal blood vessels of the ear and **(b)** spinal cord leptomeninges 3 days p.t. are shown. Trajectories of $T_{MBP\text{-}GFP}$ cells within a 20min recording period are depicted. Rolling $T_{MBP\text{-}GFP}$ cells appear as dots (yellow arrows), crawling $T_{MBP\text{-}GFP}$ cells appear as green lines (blue arrows).White arrows: Direction of the blood flow. Red: Texas Red®-labeled blood vessel and perivascular phagocytes. Scale bars: 50µm. Representative data from at least 3 independent experiments are shown.

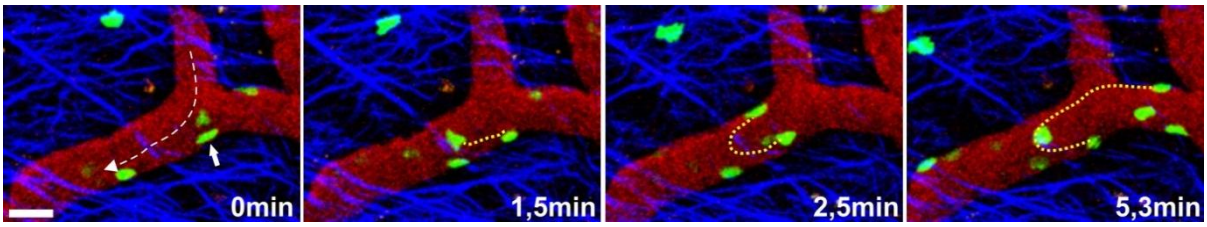

Figure 9 | Direction of the blood flow has no influence on intravascular T cell crawling. A series of snapshots acquired with intravital TPLSM during the preclinical phase of EAE (d3 p.t.) reveals the intraluminal locomotive behavior of a $T_{MBP-GFP}$ cell within a leptomeningeal blood vessel of the spinal cord. White dotted line with arrowhead: Direction of the blood flow. Yellow dotted lines: Migration path of an individual $T_{MBP-GFP}$ cell. White arrow: Initial position of the cell. Red: Texas Red®-labeled blood vessel. Green: $T_{MBP-GFP}$ cells. Blue: Reticular fibers. Scale bar: 25µm.

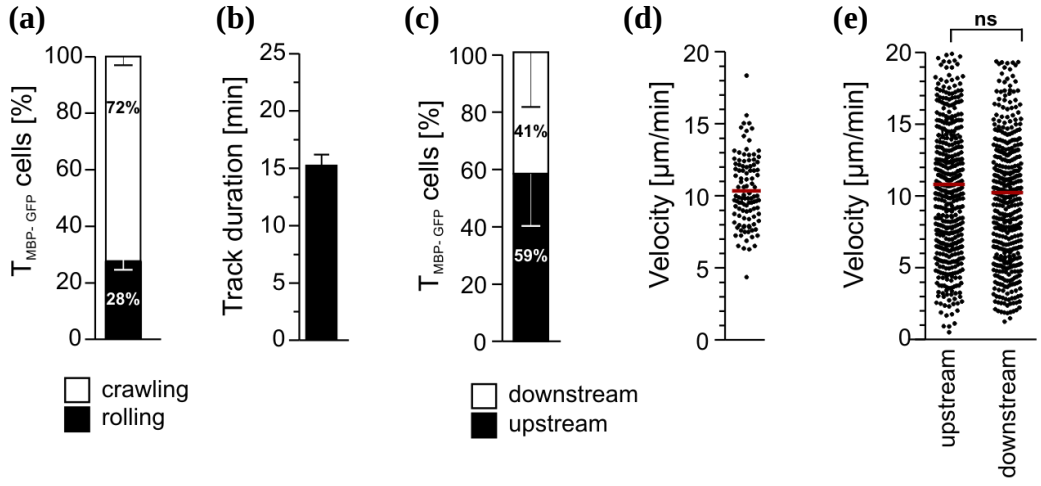

Figure 10 | Motility of encephalitogenic effector T cells within leptomeningeal blood vessels. Motility data of intravascular crawling $T_{MBP-GFP}$ cells are shown. Analyses are based on 30min intravital TPLSM imaging data acquired during the preclinical phase of EAE (d3 p.t.). Bars represent: **(a)** Proportion of intraluminal crawling vs. rolling $T_{MBP-GFP}$ cells, **(b)** average track duration of intraluminal crawling $T_{MBP-GFP}$ cells, **(c)** proportion of $T_{MBP-GFP}$ cells crawling in (downstream) or against (upstream) the direction of the blood flow, **(d)** average velocity of intraluminal crawling cells and **(e)** average velocities of individual $T_{MBP-GFP}$ cells moving downstream or upstream. Statistical significance was determined by two-tailed Mann-Whitney test. Means (and s.d. **(a-c)**) including **(a)** 135 and **(b-e)** 300 cells from at least 5 independent experiments are depicted.

3.2.2. Locomotive behavior of encephalitogenic T cells within the meningeal environment during the different phases of EAE

Following intraluminal crawling, $T_{MBP\text{-}GFP}$ cells gained access to the perivascular space by transgressing the vascular walls (BARTHOLOMÄUS et al., 2009). Software-based 4D analyses (x-y-z-t) of the acquired imaging data revealed that the majority of $T_{MBP\text{-}GFP}$ (82%) cells that had just overcome the vascular compartment (d3 p.t.) remained in close vicinity to leptomeningeal blood vessels for several hours (**Fig.11a,12a**). Coinciding with disease progression, migrating $T_{MBP\text{-}GFP}$ cells became less confined to the vascular bed and proceeded to explore the entire meningeal surface (**Fig.11b,12a**). Notably, independently from the observation time point, $T_{MBP\text{-}GFP}$ cells were scanning their environment not exclusively in an x-y-direction but also along the z-axis (not shown). With disease progression, not only the cellular distribution changed, but also the migratory behavior of encephalitogenic T cells within the meningeal compartment. Firstly, the number of arrested (stationary) cells increased while the number of motile cells decreased simultaneously. Thus, during disease recovery (d8 p.t.), 63% of $T_{MBP\text{-}GFP}$ cells were arrested compared to 12% in the preclinical and 31% in the acute phase (**Fig.12b**). Arrested T cells were defined as cells moving less than one cell diameter from their origin within a 30min recording interval. Secondly, during disease recovery, the velocity of motile cells was significantly higher (12.7µm/min) compared to the preclinical (11.1µm/min) and acute (10.7µm/min) disease phases (**Fig.13a**). Thirdly, correlating with EAE progression, the locomotion of $T_{MBP\text{-}GFP}$ cells within the leptomeninges changed significantly from a non-directed migration during preclinical (0.41) and acute EAE (0.40) towards a (more) directed movement throughout disease recovery (0.56; **Fig.13b**) as evaluated by the meandering index.

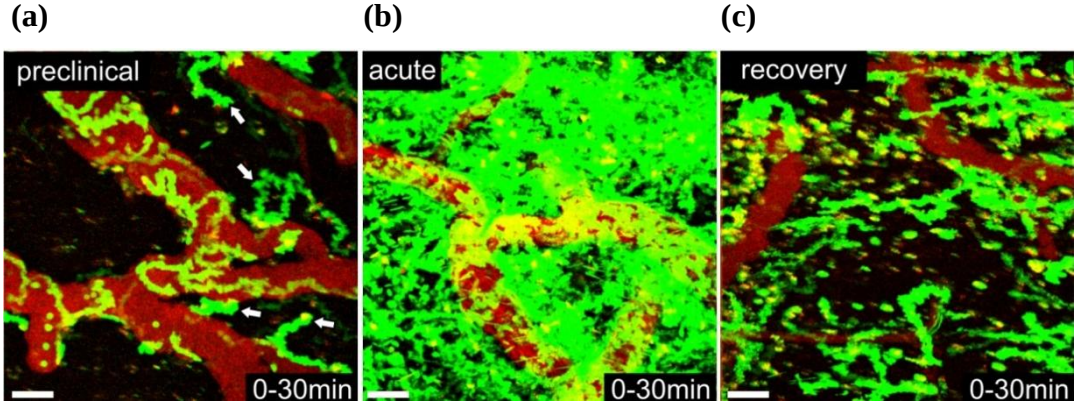

Figure 11 | Migration pattern of extravasated $T_{MBP\text{-}GFP}$ cells during the different phases of EAE. Time projections of $T_{MBP\text{-}GFP}$ cell tracks within the leptomeninges during **(a)** preclinical (3d p.t.), **(b)** acute (5d p.t.) and **(c)** recovery (d8 p.t.) phases of EAE are shown. Trajectories refer to motile $T_{MBP\text{-}GFP}$ cells within a 30min TPLSM recording period. Red: Texas Red®-labeled blood vessels. White arrows: individual extravasated $T_{MBP\text{-}GFP}$ cells. Representative recordings of at least 5 independent experiments per time point are shown.

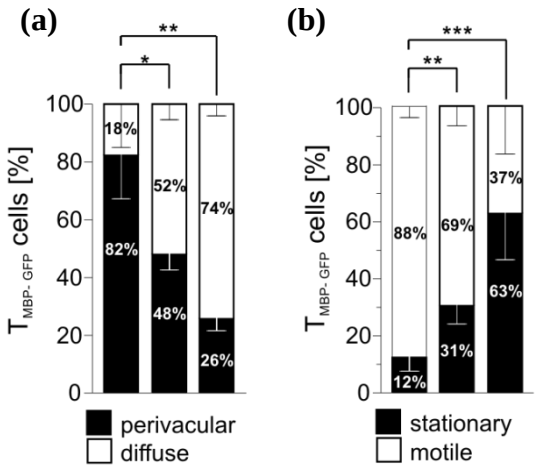

Figure 12 | Migration pattern and motility characteristics of extravasated $T_{MBP\text{-}GFP}$ cells during the different phases of EAE. (a) Percentages of $T_{MBP\text{-}GFP}$ cells found either in close vicinity to leptomeningeal blood vessels (perivascular; distance ≤1 cell diameter from respective vessels) or spread throughout the leptomeningeal surface (diffuse; distance >1 cell diameter from respective vessels) are depicted. Bars represent means and s.d. Data include 3266 extravasated $T_{MBP\text{-}GFP}$ cells within 3 independent experiments. Statistical significance was determined by Kruskal-Wallis ANOVA followed by Dunn's multiple comparison test. **(b)** Fractions of motile versus arrested (stationary) $T_{MBP\text{-}GFP}$ cells are depicted. Means and s.d. are shown. Data include 4380 cells within 5 independent experiments. Statistical significance was evaluated by Kruskal-Wallis ANOVA followed by Dunn's multiple comparison test.

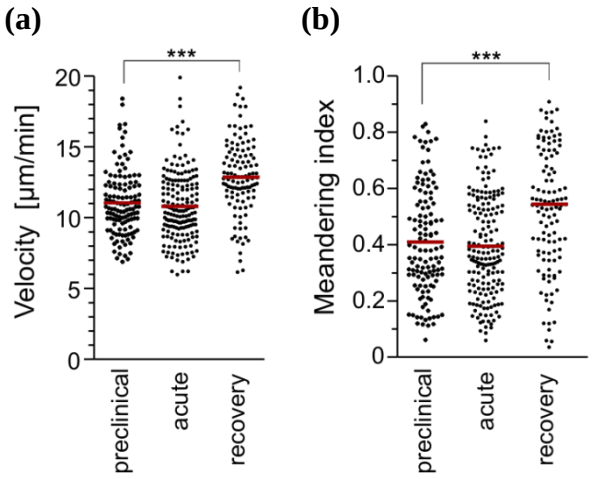

Figure 13 | Motility of extravasated $T_{MBP\text{-}GFP}$ cells within the meningeal environment during the different phases of EAE. Data are based on 30min intravital TPLSM recordings of the spinal cord leptomeninges during EAE. Average velocities **(a)** and meandering indices **(b)** of $T_{MBP–GFP}$ cells during the different phases of EAE are depicted. Red lines: Mean values. Statistical significance was determined by Kruskal-Wallis ANOVA followed by Dunn's multiple comparison test. Data include 434 cells within 5 independent experiments.

3.3. Impact of chemokines on T cell locomotion *in vivo* during EAE

The data demonstrated that T cell infiltration into the CNS and their temporospatial distribution is a highly regulated process. The next step was to identify key molecules that may contribute to this regulation. Transcriptome analysis revealed that chemokine receptors were some of the most regulated factors in *migratory* T cells (see **Fig.4**) (ODOARDI et al., 2012). Chemokines and their respective receptors are commonly known to influence immune cell migration (STEIN & NOMBELA-ARRIETA, 2005). However, their involvement in T cell migration during CNS infiltration is poorly understood.

The aim of the present study was to dissect the *in vivo* contribution of chemokine signaling on T cell migration within intra-and extravascular CNS compartments during the different phases of EAE.

3.3.1. Impact of chemokines on T cell locomotion within the lumen of leptomeningeal blood vessels during the preclinical phase of EAE

Migratory $T_{MBP\text{-}GFP}$ cells isolated from blood and spleen (d3 p.t.) expressed high levels of chemokine receptors including CXCR3, CCR5 as well as CXCR4. In contrast, expression of CCR7 was virtually absent (**Fig.14**). In order to clarify whether this expression pattern has functional consequences on T cell migration, *in vitro* chemotaxis assays on *ex vivo* isolated $T_{MBP\text{-}GFP}$ cells were performed. The data revealed that blood- and spleen-derived $T_{MBP\text{-}GFP}$ cells responded foremost to the inflammatory chemokine CXCL11 whereas CCL5 and the homeostatic chemokines CXCL12 and CCL19 did not induce any chemotactic activity (**Fig.15**).

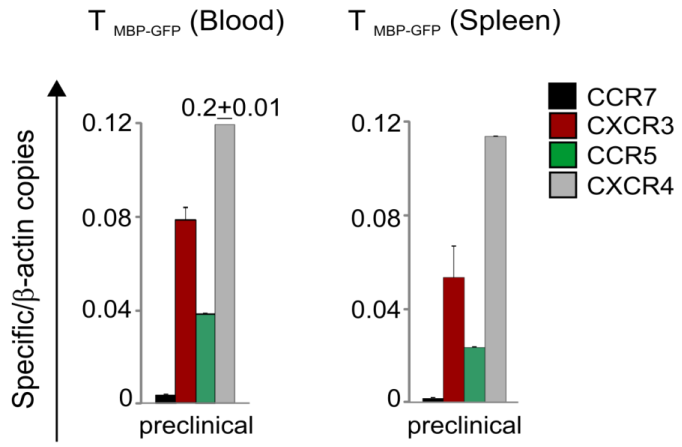

Figure 14 | Chemokine receptor expression pattern in $T_{MBP\text{-}GFP}$ cells during the preclinical phase of EAE. The mRNA expression levels of the indicated chemokine receptors within $T_{MBP\text{-}GFP}$ cells were measured using real-time PCR. Cells were isolated *ex vivo* from blood and spleen during the preclinical phase of EAE (d3 p.t.). Means and s.d. of replicate measurements are shown. Values refer to specific copies in relation to β-actin copies. A representative result of at least 3 independent experiments is shown.

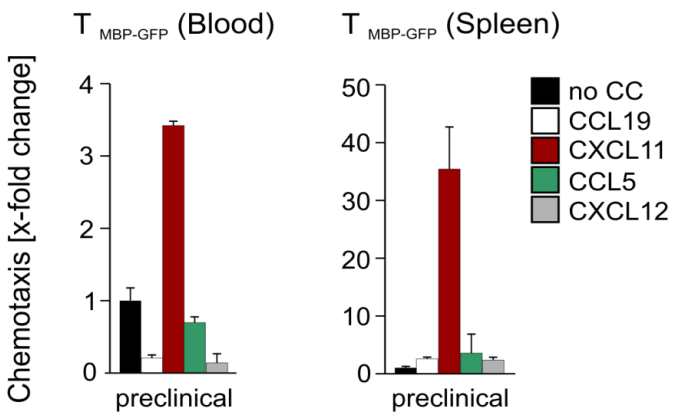

Figure 15 | Migratory $T_{MBP\text{-}GFP}$ cells respond foremost to the inflammatory chemokine CXCL11. Chemotaxis assays for the indicated chemokines were performed on $T_{MBP\text{-}GFP}$ cells isolated from blood and spleen during the preclinical phase of EAE (d3 p.t.). Numbers of $T_{MBP\text{-}GFP}$ cells were quantified via flow cytometry. Bars represent x-fold changes in specific chemotaxis towards the indicated chemokine ligands in relation to the control (w/o chemokine ligands (no CC)). Means and s.d. of a representative result from at least 3 independent experiments are shown.

In order to clarify whether these *in vitro* data were of relevance for T cell migration *in vivo*, pertussis toxin (PTx) (PITTMAN, 1979) was injected intravenously during intravital imaging at day 3 p.t. when most T cells were crawling within the lumen of leptomeningeal blood vessels (see **Fig.6**). This bacterial exotoxin interferes irreversibly with the Gαi-mediated signaling pathway of G protein-coupled receptors, including chemokine receptors (BURNS, 1988).

The effects of PTx on intravascular crawling T cells were clear: after a latent phase of approximately one hour, the number of intraluminal crawling T cells decreased rapidly. Two hours after infusion of PTx more than 80% of the initial crawling cells had disappeared from the intraluminal surface of leptomeningeal blood vessels (**Fig.16a-c**). In contrast, the number of T cells in the extravascular space remained unaltered upon treatment (**Fig.16a**). Notably, global interference with Gαi signaling did not interfere with T cell rolling since the number of rolling cells increased within the vessels after treatment (69% vs. 28%) (**Fig.17**). Together, the findings suggest that the PTx-mediated effects, that had led to reduced numbers of intraluminal crawling cells, were partially due to a disturbed transition step from rolling to crawling (**see 1.1.3, Fig.1**).

However, administration of PTx also seemed to interfere *directly* with intraluminal crawling. Analysis of the locomotion characteristics revealed that $T_{MBP\text{-}GFP}$ cells spent significantly less time on crawling within the vessels after PTx administration compared to the control situation (10.4min vs. 15.2min) (**Fig.18a,b**). This effect was simultaneously accompanied by a higher locomotion speed compared to the control (12.3µm/min vs. 10.4µm/min) (**Fig. 19**).

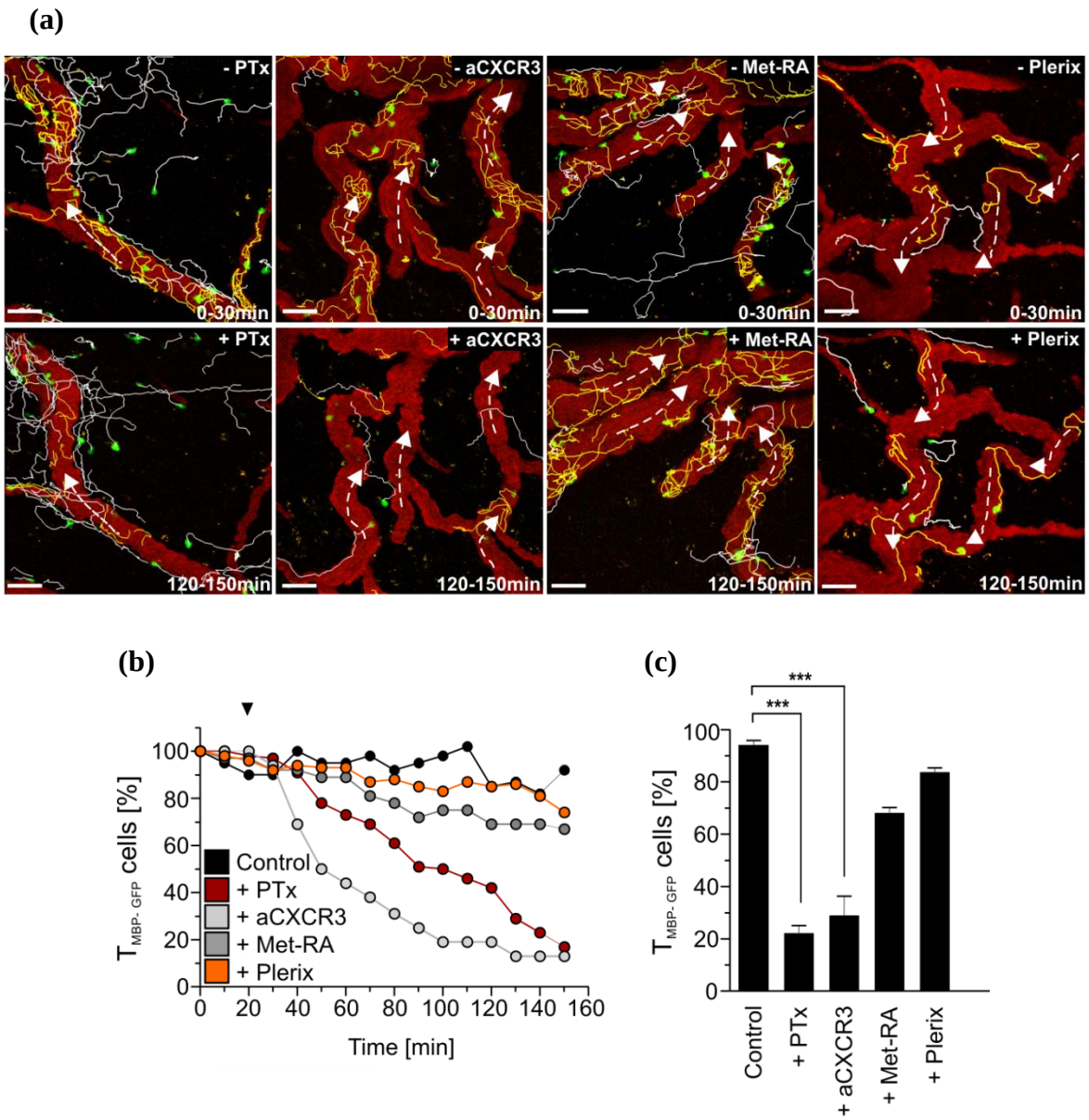

Figure 16 | Interference with chemokine signaling disturbs intraluminal T cell crawling. (a) Intravital TPLSM recordings of leptomeningeal blood vessels during the preclinical phase of EAE (d3 p.t.) are shown. Depicted are intravascular (yellow lines) and extravasated $T_{MBP\text{-}GFP}$ cell trajectories (white lines) before (upper line, 0-30min) and after the indicated treatment (lower line, 120-150min) within a 30min time interval. Green: $T_{MBP\text{-}GFP}$ cells. Red: Vessel lumen. White arrows: Direction of the blood flow. Scale bars: 50µm. Representative recordings of at least 3 independent experiments per treatment are depicted. **(b)** Graph represents relative changes in intravascular crawling $T_{MBP\text{-}GFP}$ cell numbers within an observation period of 150min. Black arrowhead: Time point of i.v. administration of PBS (Control), PTx (+ PTx), anti-CXCR3mAb (+ aCXCR3), Met-RANTES (+ Met-RA) and Plerixafor (+ Plerix). Representative data of at least 3 independent experiments per treatment are shown. **(c)** Percentages of intraluminal crawling $T_{MBP\text{-}GFP}$ cells 2h after treatment are depicted. Values for each treatment were determined in relation to the respective starting condition (time point 0). Bars represent means and s.d. of at least 3 independent experiments per treatment. Statistical significance was evaluated by Kruskal-Wallis ANOVA followed by Dunn's multiple comparison test.

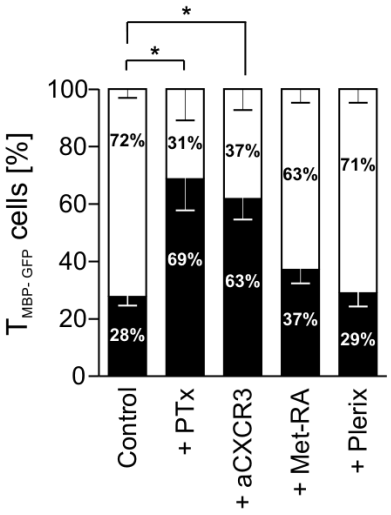

Figure 17 | Interference with chemokine signaling does not inhibit T cell rolling. Analyses are based on 30min intravital TPLSM recordings of leptomeningeal blood vessels during the preclinical phase of EAE (d3 p.t.). Percentages of rolling (black) vs. crawling $T_{MBP-GFP}$ cells (white) before (Control) or after i.v. treatment (as indicated) are depicted. Means and s.d. are shown. Data refer to at least 5 independent experiments per treatment, including 331 rolling and 608 crawling $T_{MBP-GFP}$ cells. Statistical significance was evaluated by Kruskal-Wallis ANOVA followed by Dunn's multiple comparison test.

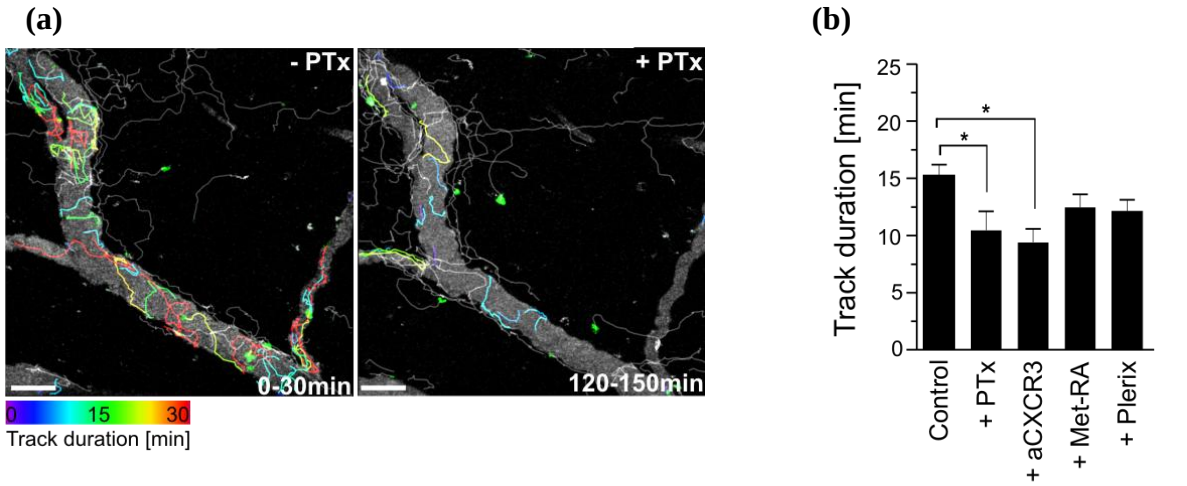

Figure 18 | Chemokine signaling is essential for the duration of T cell crawling *in vivo*. (a) Intravital TPLSM recordings of spinal cord leptomeningeal blood vessels during the preclinical phase of EAE (d3 p.t.) are depicted. Trajectories (multi-colored lines) represent individual intravascular crawling $T_{MBP-GFP}$ cells within a 30min recording interval before (left) or 2h after i.v. PTx-infusion (right). Grey: Vessel lumen (false color). Color scale (bottom line) refers to intraluminal crawling duration (interval 0 to 30min). Scale bars: 50µm. Representative images of at least 3 independent experiments are shown. **(b)** Bars represent average track durations of crawling $T_{MBP-GFP}$ cells before (Control) or 2h after i.v. treatment as indicated. Analysis is based on 30min intravital TPLSM recordings as described. Means and s.d. are depicted. Data refer to at least 5 independent experiments including 267 $T_{MBP-GFP}$ cells. Statistical significance was evaluated by Kruskal-Wallis ANOVA followed by Dunn's multiple comparison test.

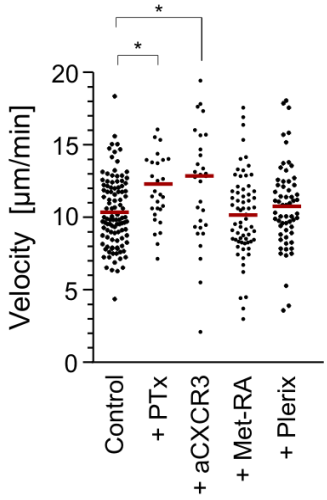

Figure 19 | Interference with chemokine signaling influences the crawling velocity. Data are based on 30min intravital TPLSM recordings performed within leptomeningeal blood vessels of the spinal cord during the preclinical phase of EAE (3d p.t.). Average velocities of intravascular crawling $T_{MBP-GFP}$ cells before (Control) or 2h after i.v. treatment are depicted. Red lines: Mean values. Data refer to at least 5 independent experiments including 267 intravascular $T_{MBP-GFP}$ cells. Statistical significance was evaluated by Kruskal-Wallis ANOVA followed by Dunn's multiple comparison test.

In order to clarify whether the effects of PTx were mainly due to interference with Gαi signaling in *T cells*, spleen-derived migratory $T_{MBP\text{-}GFP}$ cells were treated *in vitro* with PTx prior to injection into healthy recipient animals. The results were clear: unlike their Olig.-B-treated counterparts (control), PTx pre-treated T cells were incapable of crawling along the intraluminal vessel surface. Instead, they mainly rolled along the vascular walls **(Fig.20a-c)**.

As mentioned above, encephalitogenic effector T cells crawl predominantly against the direction of the blood stream (upstream). Surprisingly, intravenous administration of PTx led to a re-orientation of intraluminal crawling, i.e. 2h after treatment, $T_{MBP\text{-}GFP}$ cells were crawling mainly in the direction of the blood flow (downstream) (**Fig.21**).

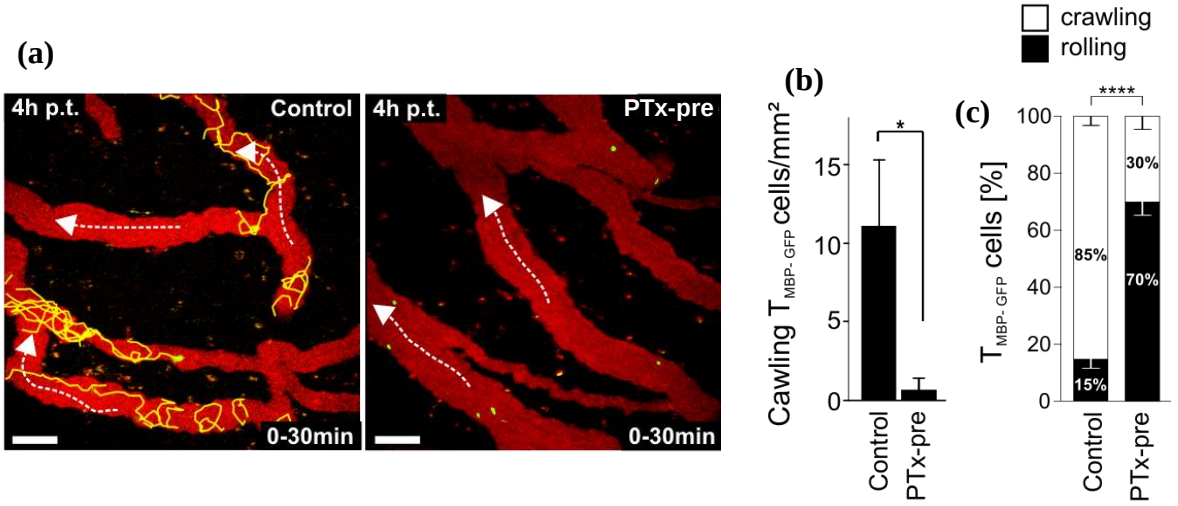

Figure 20 | PTx pre-treated migratory T cells are incapable of intravascular crawling. (a) Intravital TPLSM recordings of spinal cord leptomeninges 4h post transfer of spleen-derived migratory $T_{MBP\text{-}GFP}$ cells are shown. Trajectories (yellow) represent intraluminal tracks of individual $T_{MBP\text{-}GFP}$ cells within a 30min time interval. *Ex vivo* isolated $T_{MBP\text{-}GFP}$ cells were treated with Olig.-B (Control, left) or PTx (PTx-pre, right) prior to transfer. Red: Vessel lumen. White arrows: Direction of the blood flow. Scale bars: 50µm. Representative recordings of at least 3 independent experiments are depicted. **(b)** Correspondent quantifications of intraluminal crawling $T_{MBP\text{-}GFP}$ cells are depicted. Means and s.d. are shown. Representative data from at least 4 independent experiments are shown. **(c)** Percentages of rolling (black) vs. crawling $T_{MBP\text{-}GFP}$ cells (white) of Olig.-B (Control) or PTx pre-treated $T_{MBP\text{-}GFP}$ cells are depicted. Means and s.d. are shown. Data refer to at least 5 independent experiments per treatment, including 88 rolling and 227 crawling $T_{MBP\text{-}GFP}$ cells. Statistical significance was evaluated by Kruskal-Wallis ANOVA followed by Dunn's multiple comparison test.

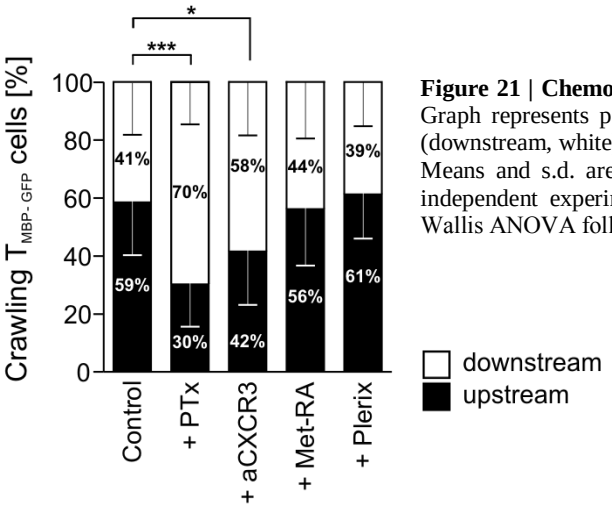

Figure 21 | Chemokines influence the orientation of intravascular crawling. Graph represents percentage of intravascular $T_{MBP\text{-}GFP}$ cells crawling either in (downstream, white) or against (upstream, black) the direction of the blood flow. Means and s.d. are shown. Data include 610 $T_{MBP\text{-}GFP}$ cells within at least 3 independent experiments. Statistical significance was determined by Kruskal-Wallis ANOVA followed by Dunn's multiple comparison test.

In general, chemokines are known to strengthen the adherence of leukocytes (under flow) onto the vessel endothelium indirectly, by triggering a high-affinity state of integrins (CONSTANTIN et al., 2000). Accordingly, blockage of VLA-4 function (but not of LFA-1; BARTHOLOMÄUS et al., 2009) via the administration of neutralizing monoclonal antibodies interfered significantly with intraluminal crawling of T cells, similar to the findings achieved with PTx. Thus, the total number of intraluminal crawling $T_{MBP\text{-}GFP}$ cells decreased after treatment (**Fig.22a**), while the remaining cells changed their intraluminal motility characteristics. The latter was demonstrated by a significant increase in the T cells' crawling speed (13.1µm/min vs. 10.3µm/min) (**Fig.22b**) and simultaneously by a reduction in the time T cells spent for crawling (11.9min vs. 15.5min) (**Fig.22c**) compared to the control situation. However, dissimilar to the findings achieved with PTx, anti-VLA-4mAb treatment did not change the T cells' preferred crawling direction against the blood stream (58% vs. 59%) (**Fig.22d**), suggesting that the orientation of intraluminal crawling is not influenced via an integrin-mediated effect.

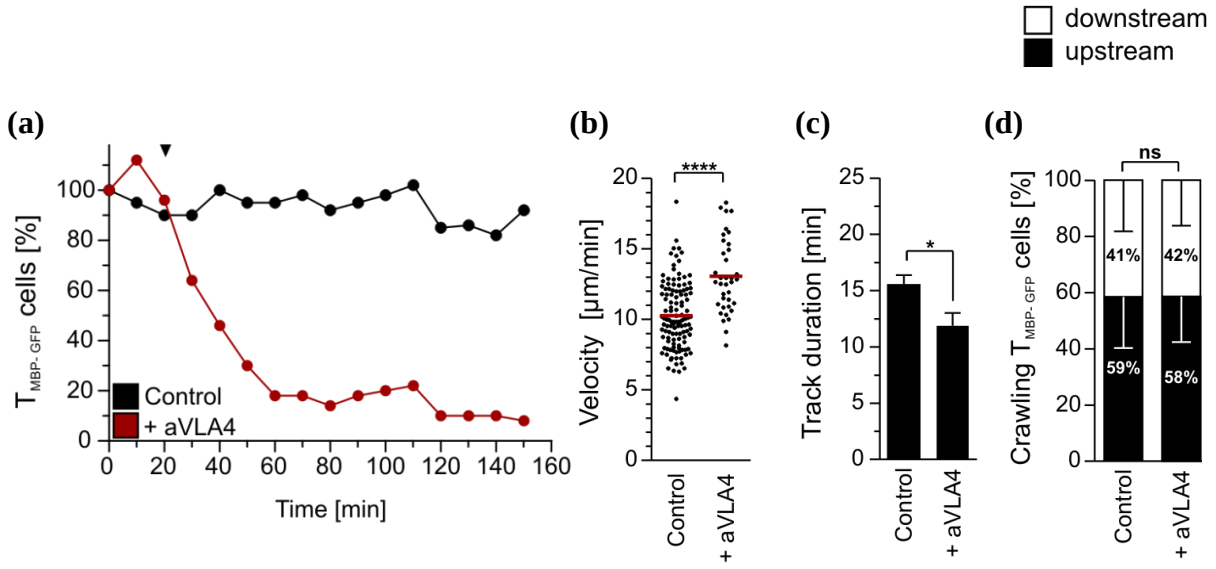

Figure 22 | α4 integrins contribute to intravascular T cell locomotion but do not influence the orientation of crawling. Data are based on 30min intravital TPLSM recordings performed within leptomeningeal blood vessels during the preclinical phase of EAE (d3 p.t.). **(a)** Graph represents relative changes in intraluminal crawling $T_{MBP\text{-}GFP}$ cell numbers within an observation period of 150min. Arrowhead: Time point of intravenous infusion of PBS (Control) or anti-VLA4mAb (+ aVLA4). Representative data from at least 3 independent experiments are shown. **(b)** Average velocities of intraluminal crawling $T_{MBP\text{-}GFP}$ cells before (Control) and after anti-VLA4mAb treatment (+ aVLA4) are depicted. Red lines: Mean values. Results include 157 $T_{MBP\text{-}GFP}$ cells within at least 3 independent experiments. **(c)** Bars represent average track durations of $T_{MBP\text{-}GFP}$ cells before and after treatment. Means and s.d. are depicted. Data refer to 157 $T_{MBP\text{-}GFP}$ cells within at least 3 independent experiments. **(d)** Mean percentages and s.d. of intraluminal T cells crawling either in (downstream) or against (upstream) the direction of the blood flow before and after treatment are shown. Data refer to 222 $T_{MBP\text{-}GFP}$ cells (3776 displacements) from at least 4 independent experiments. Statistical significance was determined by two-tailed Mann-Whitney test.

The results achieved with PTX suggested a role for chemokine receptors/chemokines on intravascular T cell locomotion. The expression data (**Fig.14**) and functional analysis (**Fig.15**) of *ex vivo* isolated T cells pointed to CXCR3 (CXCL9-11), CCR5 (CCL5) and CXCR4 (CXCL12) as potential candidates. Accordingly, specific blocking agents were administered intravenously during intravital imaging as described for PTx, i.e. a monoclonal blocking antibody against CXCR3 (MOHAN et al., 2005), Met-RANTES, an antagonist of CCR1, 2, 5 (PROUDFOOT et al., 1996) and Plerixafor (AMD3100) (HATSE et al., 2002), an antagonist of CXCR4. Intriguingly, interference with CXCR3 function almost completely reproduced the results achieved with PTx: with a delay of approximately 30min, T cells disappeared from the blood vessel (~80% after 2h) (**Fig.16**) while simultaneously the number of rolling cells increased (63% vs. 28%) **(Fig.17**). Moreover, CXCR3 was *directly* involved in mediating T cell crawling: administration of the neutralizing mAb increased the speed (12.7µm/min vs. 10.4µm/min) (**Fig.19**) and reduced drastically the duration of intraluminal crawling (9.4min vs. 15.2min) (**Fig.18b)**. Furthermore, interference with CXCR3 signaling changed the intravascular crawling orientation towards a prevalent downstream direction **(Fig.21)**. Interestingly, neither Met-RANTES nor Plerixafor had a significant impact on intravascular T cell migration **(Fig.16, 17, 19, 18b, 21)**.

3.3.2. Chemokines influence intraluminal T cell migration under inflammatory and non-inflammatory conditions

As demonstrated, chemokine signaling plays an essential role in mediating T cell migration within leptomeningeal blood vessels during the preclinical phase of EAE (d3 p.t.). Notably, although the majority of $T_{MBP\text{-}GFP}$ cells were crawling within the vessel lumen, a considerable number of cells had already transgressed the vascular walls at this early phase (not shown). These extravasated T lymphocytes contact resident antigen-presenting cells leading to a re-activation of lymphocytes and subsequently, to a release of pro-inflammatory cytokines (BARTHOLOMÄUS et al., 2009; LODYGIN et al., in press). Consequently, this series of events might lead to an early activation of the leptomeningeal vessel endothelium.

Indeed, PECAM-1 positive endothelial cells, isolated at day 3 post T cell transfer, displayed a clear up-regulation of inflammatory chemokines including ligands for CXCR3 (CXCL9-11) as well as for CCR5 (CCL5). Interestingly, this ligand up-regulation in the preclinical phase of EAE was similar to that found during acute EAE (**Fig.23**). In contrast, CXCL12 was highly expressed under non-inflammatory conditions (naïve) and during disease recovery.

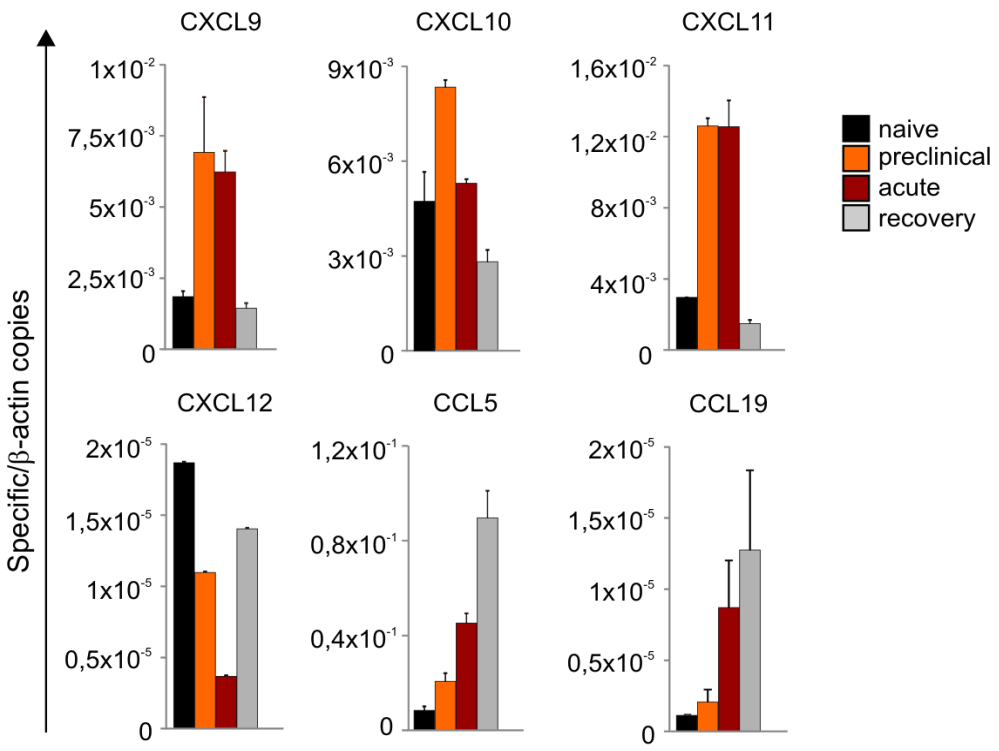

Figure 23 | Expression pattern of chemokine ligands in endothelial cells during the different phases of EAE. PECAM-1 positive endothelial cells were isolated at the indicated time points from spinal cord meninges and parenchyma. Quantitative real-time PCR was performed afterwards. Naïve= d0 p.t., preclinical= d3 p.t., acute= d5 p.t. and recovery= d8 p.t. Means and s.d. of replicate measurements are shown. Values refer to specific copies in relation to β-actin copies. Representative results of at least 3 independent experiments per time point are shown.

The expression of inflammatory chemokines within endothelial cells during preclinical EAE was accompanied by an increased permeability of the meningeal vessels at this stage. Accordingly, when small molecular weight Texas Red® dextran (3kDa) was injected during intravital imaging at d3 p.t. it came to a massive efflux of dye into the subarachnoideal space, where it was taken up by resident phagocytic cells. As a consequence, these cells appeared red after several minutes (**Fig.24a-d**). Expectedly, the disruption of the endothelial integrity was even more pronounced during the acute phase of EAE (d5 p.t. not shown). However, both leakage and phagocytic uptake of dye were absent when Texas Red® dextran was injected in naïve animals (not shown).

These changes of the endothelial status were dependent on the T cells' antigen specificity. Single transfer of brain antigen-ignorant ovalbumin-reactive T cells ($T_{OVA\text{-}GFP}$ cells) did not result in a disruption of the endothelial integrity, as demonstrated by an unaltered permeability of the vessels (**Fig.24e-h**) and did not lead to a measurable up-regulation of inflammatory chemokines compared to the naïve situation (not shown).

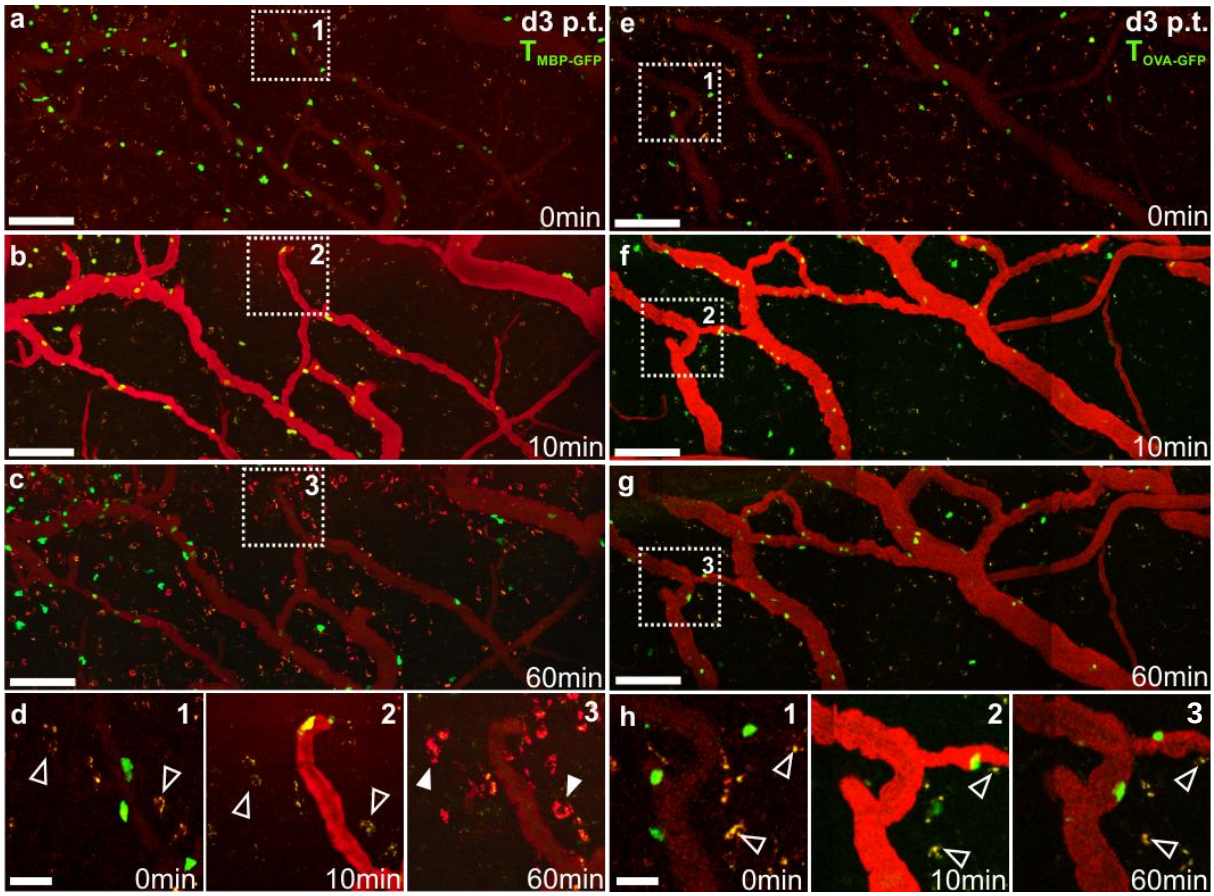

Figure 24 | Integrity of meningeal blood vessels is disrupted in the preclinical phase of EAE. Permeability of leptomeningeal blood vessels 3 days after transfer of $T_{MBP\text{-}GFP}$ cells (left) or $T_{OVA\text{-}GFP}$ cells (right) was evaluated by i.v. injection of 3kDa Texas Red®-labeled dextran. Intravital TPLSM overviews of extended imaging areas comprised of up to 3 adjacent spots were acquired before (**a,e**), at 10 (**b,f**) and 60min (**c,g**) post i.v. injection of dye. Scale bars: 120µm. Red: Leptomeningeal blood vessels. Green: GFP^+ T cells. (**d,h**) Magnification of individual regions (1-3, white dotted rectangles) originated from the overviews. Scale bars: 25µm. White arrowheads: Individual phagocytic cells before (open arrowheads) and after dextran-uptake (closed arrowheads). Representative images of at least 3 independent experiments are depicted.

Apparently, crawling (and even extravasation) of $T_{OVA\text{-}GFP}$ cells does not induce an inflammatory response. Therefore, an examination of the intraluminal migration behavior of these cells may provide insight into lymphocyte interactions with an intact meningeal vessel endothelium under non-inflammatory conditions. Notably, *migratory* $T_{OVA\text{-}GFP}$ cells follow similar migration-kinetics and undergo the same fundamental changes in their expression profile licensing them to gain access to the CNS. They up-regulate (compared to $T_{OVA\text{-}GFP}$ blasts) adhesion molecules and chemokine receptors whereas they down-regulate proliferation and activation markers (not shown).

Consequently, $T_{OVA\text{-}GFP}$ cells isolated from blood 3 days post transfer shared a similar chemokine receptor expression pattern with their myelin-reactive counterparts (**Fig.25a** vs. **Fig.14**) and responded equally to respective chemokines (**Fig.25b** vs. **Fig.15**).

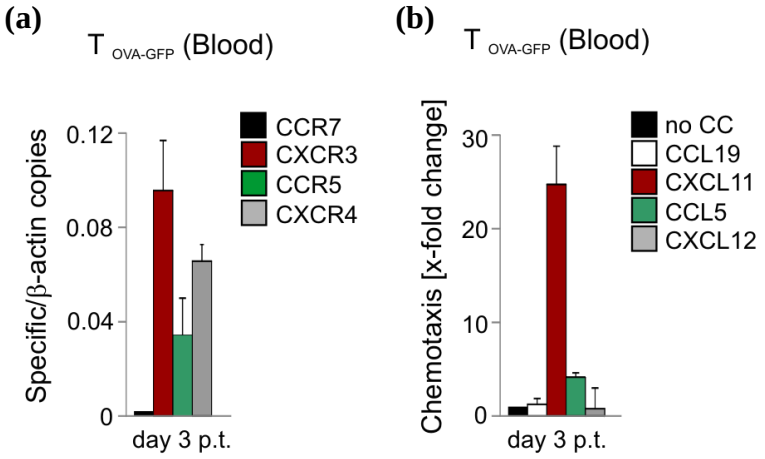

Figure 25 | Chemokine receptor expression pattern and chemotaxis of *ex vivo* isolated migratory $T_{OVA\text{-}GFP}$ cells. **(a)** The mRNA expression levels of indicated chemokine receptors within $T_{OVA\text{-}GFP}$ cells were measured using real-time PCR. Cells were isolated from blood 3 days p.t. Means and s.d. of replicate measurements are shown. Values refer to specific copies in relation to β-actin copies. A representative result of at least 3 independent experiments is shown. **(b)** Chemotaxis assays for the indicated chemokines were performed on $T_{OVA\text{-}GFP}$ cells isolated from blood 3 days p.t. Numbers of $T_{OVA\text{-}GFP}$ cells were evaluated via flow cytometry. Bars represent x-fold changes in specific migration towards the indicated chemokine ligands in relation to the control (w/o chemokine ligands (no CC)). Means and s.d. of representative results from at least 3 independent experiments are indicated.

Hence, in a next step, the role of chemokines on intraluminal T cell crawling was analyzed under non-inflammatory conditions. Intravenous administration of PTx or anti-CXCR3mAb led to a clear reduction in the number of intraluminal crawling T cells (**Fig.26**). Simultaneously, the numbers of rolling cells were elevated under both treatments (**Fig.27a**). These findings were similar to those achieved with myelin-reactive T cells (see **Fig.16,17**). Under non-inflammatory conditions, interference with chemokine signaling also *directly* affected T cell crawling. Thus, under treatment, the speed of intravascular locomotion was moderately increased, whereas the crawling duration was slightly reduced (**Fig.27b,c**). Surprisingly, administration of PTx or anti-CXCR3mAb led to a re-orientation of intraluminal crawling. Consequently, 2h after treatment, $T_{OVA\text{-}GFP}$ cells were crawling mainly in the direction of the blood flow (downstream) (**Fig.27d**).

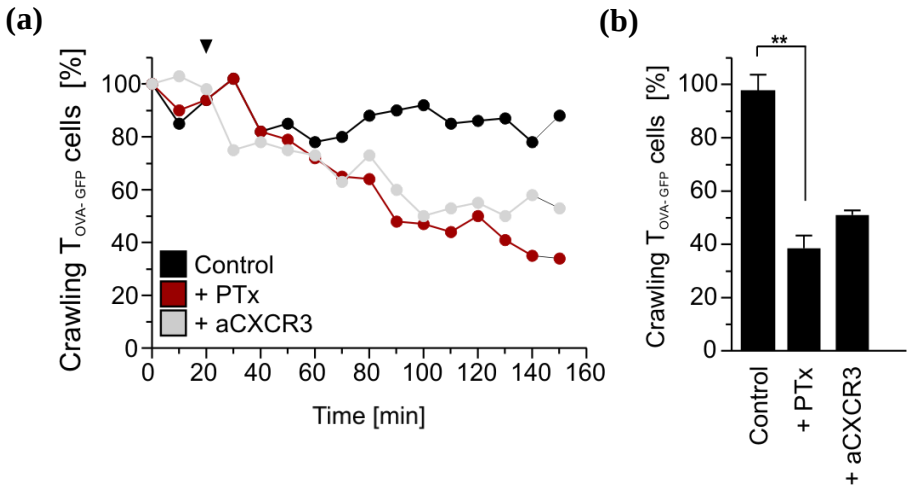

Figure 26 | Chemokine signaling contributes to crawling of T lymphocytes under non-inflammatory conditions. Data are evaluated from 30min intravital TPLSM recordings of leptomeningeal blood vessels performed 3d p.t. of $T_{OVA\text{-}GFP}$ cells. **(a)** Graph represents relative changes in intraluminal crawling $T_{OVA\text{-}GFP}$ cell numbers within an observation period of 150min. Black arrow: Time point of i.v. administration of PBS (Control), PTx (+ PTx) or anti-CXCR3mAb (+ aCXCR3). Representative experiments of at least 3 independent approaches per treatment are shown. **(b)** Quantification of intraluminal crawling $T_{OVA\text{-}GFP}$ cells 2h after treatment is shown. Values for each treatment were determined in relation to the respective starting condition (time point 0). Bars represent means and s.d. of at least 2 independent experiments per treatment. Statistical significance was evaluated by Kruskal-Wallis ANOVA followed by Dunn's multiple comparison test.

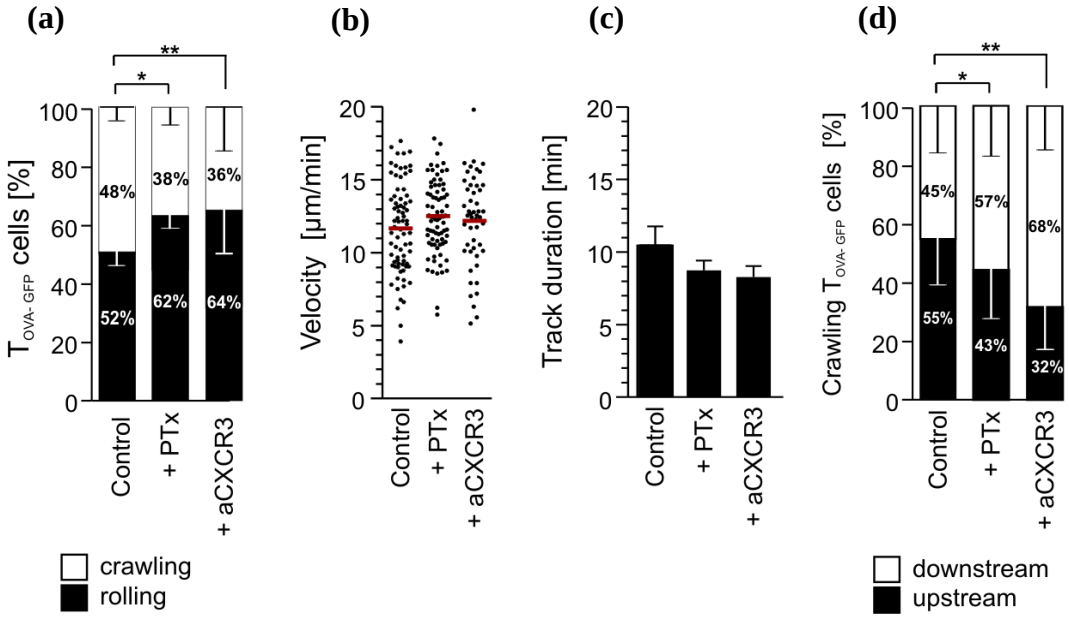

Figure 27 | Chemokines influence intravascular locomotion pattern of T cells under non-inflammatory conditions. Analyses are based on 30min intravital TPLSM recordings of leptomeningeal blood vessels 3d p.t. of $T_{OVA\text{-}GFP}$ cells. **(a)** Graph illustrates a comparison between intraluminal rolling and crawling $T_{OVA\text{-}GFP}$ cells before (Control) or after treatment with PTx (+ PTx) or anti-CXCR3mAb (+ aCXR3). Bars represent means and s.d. of 421 rolling and 306 crawling $T_{OVA\text{-}GFP}$ cells within at least 5 independent experiments. **(b)** Dot plot shows average velocities of individual intraluminal crawling $T_{OVA\text{-}GFP}$ cells before or after treatment. Red lines: Mean values. Data include 206 $T_{OVA\text{-}GFP}$ cells of at least 3 independent experiments per treatment. **(c)** Graph refers to average track durations of intravascular crawling $T_{OVA\text{-}GFP}$ cells before or after treatment. Bars represent means and s.d. of 223 crawling $T_{OVA\text{-}GFP}$ cells within at least 3 independent experiments per treatment. **(d)** Graph represents percentage of intravascular $T_{OVA\text{-}GFP}$ cells crawling either in (downstream) or against (upstream) the direction of the blood flow. Means and s.d. are shown. Data include 171 $T_{OVA\text{-}GFP}$ cells within at least 3 independent experiments. Statistical significance was determined by Kruskal-Wallis ANOVA followed by Dunn's multiple comparison test.

Although $T_{OVA\text{-}GFP}$ cells were capable of crawling within leptomeningeal blood vessels they displayed pivotal discrepancies in their intravascular locomotion behavior compared to myelin-reactive T cells. Firstly, they crawled with a higher velocity compared to $T_{MBP\text{-}GFP}$ cells (11.7µm/min vs. 10.4µm/min). Secondly, the average crawling duration was significantly shorter than those of their myelin-reactive counterparts (10.9min vs. 15.2min). Thirdly, the number of rolling $T_{OVA\text{-}GFP}$ cells was significantly elevated in comparison to $T_{MBP\text{-}GFP}$ cells (52% vs. 28%). Reasons for these differences might have been either T cell-intrinsic or due to the activation status of the vessel endothelium. In order to test whether the activation status of the endothelium has a potential impact on T cell crawling properties, $T_{OVA\text{-}GFP}$ cells were co- transferred together with myelin-reactive T cells. Intravital analyses were performed 3 days post transfer.

Now, under inflammatory conditions, $T_{OVA\text{-}GFP}$ cells changed their intraluminal locomotive behavior towards that of their myelin-reactive counterparts. Thus, more cells were crawling within the vessels compared to the single transfer situation (57% vs. 48%) (**Fig.28a** vs. **Fig.27a**). Furthermore, motility parameters were also assimilated to that of myelin-reactive cells: co-transferred $T_{OVA\text{-}GFP}$ cells crawled with lower velocity on the endothelium (10.5µm/min vs. 11.7µm/min) (**Fig.28b** vs. **Fig.27b**) and the crawling duration was significantly elevated compared to that of non-inflammatory conditions (14.8min vs. 10.9min) (**Fig.28c** vs. **Fig.27c**).

The effects of PTx on $T_{OVA\text{-}GFP}$ cells were more pronounced under these inflammatory conditions. Thus, in contrast to the single transfer, co-transferred $T_{OVA\text{-}GFP}$ cells migrated significantly faster (12.6µm/min vs. 10.5µm/min) (**Fig.28b**) and spent simultaneously less time on crawling under treatment (9.1min vs. 14.8min) (**Fig.28c**). Furthermore, the increase in the number of rolling cells was more pronounced when T_{OVA} cells were co-transferred with T_{MBP} cells. (**Fig.28a**). However, interference with Gαi signaling changed the intraluminal crawling orientation of co-transferred $T_{OVA\text{-}GFP}$ cells in a similar way compared to the single transfer (**Fig.28d**).

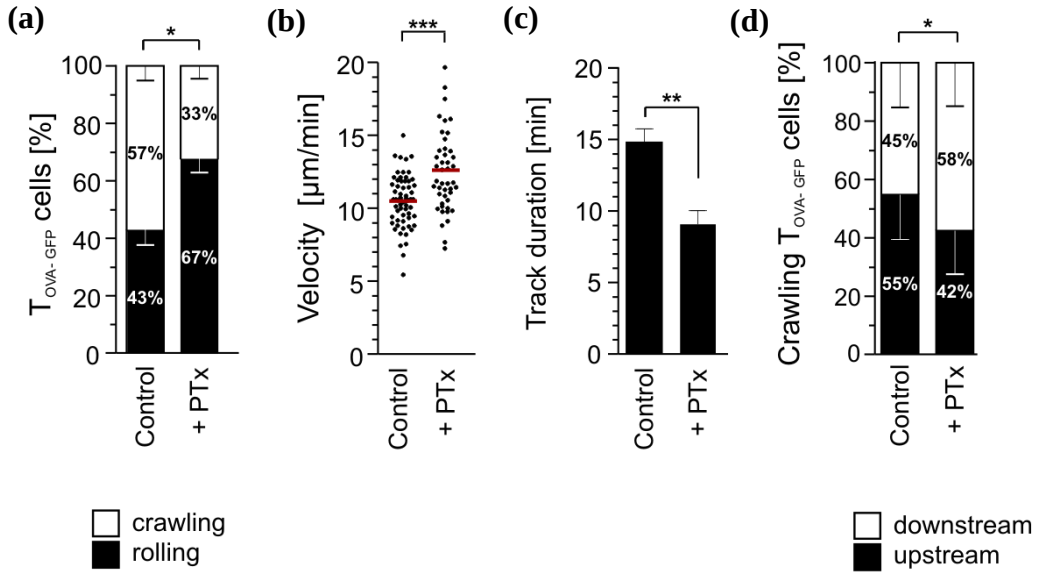

Figure 28 | Influence of chemokines on intravascular crawling is more pronounced under inflammatory conditions. Analyses are based on 30min intravital TPLSM recordings of leptomeningeal vessels 3d p.t. $T_{OVA-GFP}$ cells were transferred together with unlabeled T_{MBP} cells. **(a)** Graph illustrates comparison between intraluminal rolling and crawling $T_{OVA-GFP}$ cells before (Control) or under treatment with PTx (+ PTx). Bars represent means and s.d. of 177 rolling and 150 crawling $T_{OVA-GFP}$ cells within at least 5 independent experiments. (**b)** Dot plot shows average velocities of individual intraluminal crawling $T_{OVA-GFP}$ cells before or after treatment. Red lines: Mean values. Data include 109 $T_{OVA-GFP}$ cells of at least 3 independent experiments per treatment. **(c)** Graph refers to average track durations of intravascular crawling $T_{OVA-GFP}$ cells before or after treatment. Bars represent means and s.d. of 142 crawling $T_{OVA-GFP}$ cells within at least 3 independent experiments per treatment. **(d)** Graph represents fractions of intravascular $T_{OVA-GFP}$ cells crawling either in (downstream) or against (upstream) the direction of the blood flow. Means and s.d. are shown. Data include 134 $T_{OVA-GFP}$ cells within at least 5 independent experiments. **(a-d)** Statistical significance was determined by Kruskal-Wallis ANOVA followed by Dunn's multiple comparison test.

3.4. Impact of chemokines on T cell migration within the extravascular space during the different phases of EAE

3.4.1. Role of chemokines on the motility of extravasated T cells

Once T cells have transgressed the vascular walls, they migrate in the vicinity of leptomeningeal vessels that are embedded in a dense network of extracellular matrix (ECM) fibers (**Fig.37**). Anatomically, the leptomeninges form a boundary between the CNS parenchyma and the subarachnoideal space that contains the cerebrospinal fluid. Little is known about the migratory cues that guide encephalitogenic T cells through this environment or how they influence the migration pattern of these cells during CNS inflammation.

Quantitative PCR analysis of meningeal tissue from spinal cord suggested a putative role for chemokines in this respect. Correlating with a high expression of pro-inflammatory cytokines, namely IL-17 and IFN-γ during the preclinical (d3 p.t.) and acute (d5 p.t.) phases of EAE,

inflammatory chemokines, namely CXCL9-11 and CCL5 were strongly expressed in the meninges and up-regulated compared to the naïve situation (**Fig.29**). Notably, their expression levels remained high throughout disease recovery (d8 p.t.). In contrast, signals for CCL19 were on the border of detection at each of the examined time points. Interestingly, CXCL12 was differentially regulated since elevated levels were rather found under non-inflammatory conditions (naïve) and during disease recovery compared to the preclinical and acute phases of EAE.

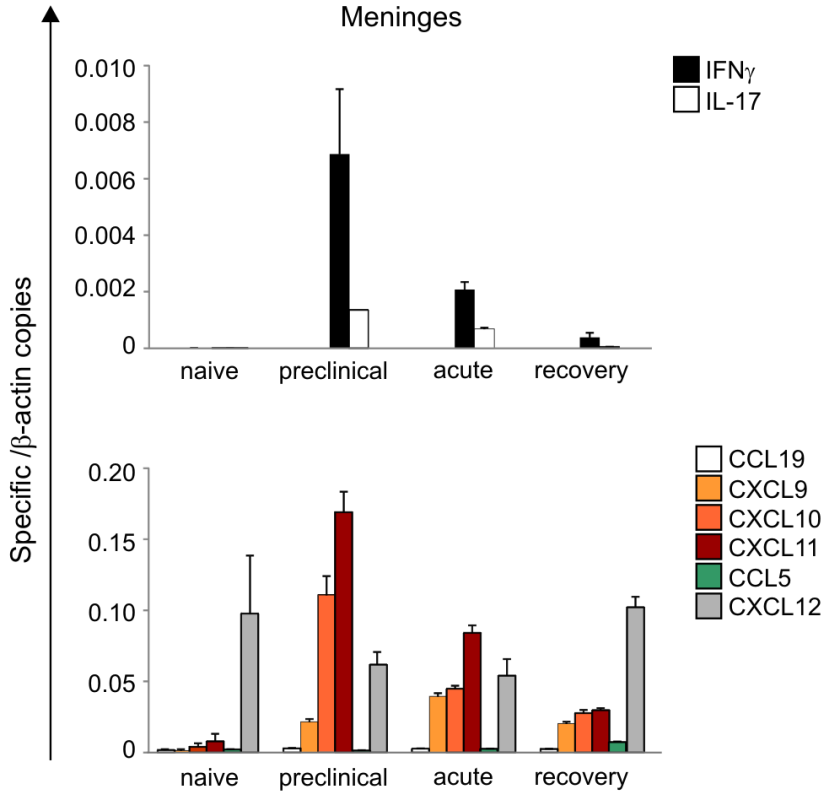

Figure 29 | Inflammatory cytokines and chemokines are up-regulated during the preclinical and acute phases of EAE. The mRNA expression pattern of pro-inflammatory cytokines (upper row) and chemokines (lower row) within spinal cord meninges was measured by real-time PCR at the indicated time points. Naïve= d0 p.t., preclinical= d3 p.t., acute= d5 p.t. and recovery= d8 p.t. Means and s.d. of replicate measurements are shown. Values refer to specific copies in relation to β-actin copies. A representative result of at least 3 independent experiments is shown.

$T_{MBP\text{-}GFP}$ cells isolated *ex vivo* from spinal cord meninges displayed high expression levels of CXCR4, CCR5 and CXCR3 during preclinical and acute EAE (**Fig.30**). During disease recovery, CXCR3 and CXCR4 expression levels remained high whereas the one of CCR5 decreased. CCR7 expression was nearly not detectable throughout all the examined time points. *In vitro* chemotaxis assays on *ex vivo* $T_{MBP\text{-}GFP}$ cells isolated from meningeal tissue revealed that myelin-reactive T cells responded foremost to CCL5 and CXCL11, whereas CCL19 and CXCL12 induced almost no chemotaxis within these cells (**Fig.31**).

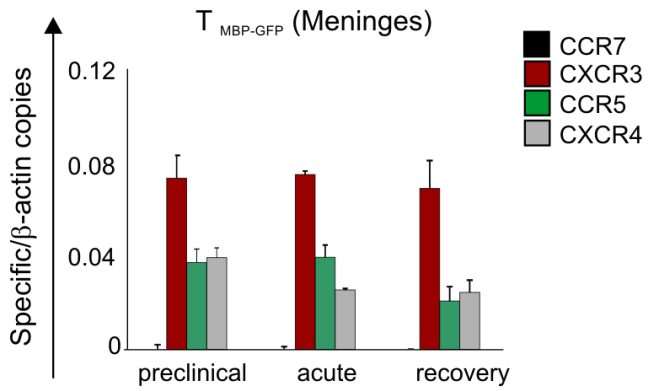

Figure 30 | Chemokine receptor expression pattern within $T_{MBP\text{-}GFP}$ cells during the course of EAE. Graphs represent mRNA expression levels of the indicated chemokine receptors within $T_{MBP\text{-}GFP}$ cells isolated from spinal cord meninges at the indicated time points. Data were evaluated by real-time PCR. Preclinical= d3 p.t., acute= d5 p.t. and recovery= d8 p.t. Means and s.d. of replicate measurements are shown. Values refer to specific copies in relation to β-actin copies. A representative result of at least 3 independent experiments is shown.

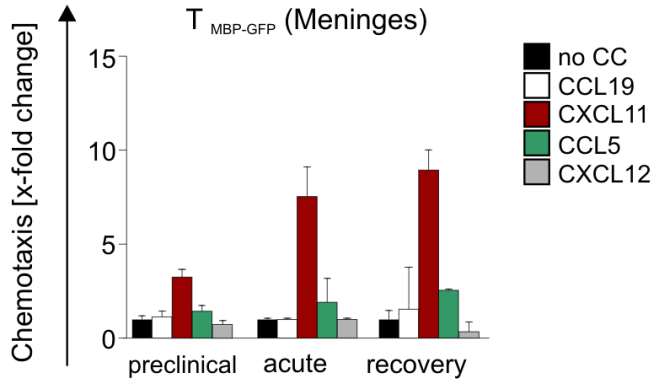

Figure 31 | Encephalitogenic effector T cells respond mainly to inflammatory chemokines. $T_{MBP\text{-}GFP}$ cells were isolated from spinal cord meninges at different time points during EAE. Chemotaxis assays for indicated chemokine ligands were performed afterwards and the numbers of $T_{MBP\text{-}GFP}$ cells were quantified via flow cytometry. Time points: Preclinical= d3 p.t., acute= d5 p.t. and recovery= d8 p.t. Bars represent x-fold changes in specific migration towards the indicated chemokine ligands in relation to the control (w/o chemokine ligands (no CC)). Means and s.d. of representative results of at least 3 independent experiments per time point are indicated.

In the next step the relevance for chemokine signaling on T cell motility in *vivo* was tested. Consequently, PTx, anti-CXCR3mAb, Met-RANTES and Plerixafor were administered during or shortly before intravital imaging. The results were unexpected: None of the blocking agents had a measurable influence on the basal velocity of $T_{MBP\text{-}GFP}$ cells within the meninges during any of the EAE phases (**Fig.32a**).

Next, the impact of chemokines on the motility pattern of extravasated encephalitogenic T cells was analyzed. As described, myelin-reactive T cells tend to be more directed in their movement during disease recovery (~0.6) compared to the preclinical (~0.4) and acute (~0.4) phases of EAE as evaluated by the meandering index. Interfering with Gαi/chemokine signaling had no measurable effect on the migration pattern of $T_{MBP\text{-}GFP}$ cells during the preclinical and acute phases of EAE (**Fig.32b**). However, administration of PTx influenced the directionality of T cell migration during disease recovery. Accordingly, myelin reactive T cells were less linear in their movement under PTx-treatment compared to the control (0.43 vs. 0.56). This effect was not observed with any of the remaining treatments.

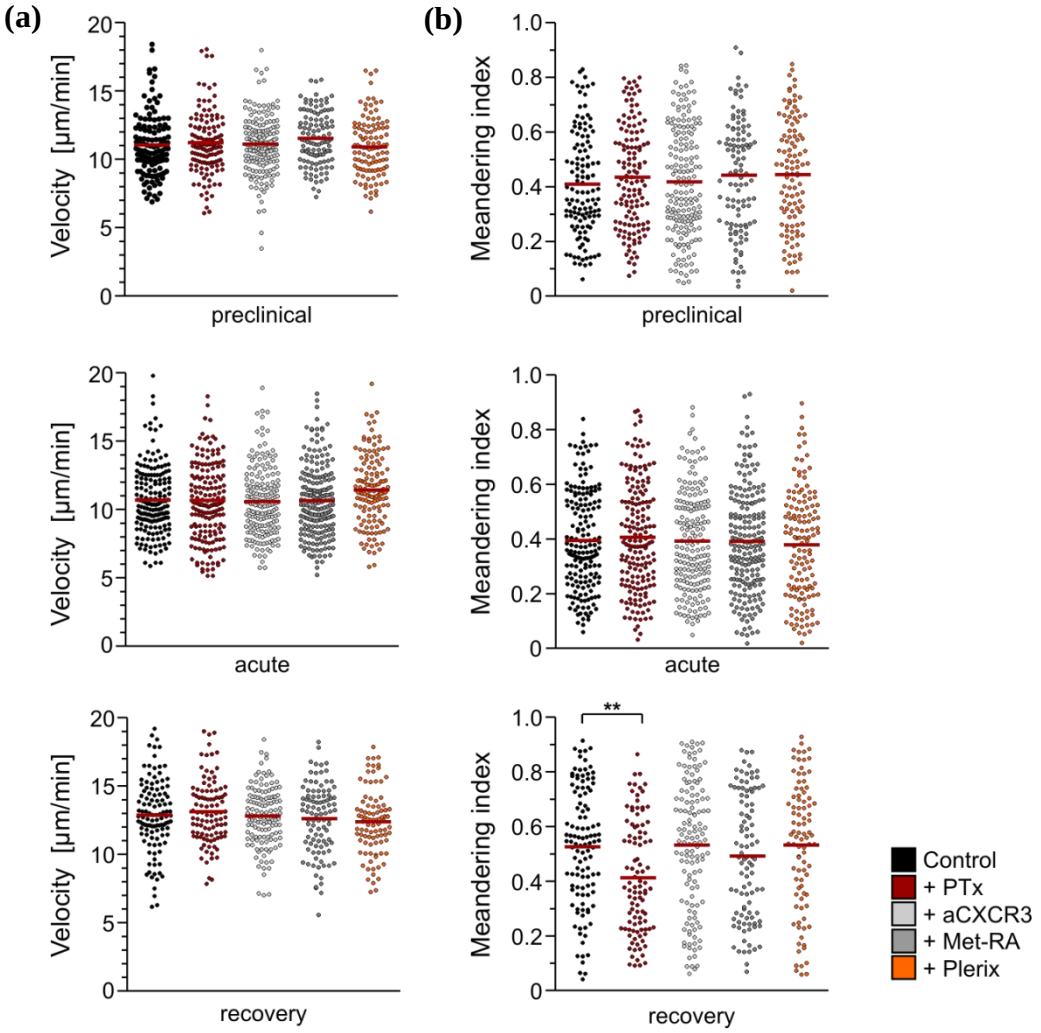

Figure 32 | Role of chemokines on the motility of extravasated $T_{MBP\text{-}GFP}$ cells during the course of EAE. Motility data are based on 30min intravital TPLSM recordings of spinal cord leptomeninges during preclinical (d3 p.t., upper line) acute (d5 p.t., center line) and recovery phases (day 8 p.t., lower line) of EAE. Dot plots represent **(a)** average velocities and **(b)** meandering indices of $T_{MBP\text{-}GFP}$ cells 4h after treatment as indicated. PBS-treatment= Control. Red lines: Mean values. Data include 2041 T_{MBP} cells from at least 3 independent experiments per treatment and time point. Statistical significance was evaluated by Kruskal-Wallis ANOVA followed by Dunn's multiple comparison test.

To test whether antigen-specificity was of relevance for T cell locomotion in the leptomeninges, $T_{OVA\text{-}GFP}$ cells were injected together with MBP-reactive T lymphocytes in healthy recipient rats. When co-transferred, $T_{OVA\text{-}GFP}$ cells enter the leptomeninges in high numbers and with similar kinetics compared to their myelin-reactive counterparts (not shown). However, co-transferred ovalbumin-reactive T cells differed partially in their motility compared to encephalitogenic T cells: $T_{OVA\text{-}GFP}$ cells migrated significantly faster during preclinical (11.9µm/min vs. 11.1µm/min) and acute EAE (12µm/min vs. 10.7µm/min) and did not increase their velocity during disease recovery **(Fig.33a)**. However, similar to the findings achieved with $T_{MBP\text{-}GFP}$ cells, PTx-treatment had no considerable effect on the speed of $T_{OVA\text{-}}$

$_{GFP}$ cells during any of the examined disease phases (**Fig.33a**).

A detailed analysis of their locomotion characteristics revealed that the co-transferred $T_{OVA-GFP}$ cells, similarly to T_{MBP} cells, displayed a more linear migration pattern during disease recovery (0.55) than in the preclinical (0.46) and acute (0.44) phases of EAE (**Fig.33b**). Administration of PTx did not affect the motility pattern of $T_{OVA-GFP}$ during preclinical and acute EAE but led to a less directed locomotion during disease recovery (0.42 vs. 0.57).

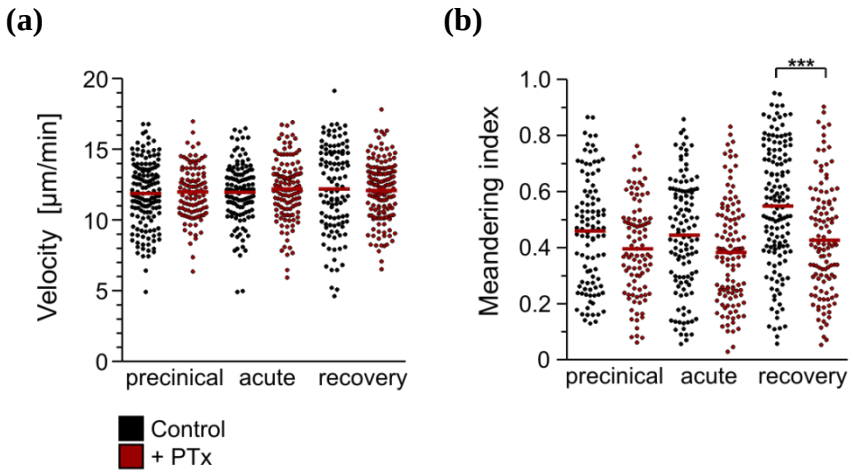

Figure 33 | Role of chemokines on the motility of extravasated $T_{OVA-GFP}$ cells during the course of EAE. Analyses are based on 30min intravital TPLSM recordings of spinal cord leptomeninges during preclinical (d3 p.t.), acute (d5 p.t.) and recovery (day 8 p.t.) phases of EAE. **(a)** Average velocities and **(b)** meandering indices of $T_{OVA-GFP}$ cells that were co-transferred with unlabeled T_{MBP} cells are shown. Red lines: Mean values. Data were evaluated 4h after treatment and include **(a)** 754 and **(b)** 684 $T_{OVA-GFP}$ cells from at least 3 independent experiments per treatment and time point. (PBS-treatment= Control). Statistical significance was determined by Kruskal-Wallis ANOVA followed by Dunn's multiple comparison test.

3.5. Impact of chemokines in stabilizing T cells during their migration in the extravascular space

These locomotion studies suggested that chemokines only moderately influence the migratory behavior of T cells within the leptomeninges. However, after application of PTx $T_{MBP\text{-}GFP}$ cells were regularly found to become detached from the meningeal surface and to be dragged along with the CSF (intravital data, not shown). This observation suggests that the adhesive forces that stabilize T cells during their migration on the meningeal surface may be potentially influenced by chemokines. Quantification of $T_{MBP\text{-}GFP}$ cells from CSF, spinal cord meninges and parenchyma after PTx- or PBS-treatment confirmed this hypothesis: the numbers of $T_{MBP\text{-}GFP}$ cells within the CSF of PTx-treated animals were significantly increased. At the same time, the numbers of cells within the meninges were significantly reduced compared to that of control animals (**Fig.34a**). Expectedly, T cell numbers within the spinal cord parenchyma were similar in both groups. Administration of PTx in animals that received ovalbumin-specific T cells together with T_{MBP} cells reproduced all findings, thereby excluding an antigen-specific component **(Fig.34b).** Moreover, anti-CXCR3mAb and Met-RANTES led to similar results compared to PTx, whereas application of Plerixafor had no measurable effect (**Fig.35**).

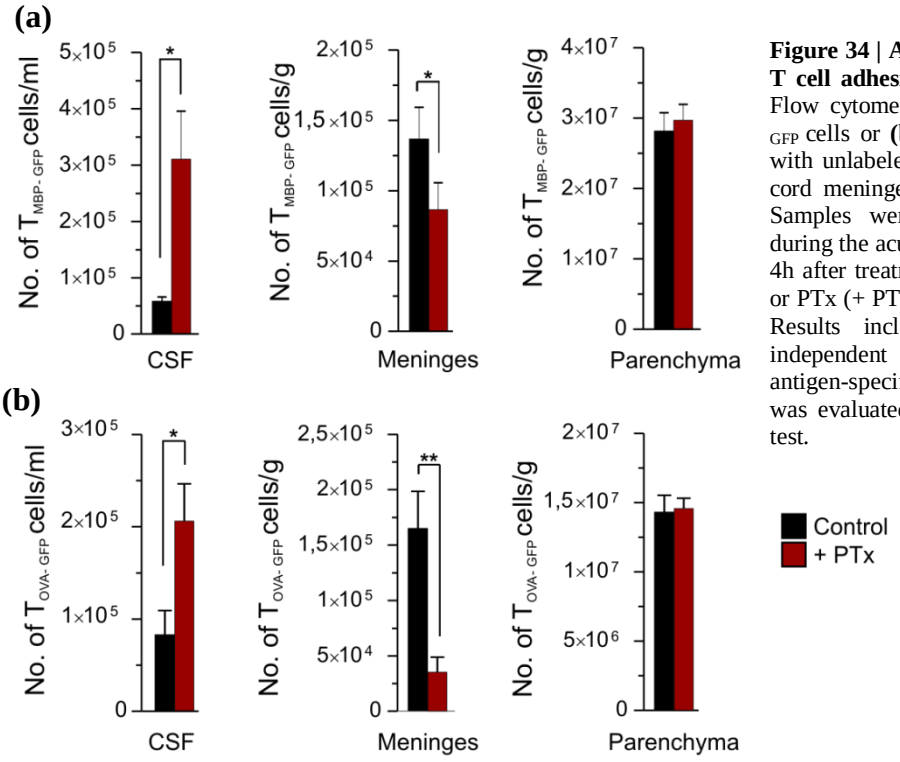

Figure 34 | Administration of PTx reduces T cell adhesion to the meningeal surface. Flow cytometric quantification of **(a)** $T_{MBP\text{-}GFP}$ cells or **(b)** $T_{OVA\text{-}GFP}$ cells co-transferred with unlabeled T_{MBP} cells from CSF, spinal cord meninges and parenchyma are shown. Samples were taken from EAE animals during the acute phase (d5 p.t.) of the disease 4h after treatment with either PBS (Control) or PTx (+ PTx). Means and s.d. are depicted. Results include data from at least 3 independent experiments per treatment and antigen-specificity. Statistical significance was evaluated by two-tailed Mann-Whitney test.

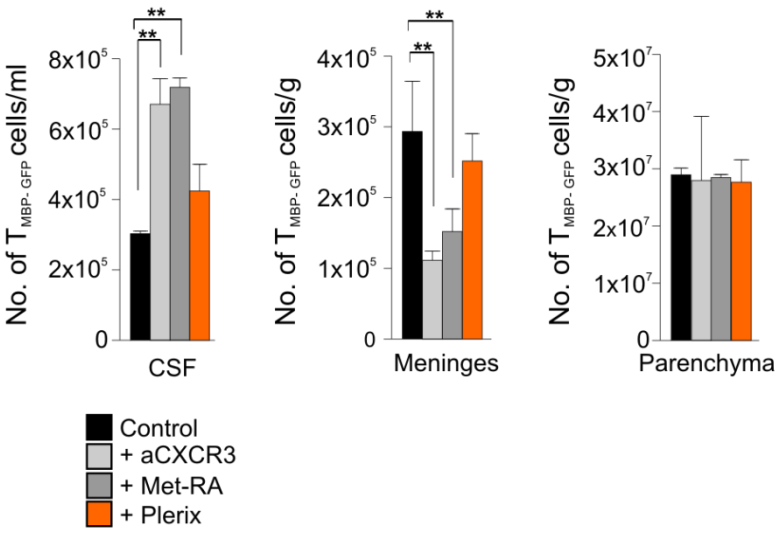

Figure 35 | Inflammatory chemokines stabilize T cell adhesion to the meningeal surface during EAE. Flow cytometric quantification of $T_{MBP\text{-}GFP}$ cells isolated from CSF, spinal cord meninges and parenchyma during the acute phase of EAE (d5 p.t.) are shown. Samples were taken from EAE animals 4h after injection of either PBS (Control), anti-CXCR3mAb, Met-RANTES or Plerixafor. Means and s.d. are depicted. Results include data from at least 3 independent experiments per treatment. Statistical significance was determined by Kruskal-Wallis ANOVA followed by Dunn's multiple comparison test.

To consolidate these findings, spleen derived-migratory $T_{MBP\text{-}GFP}$ cells were treated *in vitro* with PTx prior to injection into the cisterna magna of healthy recipient animals. 24 hours after i.th. injection intravital TPLSM imaging of spinal cord leptomeninges was performed. The data revealed that PTx-treated T cells obviously failed to adhere to the meningeal surface since their numbers there were significantly lower than those of Olig.-B-treated cells (**Fig.36**).

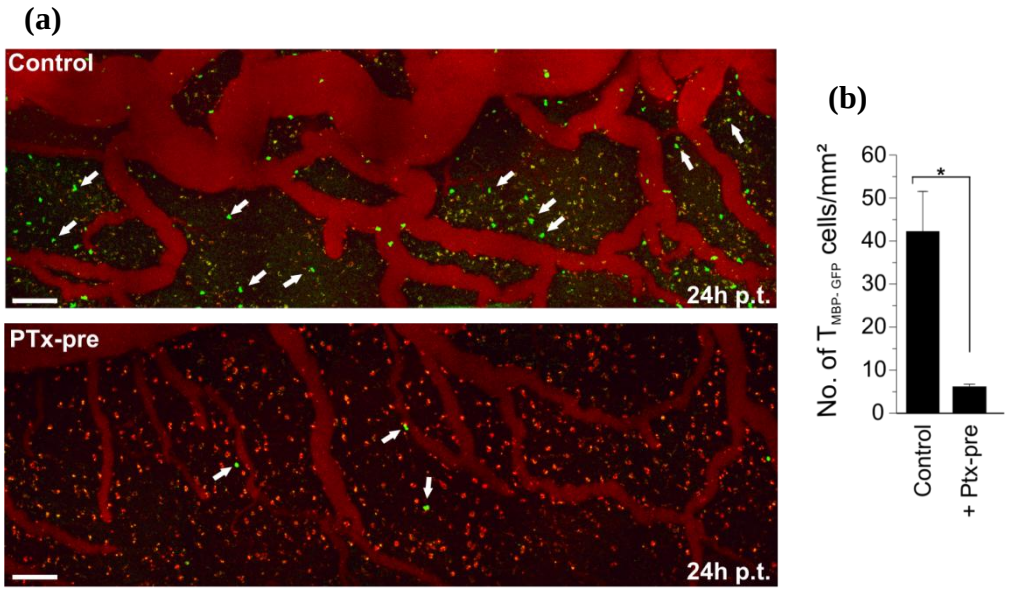

Figure 36 | PTx pre-treated migratory T cells fail to adhere to the leptomeningeal surface after i.th. transfer. (a) Intravital TPLSM recordings of spinal cord leptomeninges were performed 24h after i.th. injection of spleen-derived migratory $T_{MBP\text{-}GFP}$ cells pre-treated *in vitro* with either Olig.-B (Control, upper image) or PTx (+ PTx-pre, lower image) in healthy recipient rats. White arrows: Positions of individual $T_{MBP\text{-}GFP}$ cells. Red: Blood vessels, phagocytes. Green: $T_{MBP\text{-}GFP}$ cells. Scale bars: 100µm. Representative images of at least 3 independent experiments are depicted. **(b)** Correspondent quantification of $T_{MBP\text{-}GFP}$ cells per mm² is shown. Means and s.d. are depicted. Data include 291 cells from at least 3 independent experiments. Statistical significance was evaluated by two-tailed Mann-Whitney test.

3.5.1. Role of chemokines on the interaction between T cells and meningeal phagocytes

Embedded in the reticular fiber network of the leptomeninges are tissue resident phagocytes that are distributed throughout the entire meningeal surface and often found collocated in close proximity to leptomeningeal vessels (**Fig.37**). These tissue resident cells scan their environment by vividly protruding and retracting their cellular processes and are thought to represent the first line of APCs that present CNS-derived antigen to infiltrating T cells (BARTHOLOMÄUS et al., 2009). Due to their phagocytic activity, these cells can be visualized by applying small molecular fluorescently-labeled dextrans into the cisterna magna of animals prior to intravital imaging (**Fig.37**).

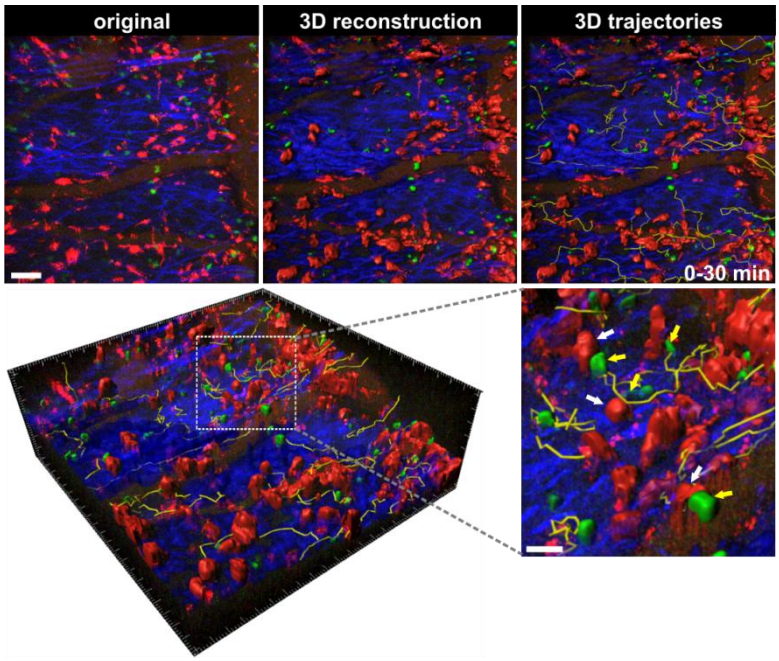

Figure 37 | Extravasated T cells interact with meningeal phagocytes that are embedded in fibrillar ECM structures. TPLSM of the dorsal spinal cord leptomeninges reveals interactions between $T_{MBP\text{-}GFP}$ cells (green, yellow arrows) and Texas Red®-labeled meningeal phagocytes (red, white arrows), embedded in a dense network of reticular fibers (blue, 2nd harmonic signal). Original picture and 3D reconstructions with or without 3D trajectories (yellow lines) throughout a 30min time interval are depicted. Scale bar: 50µm. Lower right: Magnified region, originated from the picture to the left as indicated by the white dotted rectangle. Scale bar: 20µm.

Interactions between these tissue resident phagocytes and encephalitogenic effector T cells were frequently observed during all three phases of EAE. Notably, contacts did not appear exclusively in close proximity to the vasculature but also over the entire meningeal surface (**Fig.37**). The average time T cells spent on contacting a single phagocyte within a 30min observation period was ~5min during both, the preclinical (4.9min) and acute (5.4min)

phases of EAE, whereas the contact duration in the recovery phase was significantly shorter (3.9min**)**. Apart from these relatively short contacts, T lymphocytes were found to establish more intense interactions with resident phagocytes. The T cells remained locally arrested at meningeal phagocytic cells throughout the entire observation period. Accordingly, these interactions were defined as long-lasting contacts (≥30min).

Ex vivo isolated meningeal phagocytes expressed MHC class II molecules and integrins that were highly up-regulated during the preclinical and acute disease phases compared to the naïve situation (not shown). Moreover, inflammatory chemokines, namely CXCL9-11 and CCL5 were highly up-regulated during preclinical and acute EAE compared to the naïve situation and disease recovery. Vice versa, CXCL12 was up-regulated exclusively under non-inflammatory conditions and during disease recovery (**Fig.38**).

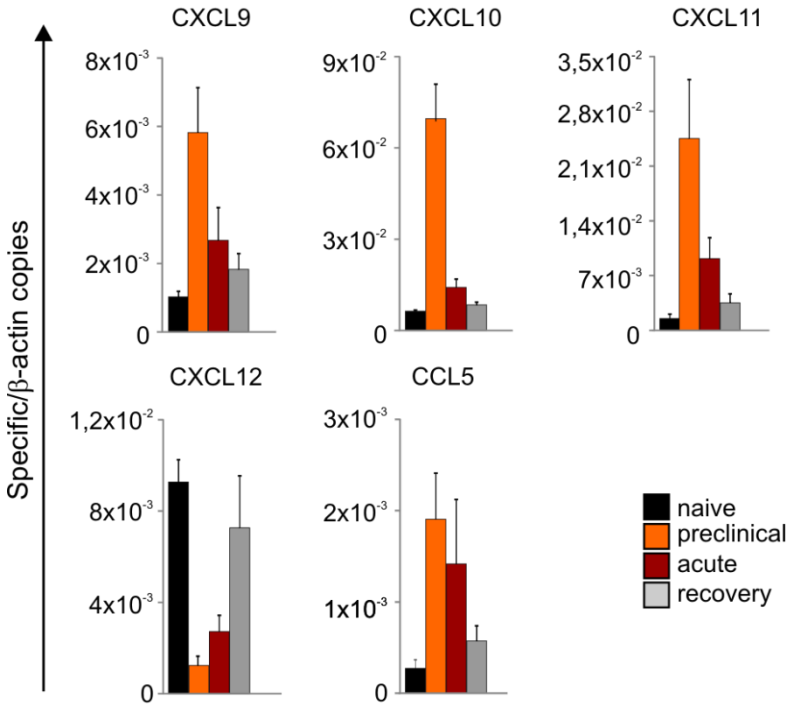

Figure 38 | Inflammatory chemokines are up-regulated in meningeal phagocytes during the preclinical and acute phases of EAE. Texas Red® dextran-labeled phagocytes were isolated at the indicated time points after T_{MBP} cell transfer from spinal cord meninges and parenchyma. Naïve= d0 p.t., preclinical= d3 p.t., acute= d5 p.t. and recovery= d8 p.t. Quantitative real-time PCR for the indicated chemokines was performed afterwards. Means and s.d. from replicate measurements are depicted. Values refer to specific copies in relation to β-actin copies. A representative result of at least 3 independent experiments is shown.

In order to investigate whether chemokines are involved in forming and/or stabilizing interactions between T cells and CNS-resident phagocytes, PTx as well as anti-CXCR3mAb, Met-RANTES and Plerixafor were administered prior to intravital imaging during the preclinical, acute and recovery phases of EAE.

Administration of PTx reduced significantly the contact durations between $T_{MBP\text{-}GFP}$ cells and resident phagocytes in each EAE phase (preclinical: 3 vs. 4.9min, acute: 3.5 vs. 5.4min and recovery: 2.5 vs. 3.9min) in comparison with the control situation (**Fig.39a**). Simultaneously, the number of phagocytes contacted by an individual T cell increased significantly within a 30min observation period compared to the control **(Fig.39b**). This coincidence might explain why T cell velocities remained unaltered under treatment during all three phases of EAE (see **Fig.32a**). Interestingly, both anti-CXCR3mAb and Met-RANTES reproduced all findings achieved with PTx (**Fig.39**). In contrast, administration of Plerixafor had no measurable effect on the examined parameters. Interestingly, interference with chemokine signaling had no influence on established stable interactions between arrested T cells and local phagocytes during any of the three EAE phases (**Fig.40**).

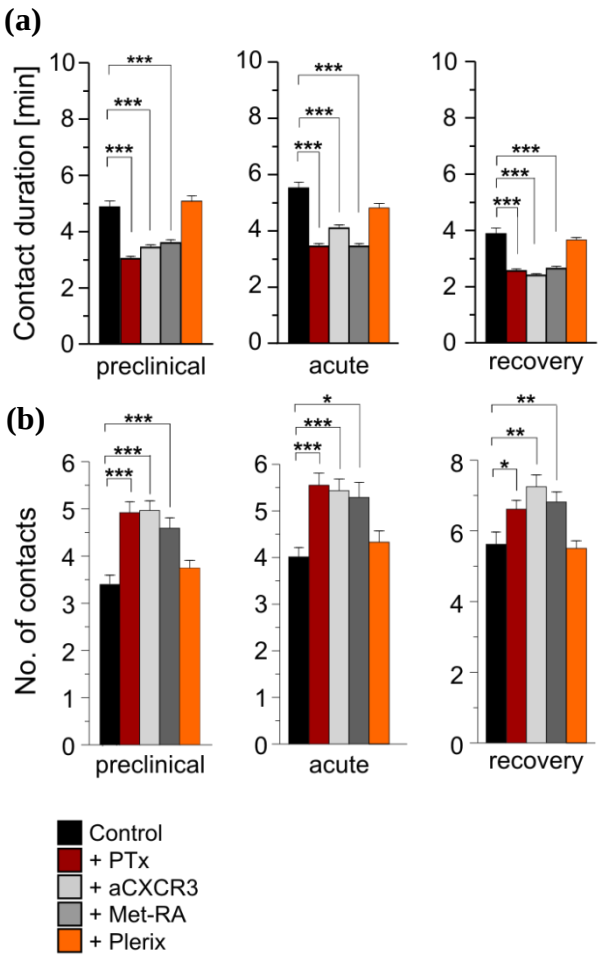

Figure 39 | Interference with chemokine signaling influences short-lasting contacts between $T_{MBP\text{-}GFP}$ cells and resident meningeal phagocytes. Analysis are based on 30min intravital TPLSM recordings during preclinical (d3 p.t.), acute (d5 p.t.) and recovery (d8 p.t.) phases of EAE. Animals received either PBS (Control), PTx, anti-CXCR3mAb, Met-RANTES or Plerixafor 4h prior to imaging. **(a)** Contact durations between motile $T_{MBP\text{-}GFP}$ cells and meningeal phagocytes within a 30min recording period are shown. Means and s.d. are depicted. Results include 4587 contacts from at least 3 independent experiments per treatment and time point. **(b)** Graphs show the mean numbers of phagocytes that were contacted by individual T cells within a 30min observation period. **(a,b)** Statistical significance was evaluated by Kruskal-Wallis ANOVA followed by Dunn's multiple comparison test.

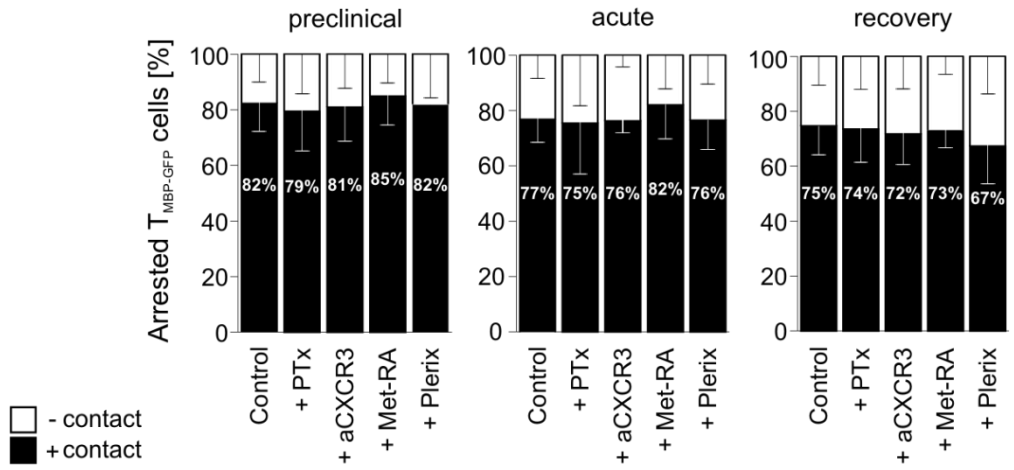

Figure 40 | Interference with chemokine signaling does not influence long-lasting contacts between $T_{MBP-GFP}$ cells and resident meningeal phagocytes. Graphs represent percentages of stationary $T_{MBP-GFP}$ cells either arrested to (+ contact) or not in contact with phagocytes (- contact) within a 30min intravital observation period. PBS-treatment= Control. Animals were treated 4h prior to imaging. Means and s.d. are depicted. Results include 1765 $T_{MBP-GFP}$ cells from at least 3 independent experiments per treatment and time point.

In order to investigate whether these results were specific for myelin-reactive cells, interactions between ovalbumin-reactive T cells, (co-transferred together with T_{MBP} cells) and meningeal phagocytes were examined. Compared with MBP-reactive cells, motile $T_{OVA-GFP}$ cells contacted resident phagocytic cells only in a very short, transient manner throughout all observation time points (preclinical: 3.8min vs. 4.9min, acute: 3.8min vs. 5.4min and recovery: 2.9min vs. 3.9min) (**Fig.41a** vs. **Fig.39a**).

The findings upon PTx treatment were in contrast to that of myelin-reactive cells. Administration of PTx did not further reduce the interaction durations between $T_{OVA-GFP}$ cells and their phagocytic counterparts. Furthermore, $T_{OVA-GFP}$ cells did not contact significantly more local phagocytes under treatment during a 30min observation period (**Fig.41b** vs. **Fig.39b**).

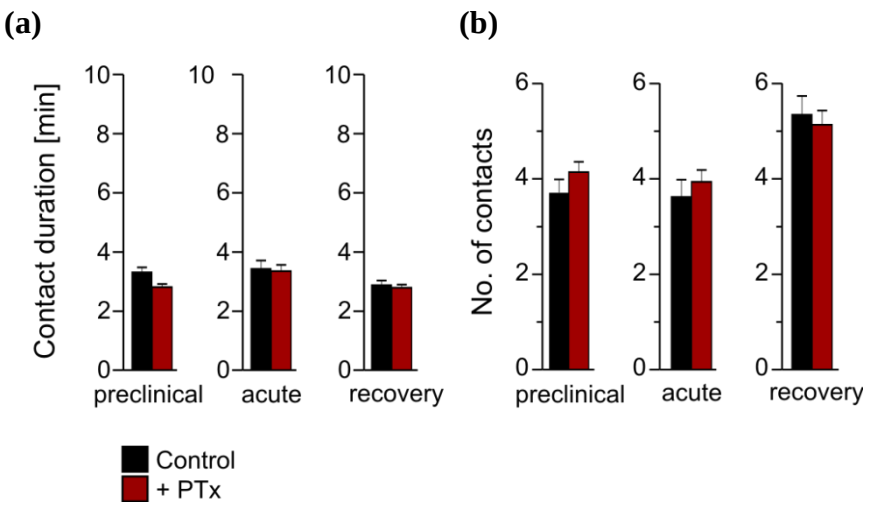

Figure 41 | Interference with chemokine signaling has no impact on interactions between motile $T_{OVA\text{-}GFP}$ cells and meningeal phagocytes. Analysis are based on 30min intravital TPLSM recordings during preclinical (d3 p.t.), acute (d5 p.t) and recovery (d8 p.t) phases of EAE. $T_{OVA\text{-}GFP}$ cells were transferred together with unlabeled T_{MBP} cells. Animals were injected with either PBS (Control) or PTx (**a)** Contact durations between motile $T_{OVA\text{-}GFP}$ cells and meningeal phagocytes within a 30min recording period are shown**.** Means and s.d. are depicted. Results include 904 contacts from at least 3 independent experiments per treatment and time point. **(b)** Graphs show the mean numbers of phagocytes contacted by individual T cells within a 30min observation period. Data were evaluated from 249 $T_{OVA\text{-}GFP}$ cells within at least 3 independent experiments.

3.5.2. Role of chemokines during the re-activation of encephalitogenic T cells within the living CNS tissue

In order to visualize T cell (re-) activation within the living milieu, myelin-reactive T cells were used that co-expressed fluorescent sensors of nuclear factor of activated T cells (YFP-NFAT) and histone protein H2B (mCherry-H2B). These sensors allow visualization and real-time tracking of T cell activation *in vivo*, when cytosolic NFAT is translocated to the nucleus upon TCR activation (LODYGIN et al., in press).

Intravital microscopy revealed that encephalitogenic T cells did not show any signs of activation either during their accumulation in the periphery or during intravascular crawling before transgressing the leptomeningeal blood vessels (LODYGIN et al., in press). In contrast, 20% of extravasated T cells within the meninges were found to bear the NFAT sensor in the nucleus, clearly indicating the structural compartment of the CNS where T cell activation takes place (LODYGIN et al., in press). Surprisingly, the majority of *de novo* translocation events in effector T cells were evoked by short-lasting contacts with meningeal phagocytes. The time-span between an initial phagocyte contact and the translocation of NFAT into the T cell's nucleus was relatively short, ranging between 4 -5 minutes (**Fig.42**).

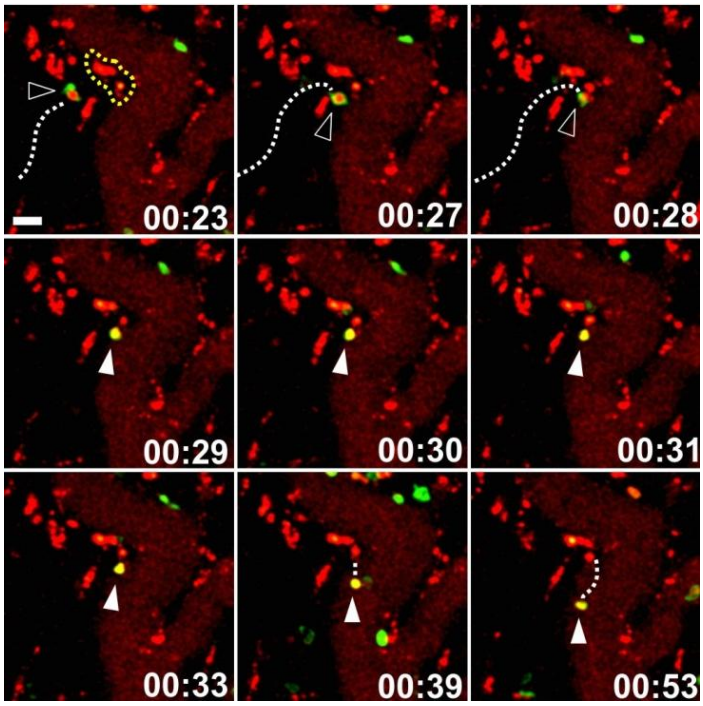

Figure 42 | Short-lasting contacts with resident phagocytes prompt *de novo* NFAT-translocations in T_{MBP} cells. Series of selected single frames of a 60min TPLSM recording during the preclinical phase of EAE are shown. A myelin-reactive T cell with cytosolic NFAT (open arrowhead) establishes a short-lasting contact with a Texas Red® dextran-labeled resident phagocyte (dotted yellow line), leading subsequently to the translocation of NFAT to the T cell's nucleus. Red: Blood vessels and meningeal phagocytes. White dotted lines: T cell track; Scale bar: 20µm. (Data published in LODYGIN et al., in press).

Apparently, short-lasting contacts between T cells and resident phagocytes are sufficient to trigger T cell re-activation *in vivo*. Since interference with chemokine signaling was shown to disturb these short-lasting contacts (**Fig.39a**) the attempt was made to clarify whether this "disturbance" had functional consequences for T cell re-activation. Accordingly, PTx and anti-CXCR3mAb were injected prior to intravital imaging. Unexpectedly, neither PTx- nor anti-CXCR3mAb treatment resulted in a significantly lower fraction of NFAT-translocated T cells. In contrast, administration of the calcineurin-inhibitor FK506 (GOTO et al., 1987) or local application of soluble MBP (ODOARDI et al., 2007) led respectively to a strong decrease or increase of T cells that carried the NFAT sensor within the nucleus (**Fig.43**).

To corroborate these findings, the expression of activation markers, i.e. IFN-γ and IL-17 within $T_{MBP\text{-}GFP}$ cells was analyzed by quantitative real-time PCR. Encephalitogenic T cells were isolated *ex vivo* from animals that were treated either with PTx or anti-CXCR3mAb for 6, 12 and 24h during acute EAE. Compared to control animals neither global interference with Gαi signaling nor specific blockage of CXCR3 function led to a measurable reduction in T cell activation at any examined time point (**Fig.44**). Furthermore, flow cytometric evaluations did not reveal any changes on the surface expression of activation markers such as OX-40 and CD25 within $T_{MBP\text{-}GFP}$ cells that were isolated from CNS meninges (not shown). In contrast, after administration of FK506, myelin-reactive T cells were significantly less

activated compared to cells isolated from control animals. Vice versa, application of soluble antigen (MBP) resulted in a massive elevation in T cell activation markers on both mRNA **(Fig.44)** and protein level (not shown).

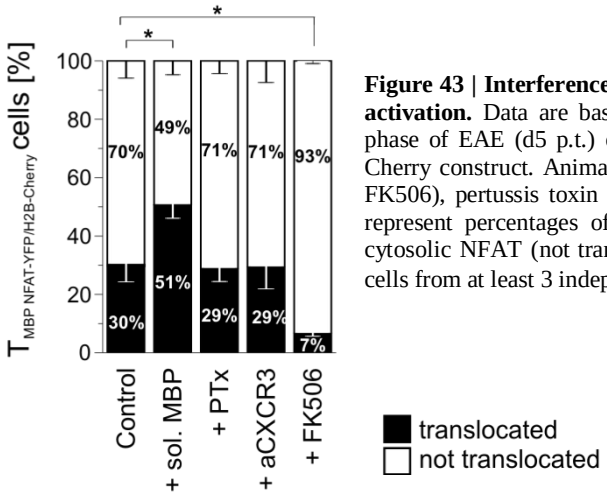

Figure 43 | Interference with chemokine signaling has no influence on early T cell activation. Data are based on 30min intravital TPLSM recordings during the acute phase of EAE (d5 p.t.) of MBP-reactive T cells co-expressing the NFAT-YFP/H2B-Cherry construct. Animals were treated with soluble antigen (+ sol. MBP), FK506 (+ FK506), pertussis toxin (+ PTx) or with DMSO (Control) 4h prior to imaging. Bars represent percentages of MBP-reactive T cell with either nuclear (translocated) or cytosolic NFAT (not translocated). Means and s.d. are depicted. Results include 1605 cells from at least 3 independent experiments per treatment and time point.

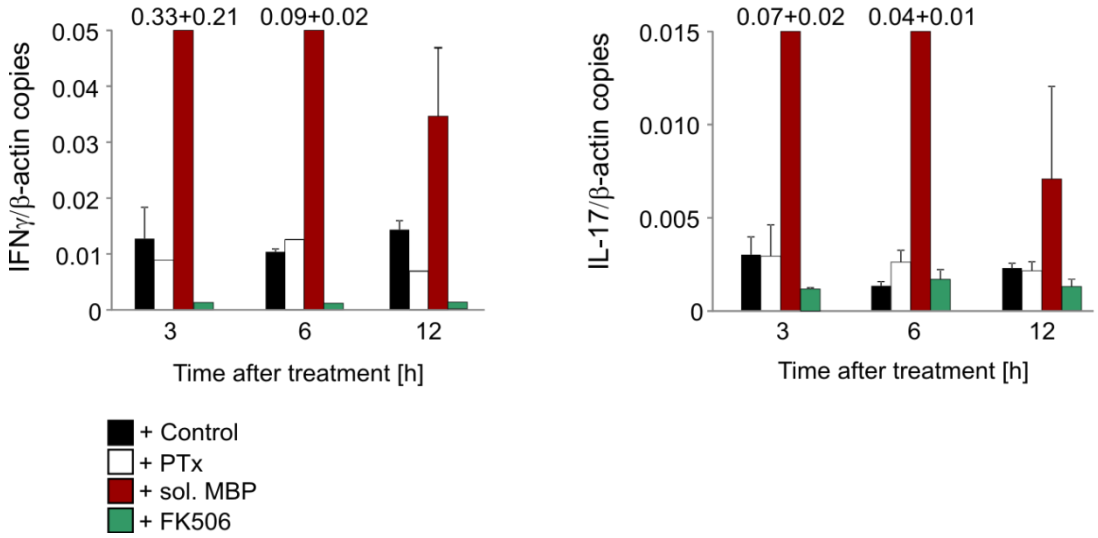

Figure 44 | Inhibition of chemokine signaling does not interfere with T cell activation. Graphs represent mRNA expression levels of IFN-γ (left) and IL-17 (right) within *ex vivo* isolated T cell from spinal cord meninges. Animals were treated with DMSO (control), FK506, PTx or with soluble MBP during acute inflammation (day 4.5 p.t.). CNS meninges were isolated at 6, 12 and 24h post treatment. Means and s.d. of replicate measurements are shown. Values refer to specific copies in relation to β-actin copies. A representative result of at least 3 independent experiments is shown.

4. Discussion

In experimental autoimmune encephalomyelitis (EAE), an animal model for multiple sclerosis (MS), encephalitogenic T cells breach distinct cerebral barriers in order to gain access to their target tissue, the CNS. However, it remains poorly understood *how* exactly auto-reactive T cells overcome these boundaries. The data of the present work displayed in real-time the behavior of GFP^+ $CD4^+$ MBP-reactive T cells ($T_{MBP\text{-}GFP}$ cells) within leptomeningeal blood vessels and provided insights into their migration within the living meningeal environment.

4.1. Migratory behavior of effector T cells within the lumen of leptomeningeal blood vessels

4.1.1. Intraluminal crawling of effector T cells

During *t*EAE of the Lewis rat the majority of encephalitogenic effector T cells accumulated within the CNS only after an obligatory delay of 2-3 days (p.t.). The T cells first arrived at the level of leptomeningeal blood vessels of the lumbar/sacral spinal cord. There, they did not roll along the vessels walls as expected from observations in peripheral vascular beds but rather they crawled extensively in the immediate vicinity of the vessels. Up to this point it was unclear whether these cells crawled along the abluminal surface or within the vascular lumen. Several pieces of evidence confirmed that the vast majority of these cells were indeed crawling along the inner vessel walls (BARTHOLOMÄUS et al., 2009; KAWAKAMI & FLÜGEL, 2010). This specific migratory phenotype has been reported for other types of leukocytes, i.e. neutrophils (PHILLIPSON et al., 2006), NK-T cells (GEISSMANN et al., 2005) and monocytes (AUFFRAY et al., 2007) but never before in (auto-reactive) effector T cells.

Morphologically, intraluminal crawling resembles an amoeboid movement, a well described phenotype for leukocytes migrating within a 2D environment (FRIEDL & WEIGELIN, 2008; LÄMMERMANN & SIXT, 2009). A detailed view on the locomotion characteristics revealed that myelin-reactive T cells were not moving in the direction of the blood stream, as might have been expected, but rather against the blood flow (**Fig.10c**). Furthermore, the crawling behavior was influenced by the activation status of the vessel endothelium: brain antigen-ignorant, ovalbumin-specific T cells crawled for a shorter time and with a higher speed compared to their myelin-reactive counterparts. However, under inflammatory conditions, ovalbumin-reactive T cells assimilated their intraluminal migration pattern to that of myelin-

reactive T cells.

Interestingly, intraluminal crawling was apparently a peculiarity of CNS vessels, since it was less obvious within the periphery (BARTHOLOMÄUS et al., 2009). Within the latter, effector T cells mainly rolled along the vessel endothelium, i.e. T cells appeared as several round shaped dots, moving solely in the direction of the blood stream (BARTHOLOMÄUS et al., 2009). This discrepant locomotion behavior can hardly be explained by T cell intrinsic properties but rather points to different endothelial characteristics between CNS and peripheral vessels.

De novo crawling of effector T cells within CNS vessels resulted regularly from preceding rolling, but also occurred immediately after capture from T lymphocytes to the inner vascular walls (unpublished data). In this respect it should be noted that crawling of myelin-reactive T cells is no peculiarity of LEWIS rat *t*EAE since the findings were reproduced in SJL mice inoculated with PLP-reactive T cells (BARTHOLOMÄUS et al., 2009). Furthermore, this new migratory characteristic was no *in vitro* artifact of T cell culturing since memory T cells that had been reactivated by immunizing carriers with MBP (KAWAKAMI et al., 2005 (II)) were also capable of crawling (BARTHOLOMÄUS et al., 2009). Intraluminal crawling seems to be a singularity of migratory T cells, i.e. T cells that had undergone a profound reprogramming in the periphery before they arrive at the CNS vasculature (ODOARDI et al. 2012). In contrast, *in vitro*-activated T lymphoblasts that had been injected intraarterially were shown to be firmly arrested to spinal cord vessels immediately after transfer (VAJKOCZY et al., 2001).

Up to now, the biological relevance of intraluminal crawling is poorly understood. Most likely, it resembles a scanning behavior for T lymphocytes in order to spot special exit ports that may facilitate transendothelial migration (SCHENKEL et al., 2004).

4.1.2. Intraluminal crawling of effector T cells is dependent on chemokine signaling

The data of the present work implies a crucial role for chemokines in T cell-mediated infiltration of the CNS. Especially, chemokines influenced the intraluminal crawling behavior of effector T cells within leptomeningeal blood vessels and thereby the initial step of CNS autoimmunity in the context of EAE. In order to clarify how (and which) chemokines

influence the behavior of migrating T cells within different CNS compartments and during distinct infiltration steps, it became indispensable to use various blocking agents, i.e. Met-RANTES (PROUDFOOT et al., 1996), Plerixafor/AMD3100 (HATSE et al., 2002), a monoclonal blocking antibody against CXCR3 (MOHAN et al., 2005) and pertussis toxin (PTx) (PITTMAN, 1979). The effectiveness of the treatment was tightly controlled via chemotaxis assays from *ex vivo* isolated cells. Importantly, any one blocking agent was administered only immediately before or during live analyses of effector T cells. Thereby, compensatory or unspecific mechanisms that could potential influence the migratory behavior of effector T cells were minimized. Furthermore, by treating the animals only in a short-term range of less than 3 hours, the reported potential harmful side-effects of PTx on the vessel endothelium were circumvented as far as possible (BRÜCKENER et al., 2003; BEN-NUN et al., 1997).

Whereas blocking peptides (Met-RANTES, Plerixafor) and antibodies (anti-CXCR3mAb) exhibit their antagonistic/neutralizing activities immediately after binding to the respective receptors, PTx, composed of an enzymatic A-subunit and a B-oligiomeric subunit (STEIN et al, 1994; TAMURA et al., 1982) needs to get access to the cytosol of a given cell. Thereby, the non-enzymatic B-subunit mediates membrane binding via glycoconjugate receptors (WITVLIET et al., 1989; BRENNAN et al., 1988). Thereafter, PTx is retrogradely transported by endosomal uptake followed by shuttling via the Golgi network and the endoplasmatic reticulum (HAZES & READ, 1997; PLAUT & CARBONETTI, 2008). Dissociation of the holotoxin and translocation of the enzymatic A-subunit from the endoplasmatic reticulum to the cytosol finally leads to the ADP-ribosylation of heterotrimeric G proteins (PLAUT & CARBONETTI, 2008). The time period from toxin-uptake to unfold enzymatic activity is approximately 1h but depends largely on the responding cell line (EL BAYÂ et al., 1999). This may explain why the first measurable reduction in the number of intraluminal crawling T cells was evident only after ~60min of PTx treatment (30% reduction), whereas anti-CXCR3 blockade led to the same decrease already after 20 minutes. Interference with chemokine signaling – non-specifically (via PTx) or specifically (via anti-CXCR3 mAbs) – affected intraluminal T cell locomotion on several levels:

(1) Inhibition of chemokine signaling led to a significant reduction of intraluminal crawling T cells while simultaneously the number of rolling T cells increased. (2) Interference with chemokine signaling also directly affected intraluminal crawling as shown by a reduction in the time T cells spent scanning the luminal surface and by an acceleration of the crawling

velocity. These findings suggest that chemokines mediate not only the shift from initial transient adhesion (rolling) towards firm interaction of T cells with the vessel walls (crawling) but also the maintenance of intraluminal crawling. This interpretation is in accordance with the general view that chemokine signaling intensifies interactions of leukocytes with endothelial cells via integrin-mediated adhesion (CAMPBELL et al., 1998; PELED et al., 1999; CONSTANTIN et al., 2000; SHAMRI et al., 2005; SHULMAN et al., 2009).
(3) Inhibition of chemokine signaling led to an alteration of the T cells' preferred upstream crawling direction towards a migration with the blood stream (**Fig.21**). This phenomenon cannot be solely explained by an indirect effect via integrins, since blockage of the integrin VLA-4 did not influence the crawling direction. These findings may argue in favor of an endothelial chemokine gradient as functional basis for intraluminal crawling. Such gradients might emerge from chemokines that are directly produced by endothelial cells (or shuttled via transcytosis from the abluminal to the luminal vessel surface (MIDDLETON et al., 1997; HUANG et al., 2000). This interpretation is supported by recent observations on intraluminally crawling leukocytes that were guided by immobilized chemokine gradients within venules of the cremasteric muscle (MASSENA et al., 2010) or within the lumen of liver sinusoids in a model of sterile inflammation (MCDONALD et al., 2010).

Interestingly, the observation that ovalbumin-reactive effector T cells crawl evenly within the leptomeningeal vessels in a chemokine-dependent manner implicated a certain involvement of chemokine-signaling in mediating endothelial interactions even under non-inflammatory conditions. There are two reasons why the endothelium was considered as unprimed within this experimental constellation: (1) Crawling and even extravasation of T_{OVA} cells did not lead to an elevation of inflammatory chemokines on the vessel endothelium (not shown) and (2) there was no measurable disruption of the endothelial integrity, compared to the naïve situation. However, it should be emphasized that inflammatory chemokines (CXCL9-11) are present at basal levels within naïve meningeal endothelial cells. This fact might explain why specific blocking of CXCR3 signaling affected crawling of both T_{MBP} and T_{OVA} cells.

4.2. Effects of chemokines on extravasated T cells

4.2.1. Role of chemokines as chemoattractants for encephalitogenic T cells

Once myelin-reactive T cells had transgressed the pial vessels they scanned the outer side of the vascular walls and distributed throughout the meningeal surface (BARTHOLOMÄUS et al., 2009). This milieu is characterized by a network of fibers that can be visualized by second harmonic generation imaging (**Fig.37**). It is well known that stromal cells in the leptomeninges produce extracellular matrix (ECM) components e.g. collagen, fibronectin and laminin (RUTKA et al., 1986; SILVA et al., 1999). Furthermore, a reticular fiber network has been described to occur in inflammatory lesions of the brain during toxoplasmic encephalitis, and Toxoplasma gondii-specific T cells were found to move along these ECM structures (WILSON et al., 2009). However, the molecular factors that guide these cells within this extravascular (interstitial) environment are largely unknown.

Within the interstitial space, leukocytes are in principle able to migrate via haptokinesis or contact guidance along ECM structures without the need of chemoattractant factors (FRIEDL & WEIGELIN, 2008). However, during inflammation it is unlikely that lymphocytes move irrespective of chemoattractant gradients. Immunohistological examinations provided indirect evidence for the contribution of chemokines in leukocyte migration, since levels of inflammatory chemokines and their respective receptors on mononuclear infiltrates had been detected within acute lesions of MS patients (SØRENSEN et al., 1999) and EAE diseased animals (KARPUS & RANSOHOFF, 1998; FIFE et al., 2001). The results of the present work are in accordance with these studies, namely the presence of elevated levels of inflammatory chemokines (CXCL9-11, CCL5) within the CNS during preclinical EAE and disease progression compared to the naïve situation. Furthermore, *ex vivo* isolated T cells from CNS meninges carried the respective receptors (CXCR3, CCR5) and were able to respond to chemokine gradients in *in vitro* chemotaxis assays.

Chemokine gradients are likely to appear *in vivo* in a soluble form or immobilized on ECM structures (SCHUMANN et al., 2010; YANG et al., 2007; PELLETIER et al., 2000). Lymphocytes carrying the respective receptors can respond to soluble gradients via chemotaxis or in a haptotactic manner to immobilized chemokines (FRIEDL & WEIGELIN, 2008). Such a cellular response would result in a directed movement towards the chemokine source that can be evaluated by the meandering index. Conversely, blockage of chemokine

signaling would disrupt such a directed movement (MCDONALD et al., 2010).

However, during the preclinical and acute phases of EAE the extravasated effector T cells apparently migrated in a non-directed manner that was not changed by chemokine interference (**Fig.32b**). There are several explanations that may justify this seemingly "random" locomotive pattern. Firstly, the presence of chemokine ligands within the meningeal tissue was evaluated only on a transcriptional level and might therefore not reflect the actual protein expression. However, this appears unlikely since chemokines have been reported to be expressed at the protein level within the CNS, at least in diseased animals (KARPUS & RANSOHOFF, 1998). Secondly, during inflammation, abundant levels of ligands may reduce the migrating cell's responsiveness to chemokines due to cellular adaption mechanisms, like receptor desensitization/internalization (FERGUSON & CARON, 1998). This hypothesis is questioned by the fact that the *ex vivo* isolated T cells from the meninges readily responded to chemokine ligands in chemotaxis assays (*in vitro*). Thirdly, and perhaps most likely, T cells might not able to detect distinct chemokine gradients due the high spatial density of chemokine-producing cells during inflammation. Thus, the meningeal phagocyte population that was clearly shown to express pro-inflammatory chemokines densely covers the vessels and the meningeal plane (**Fig.37**).

4.2.2. Chemokines stabilize T cell migration within the meningeal environment

Upon chemokine blockage, effector T cells became detached from the leptomeningeal surface and accumulated in the CSF. This phenomenon was similar to that within the vascular lumen where crawling cells became detached from the vessel endothelium. Notably, this detachment in the meninges did not reach the level seen in the blood circulation (**Fig.34,35**). This might be due to the specialized composition of the leptomeningeal milieu. Thus, the fibers around the vessels and on the meningeal plane form a 3D network that is bathed in the CSF. T cells migrating within this ECM network might be protected from being dragged away by the CSF, whereas cells crawling on its surface are exposed to the shear forces exerted by the CSF. Adhesion might require the induction of high-affinity integrin forces (WOOLF et al., 2007). Interference with chemokine signaling by PTx, anti-CXCR3mAb or Met-RANTES would then lead to a detachment of T cells from the meningeal surface by interrupting these adhesive bonds.

4.2.3. Chemokines stabilize interactions between T cells and meningeal phagocytes but do not affect T cell activation

It is important to note that meningeal phagocytes not only produce inflammatory chemokines, but at least partially also MHC class II molecules on their surface (LODYGIN et al., in press). Moreover, these cells were found to be able to present myelin components to the invading T cells leading to subsequent T cell activation (BARTHOLOMÄUS et al., 2009; LODYGIN et al., in press) and can be therefore considered as potential antigen presenting cells (APCs).

In general, two different forms of interactions between T lymphocytes and meningeal APCs were distinguishable *in vivo*: dynamic, short-lasting interactions (<10min) between motile T cells and their antigen-presenting counterparts or stable, long-lasting contacts (≥30min) between arrested T cells and meningeal APCs.

Stable interactions between T cells and APCs were reported to lead to the formation of a specialized contact area that is commonly known as immunological synapse (GRAKOUI et al., 1999). The initiation of this interaction requires strong adhesive forces that are believed to be mediated predominantly by integrins (DUSTIN, 2009). Chemokines were speculated to play a role in strengthening these forces (CONSTANTIN et al., 2000). This view is supported by the observation that the durations of short-lasting contacts that might be considered as predecessors of the stable synapses, were indeed dependent on chemokines: blockage of chemokine signaling by administration of PTx, anti-CXCR3mAb or Met-RANTES significantly shortened interactions between motile T cells and resident APCs during all three phases of EAE (**Fig.39a**). In contrast, long-lasting contacts between encephalitogenic effector T cells and the meningeal phagocytes were not influenced by chemokine blockage. Interestingly, interference with chemokine signaling did not affect the transient contacts between brain-ignorant ovalbumin-reactive T cells and the meningeal phagocytes. It is important to note that even in the absence of chemokine blockage these interactions were significantly shorter than those between myelin-reactive T cells and their antigen-presenting partners. From these data a three step model of T cell activation within the meninges during EAE can be proposed.

(1) The first “explorative touches” (duration: ~3.5min) of T cells with their meningeal counterparts are antigen and chemokine-independent. This can be observed in brain antigen-ignorant T_{OVA} cells or in T_{MBP} cells that had been treated with chemokine blockers. Step 1 can subsequently lead to a second phase, designated as (2) “priming contacts” (5-6min) where

T cells encounter their antigen (antigen-dependent) and get re-activated upon TCR stimulation (**Fig.42**). These priming contacts require chemokine signaling, as demonstrated in myelin-reactive effector T cells after blockage with PTx, anti-CXCR3mAb or Met-RANTES. Step 2 can finally proceed to (3) "long-lasting contacts" (≥30min), where both interaction partners remain locally arrested. This step is again dependent on the antigen specificity of the T cells since only a minority of OVA-reactive cells is found to be arrested (not shown). Interestingly, this interaction seems be chemokine independent: neither PTx nor anti-CXCR3mAb nor Met-RANTES had any effect on the numbers of these stable T cell – phagocyte contacts.

Surprisingly, interference with chemokine signaling did not influence T cell activation. This was demonstrated by similar numbers of NFAT-translocated cells in treated and un-treated animals and by similar expression of T cell activation markers within both groups. Obviously, the priming contacts between T cells and phagocytes are sufficient to drive T cell activation; however, they do not seem to be absolutely required. The reduced contact durations between T cells and APCs upon interference with chemokine signaling might be compensated by the establishment of significantly more interactions within the same time period compared to the control situation (**Fig.39b**). This explanation would be in agreement with the serial encounter model proposed by Friedl and Gunzer (FRIEDL & GUNZER, 2001).

5. Summary and Conclusion

During transfer EAE, effector T cells appear within the CNS only after a latency period of 2-3 days. This delay is due to a preceding extensive journey through lungs and secondary lymphatic organs where the cells undergo profound functional alterations resulting in a "migratory" phenotype that allows them to re-enter the circulation and finally arrive at their destination, the CNS (FLÜGEL et al., 2001; ODOARDI et al., 2012). The present work focuses in detail on factors controlling the locomotion behavior of $CD4^+$ effector T cells (FLÜGEL et al., 1999) from their first arrival within pial blood vessels and throughout their journey within the meningeal environment at distinct time points during *t*EAE.

During the preclinical phase, encephalitogenic effector T cells were crawling along the inner surface of leptomeningeal vessels predominately against the direction of the blood stream. Intravenous administration of PTx or a neutralizing anti-CXCR3mAb displayed a crucial impact of chemokines on intravascular T cell crawling since the cells changed their motility properties and their predominant crawling direction upon blockage. Similar observations were obtained with brain-antigen ignorant T_{OVA} cells, which suggest that chemokines impact on T cell-mediated immune surveillance in a non-inflamed CNS.

Once myelin-reactive T cells transgressed the vascular barriers they continued their scan throughout the meningeal surface. Interference with chemokine signaling at this stage had only a moderate impact on the basal T cell motility. However, chemokines were crucial in stabilizing the contacts between T cells and resident phagocytic cells in the leptomeningeal milieu. Furthermore, administration of PTx, anti-CXCR3mAb or Met-RANTES led to a substantial detachment of T cells into the CSF.

In summary, the data indicate that chemokines regulate the exit of effector T cells from CNS blood vessels into the meninges. Furthermore, by stabilizing the cells in the meningeal milieu they control the distribution of T cells in the CSF and the CNS parenchyma.

6. References

Abbott NJ.
Dynamics of CNS barriers: evolution, differentiation, and modulation.
Cell Mol Neurobiol. 2005; 25(1):5-23.

Abbott NJ, Patabendige AA, Dolman DE, Yusof SR, Begley D.
Structure and function of the blood-brain barrier.
Neurobiol Dis. 2010; 37(1):13-25.

Anandasabapathy N, Victora GD, Meredith M, Feder R, Dong B, Kluger C, Yao K, Dustin ML, Nussenzweig MC, Steinman RM, Liu K.
Flt3L controls the development of radiosensitive dendritic cells in the meninges and choroid plexus of the steady-state mouse brain.
J Exp Med. 2011; 208(8):1695-705.

Auffray C, Fogg D, Garfa M, Elain G, Join-Lambert O, Kayal S, Sarnacki S, Cumano A, Lauvau G, Geissmann F.
Monitoring of blood vessels and tissues by a population of monocytes with patrolling behavior.
Science. 2007; 317(5838):666-70.

Austrup F, Vestweber D, Borges E, Löhning M, Bräuer R, Herz U, Renz H, Hallmann R, Scheffold A, Radbruch A, Hamann A.
P- and E-selectin mediate recruitment of T-helper-1 but not T-helper-2 cells into inflammed tissues.
Nature. 1997; 385(6611):81-3.

Bajénoff M, Egen JG, Koo LY, Laugier JP, Brau F, Glaichenhaus N, Germain RN.
Stromal cell networks regulate lymphocyte entry, migration, and territoriality in lymph nodes.
Immunity. 2006; 25(6):989-1001.

Bartholomäus I, Kawakami N, Odoardi F, Schläger C, Miljkovic D, Ellwart JW, Klinkert WE, Flügel-Koch C, Issekutz TB, Wekerle H, Flügel A.
Effector T cell interactions with meningeal vascular structures in nascent autoimmune CNS lesions.
Nature. 2009; 462(7269):94-8.

Ben-Nun A, Wekerle H, Cohen IR.
The rapid isolation of clonable antigen-specific T lymphocyte lines capable of mediating autoimmune encephalomyelitis.
Eur J Immunol. 1981; 11(3):195-9.

Ben-Nun A, Mendel I, Kerlero de Rosbo N.
Immunomodulation of murine experimental autoimmune encephalomyelitis by pertussis toxin: the protective activity, but not the disease-enhancing activity, can be attributed to the nontoxic B-oligomer.
Proc Assoc Am Physicians. 1997; 109(2):120-5.

Berlin C, Bargatze RF, Campbell JJ, von Andrian UH, Szabo MC, Hasslen SR, Nelson RD, Berg EL, Erlandsen SL, Butcher EC.
alpha 4 integrins mediate lymphocyte attachment and rolling under physiologic flow.
Cell. 1995; 80(3):413-22.

Bradbury MW, Cserr HF, Westrop RJ.
Drainage of cerebral interstitial fluid into deep cervical lymph of the rabbit.
Am J Physiol. 1981; 240(4):F329-36.

Braun A, Worbs T, Moschovakis GL, Halle S, Hoffmann K, Bölter J, Münk A, Förster R.
Afferent lymph-derived T cells and DCs use different chemokine receptor CCR7-dependent routes for entry into the lymph node and intranodal migration.
Nat Immunol. 2011; 12(9):879-87.

Brennan MJ, David JL, Kenimer JG, Manclark CR.
Lectin-like binding of pertussis toxin to a 165-kilodalton Chinese hamster ovary cell glycoprotein.
J Biol Chem. 1988; 263(10):4895-9.

Brückener KE, el Bayâ A, Galla HJ, Schmidt MA.
Permeabilization in a cerebral endothelial barrier model by pertussis toxin involves the PKC effector pathway and is abolished by elevated levels of cAMP.
J Cell Sci. 2003; 116(Pt 9):1837-46.

Burns DL.
Subunit structure and enzymic activity of pertussis toxin.
Microbiol Sci. 1988; 5(9):285-7.

Butcher EC.
Leukocyte–endothelial cell recognition: three (or more) steps to specificity and diversity.
Cell. 1991; 67(6):1033–1036.

Campbell JJ, Hedrick J, Zlotnik A, Siani MA, Thompson DA, Butcher EC.
Chemokines and the arrest of lymphocytes rolling under flow conditions.
Science. 1998; 279(5349):381-4.

Chow CW, Rincón M, Davis RJ.
Requirement for transcription factor NFAT in interleukin-2 expression.
Mol Cell Biol. 1999; 19(3):2300-7.

Clipstone NA, Crabtree GR.
Identification of calcineurin as a key signalling enzyme in T-lymphocyte activation.
Nature. 1992; 357(6380):695-7.

Constantin G, Majeed M, Giagulli C, Piccio L, Kim JY, Butcher EC, Laudanna C.
Chemokines trigger immediate beta2 integrin affinity and mobility changes: differential regulation and roles in lymphocyte arrest under flow.
Immunity. 2000; 13(6):759-69.

Crabtree GR, Olson EN.
NFAT signaling: choreographing the social lives of cells.
Cell. 2002; 109 Suppl:S67-79.

Cserr HF, Knopf PM.
Cervical lymphatics, the blood-brain barrier and the immunoreactivity of the brain: a new view.
Immunol Today. 1992; 13(12):507-12.

Denk W, Strickler JH, Webb WW.
Two-photon laser scanning fluorescence microscopy.
Science. 1990; 248 (4951):73-6.

Denk W, Svoboda K.
Photon upmanship: why multiphoton imaging is more than a gimmick.
Neuron. 1997; 18(3):351-7.

Diaspro A, Robello M.
Two-photon excitation of fluorescence for three-dimensional optical imaging of biological structures.
J Photochem Photobiol B. 2000; 55(1):1-8.

Dogan RN, Karpus WJ.
Chemokines and chemokine receptors in autoimmune encephalomyelitis as a model for central nervous system inflammatory disease regulation.
Front Biosci. 2004; 9:1500-5.

Dustin ML.
Modular design of immunological synapses and kinapses.
Cold Spring Harb Perspect Biol. 2009; 1(1):a002873.

el Bayâ A, Brückener K, Schmidt MA.
Nonrestricted differential intoxication of cells by pertussis toxin.
Infect Immun. 1999; 67(1):433-5.

Engelhardt B, Ransohoff RM.
The ins and outs of T-lymphocyte trafficking to the CNS: anatomical sites and molecular mechanisms.
Trends Immunol. 2005; 26(9):485-95.

Engelhardt B.
Immune cell entry into the central nervous system: involvement of adhesion molecules and chemokines.
J Neurol Sci. 2008; 274(1-2):23-6.

Engelhardt B, Ransohoff RM.
Capture, crawl, cross: the T cell code to breach the blood-brain barriers.
Trends Immunol. 2012; 33(12):579-89.

Eylar EH, Kniskern PJ, Jackson JJ.
Myelin basic proteins.
Methods Enzymol. 1974; 32:323-41.

Ferguson SS, Caron MG.
G protein-coupled receptor adaptation mechanisms.
Semin Cell Dev Biol. 1998; 9(2):119-27.

Fife BT, Paniagua MC, Lukacs NW, Kunkel SL, Karpus WJ.
Selective CC chemokine receptor expression by central nervous system-infiltrating encephalitogenic T cells during experimental autoimmune encephalomyelitis.
J Neurosci Res. 2001; 66(4):705-14.

Flügel A, Willem M, Berkowicz T, Wekerle H.
Gene transfer into CD4+ T lymphocytes: green fluorescent protein-engineered, encephalitogenic T cells illuminate brain autoimmune responses.
Nat Med. 1999; 5(7):843-7.

Flügel A, Berkowicz T, Ritter T, Labeur M, Jenne DE, Li Z, Ellwart JW, Willem M, Lassmann H, Wekerle H.
Migratory activity and functional changes of green fluorescent effector cells before and during experimental autoimmune encephalomyelitis.
Immunity. 2001; 14 (5):547-60.

Flügel A, Schläger C, Lühder F, Odoardi F.
Autoimmune disease in the brain – how to spot the culprits and how to keep them in check.
J Neurolo Sci. 2011; 311 S1 S3–S11.

Friedl P, Gunzer M.
Interaction of T cells with APCs: the serial encounter model.
Trends Immunol. 2001; 22(4):187-91.

Friedl P, Weigelin B.
Interstitial leukocyte migration and immune function.
Nat Immunol. 2008; 9(9):960-9.

Fugger L.
Human autoimmunity genes in mice.
Curr Opin Immunol. 2000; 12(6):698-703.

Galea I, Palin K, Newman TA, Van Rooijen N, Perry VH, Boche D.
Mannose receptor expression specifically reveals perivascular macrophages in normal, injured, and diseased mouse brain.
Glia. 2005; 49(3):375-84.

Galea I, Bechmann I, Perry VH.
What is immune privilege (not)?
Trends Immunol. 2007; 28(1):12-8.

Geissmann F, Cameron TO, Sidobre S, Manlongat N, Kronenberg M, Briskin MJ, Dustin ML, Littman DR.
Intravascular immune surveillance by CXCR6+ NKT cells patrolling liver sinusoids.
PLoS Biol. 2005; 3(4):e113.

Goto T, Kino T, Hatanaka H, Nishiyama M, Okuhara M, Kohsaka M, Aoki H, Imanaka H.
Discovery of FK-506, a novel immunosuppressant isolated from Streptomyces tsukubaensis.
Transplant Proc. 1987; 19(5 Suppl 6):4-8.

Goverman J.
Autoimmune T cell responses in the central nervous system.
Nat Rev Immunol. 2009; 9(6):393-407.

Grakoui A, Bromley SK, Sumen C, Davis MM, Shaw AS, Allen PM, Dustin ML.
The immunological synapse: a molecular machine controlling T cell activation.
Science. 1999; 285(5425):221-7.

Gröne HJ, Weber C, Weber KS, Gröne EF, Rabelink T, Klier CM, Wells TN, Proudfood AE, Schlöndorff D, Nelson PJ.
Met-RANTES reduces vascular and tubular damage during acute renal transplant rejection: blocking monocyte arrest and recruitment.
FASEB J. 1999; 13(11):1371-83.

Hatse S, Princen K, Bridger G, De Clercq E, Schols D.
Chemokine receptor inhibition by AMD3100 is strictly confined to CXCR4.
FEBS Lett. 2002; 527(1-3):255-62.

Hazes B, Read RJ.
Accumulating evidence suggests that several AB-toxins subvert the endoplasmic reticulum-associated protein degradation pathway to enter target cells.
Biochemistry. 1997; 36(37):11051-4.

Helmchen F, Denk W.
Deep tissue two-photon microscopy.
Nat Methods. 2005; 2:932–940.

Hickey WF, Hsu BL, Kimura H.
T-lymphocyte entry into the central nervous system.
J Neurosci Res. 1991; 28(2):254-60.

Hojo M, Maghni K, Issekutz TB, Martin JG.
Involvement of alpha-4 integrins in allergic airway responses and mast cell degranulation in vivo.
Am J Respir Crit Care Med. 1998; 158(4):1127-33.

Holda JH, Swanborg RH.
Autoimmune effector cells. II. Transfer of experimental allergic encephalomyelitis with a subset of T lymphocytes.
Eur J Immunol. 1982; (12): 453–455.

Holman DW, Klein RS, Ransohoff RM.
The blood-brain barrier, chemokines and multiple sclerosis.
Biochim Biophys Acta. 2011; 1812(2):220-30.

Huang YH, Lei HY, Liu HS, Lin YS, Liu CC, Yeh TM.
Dengue virus infects human endothelial cells and induces IL-6 and IL-8 production.
Am J Trop Med Hyg. 2000; 63(1-2):71-5.

Jain A, Munn LL.
Determinants of leukocyte margination in rectangular microchannels.
PLoS One. 2009; 4 (9):e7104.

Karpus WJ, Ransohoff RM.
Chemokine regulation of experimental autoimmune encephalomyelitis: temporal and spatial expression patterns govern disease pathogenesis.
J Immunol. 1998; 161(6):2667-71.

Kawakami N, Lassmann S, Li Z, Odoardi F, Ritter T, Ziemssen T, Klinkert WE, Ellwart JW, Bradl M, Krivacic K, Lassmann H, Ransohoff RM, Volk HD, Wekerle H, Linington C, Flügel A.
The activation status of neuroantigen-specific T cells in the target organ determines the clinical outcome of autoimmune encephalomyelitis.
J Exp Med. 2004; 199(2):185-97.

Kawakami N, Nägerl UV, Odoardi F, Bonhoeffer T, Wekerle H, Flügel A. (1)
Live imaging of effector cell trafficking and autoantigen recognition within the unfolding autoimmune encephalomyelitis lesion.
J Exp Med. 2005; 201(11):1805-14.

Kawakami N, Odoardi F, Ziemssen T, Bradl M, Ritter T, Neuhaus O, Lassmann H, Wekerle H, Flügel A. (2)
Autoimmune CD4+ T cell memory: lifelong persistence of encephalitogenic T cell clones in healthy immune repertoires.
J Immunol. 2005; 175(1):69-81.

Kawakami N, Flügel A.
Knocking at the brain's door: intravital two-photon imaging of autoreactive T cell interactions with CNS structures.
Semin Immunopathol. 2010; 32(3):275-87.

Kerfoot, SM & Kubes P.
Overlapping roles of P‑selectin and α4 integrin to recruit leukocytes to the central nervous system in experimental autoimmune encephalomyelitis.
J Immunol. 2002; 169:1000–1006.

Kiani A, García-Cózar FJ, Habermann I, Laforsch S, Aebischer T, Ehninger G, Rao A.
Regulation of interferon-gamma gene expression by nuclear factor of activated T cells.
Blood. 2001; 98(5):1480-8.

Kida S, Pantazis A, Weller RO.
CSF drains directly from the subarachnoid space into nasal lymphatics in the rat: anatomy, histology and immunological significance.
*Neuropathol Appl Neurobiol.*1993; 19:480-488.

Kim M, Carman CV, Springer TA.
Bidirectional transmembrane signaling by cytoplasmic domain separation in integrins.
Science. 2003; 301(5640):1720-5.

Kinashi T.
Intracellular signalling controlling integrin activation in lymphocytes.
Nat Rev Immunol. 2005; 5(7):546-59.

Kivisäkk P, Mahad DJ, Callahan MK, Sikora K, Trebst C, Tucky B, Wujek J, Ravid R, Staugaitis SM, Lassmann H, Ransohoff RM.
Expression of CCR7 in multiple sclerosis: implications for CNS immunity.
Ann Neurol. 2004; 55(5):627-38.

Klinkert WE.
Homing of antigen-specific T cells in the Lewis rat. Accumulation of antigen-reactive cells in the perithymic lymph nodes.
*The Journal of Immunology.*1987; 139: 1030–1036.

Kniesel U, Wolburg H.
Tight junctions of the blood-brain barrier.
Cell Mol Neurobiol. 2000; 20(1):57-76.

Krumbholz M, Theil D, Steinmeyer F, Cepok S, Hemmer B, Hofbauer M, Farina C, Derfuss T, Junker A, Arzberger T, Sinicina I, Hartle C, Newcombe J, Hohlfeld R, Meinl E.
CCL19 is constitutively expressed in the CNS, up-regulated in neuroinflammation, active and also inactive multiple sclerosis lesions.
J Neuroimmunol. 2007; 190(1-2):72-9.

Kunkel EJ, Butcher EC.
Chemokines and the tissue-specific migration of lymphocytes.
Immunity. 2002; 16(1):1-4.

Lämmermann T, Sixt M.
Mechanical modes of 'amoeboid' cell migration.
Curr Opin Cell Biol. 2009; 21(5):636-44.

Lassmann H, Brück W, Lucchinetti CF.
The immunopathology of multiple sclerosis: an overview.
Brain Pathol. 2007; 17(2):210-8.

Lawrence, M. B., Kansas, G. S., Ghosh, S., Kunkel, E. J.& Ley, K.
Threshold levels of fluid shear promote leukocyte adhesion through selectins (CD62L, P, E).
J Cell Biol. 1997; 136:717–727.

Ley K.
Molecular mechanisms of leukocyte recruitment in the inflammatory process.
Cardiovasc Res. 1996; 32(4):733-42.

Ley K, Laudanna C, Cybulsky MI, & Nourshargh S.
Getting to the site of inflammation: the leukocyte adhesion cascade updated.
Nature Rev Immunol. 2007; 7:678-689.

Lipton MM, Freund J.
The transfer of experimental allergic encephalomyelitis in the rat by means of parabiosis.
J Immunol. 1953; 71(5):380-4.

Lodygin D, Odoardi F, Schläger C, Körner H, Kitz A, Nosov M, van den Brandt J, Reichardt HM, Haberl M, Flügel A.
A combination of fluorescent NFAT and H2B sensors uncovers dynamics of T cell activation in real time during CNS autoimmunity.
Nat Med. In press

Mannie M, Swanborg RH, Stepaniak JA.
Experimental autoimmune encephalomyelitis in the rat.
Curr Protoc Immunol. 2009; Chapter 15: Unit 15.2.

Markowitz DG, Goff SP, Bank A.
Safe and efficient ecotropic and amphotropic packaging lines for use in gene transfer experiments.
Trans Assoc Am Physicians. 1988; 101:212-8.

Marshall BT, Long M, Piper JW, Yago T, McEver RP, Zhu C.
Direct observation of catch bonds involving cell-adhesion molecules.
Nature. 2003; 423(6936):190-3.

Marty C, Ye RD.
Heterotrimeric G protein signaling outside the realm of seven transmembrane domain receptors.
Mol Pharmacol. 2010; 78(1):12-8.

Massena S, Christoffersson G, Hjertström E, Zcharia E, Vlodavsky I, Ausmees N, Rolny C, Li JP, Phillipson M.
A chemotactic gradient sequestered on endothelial heparan sulfate induces directional intraluminal crawling of neutrophils.
Blood. 2010; 116 (11):1924-31.

Matthys P, Hatse S, Vermeire K, Wuyts A, Bridger G, Henson GW, De Clercq E, Billiau A, Schols D.
AMD3100, a potent and specific antagonist of the stromal cell-derived factor-1 chemokine receptor CXCR4, inhibits autoimmune joint inflammation in IFN-gamma receptor-deficient mice.
J Immunol. 2001; 167(8):4686-92.

McDonald B, Pittman K, Menezes GB, Hirota SA, Slaba I, Waterhouse CC, Beck PL, Muruve DA, Kubes P.
Intravascular danger signals guide neutrophils to sites of sterile inflammation.
Science. 2010; 330(6002):362-6.

McEver RP & Cummings, RD.
Role of PSGL‑1 binding to selectins in leukocyte recruitment.
J Clin Invest. 1997; 100, 485–491.

Middleton J, Neil S, Wintle J, Clark-Lewis I, Moore H, Lam C, Auer M, Hub E, Rot A.
Transcytosis and surface presentation of IL-8 by venular endothelial cells.
Cell. 1997; 91(3):385-95.

Middleton J, Patterson AM, Gardner L, Schmutz C, Ashton BA.
Leukocyte extravasation: chemokine transport and presentation by the endothelium.
Blood. 2002; 100(12):3853-60.

Millar RP, Newton CL.
The year in G protein-coupled receptor research.
Mol Endocrinol. 2010; 24(1):261-74.

Miyasaka M, Tanaka T.
Lymphocyte trafficking across high endothelial venules: dogmas and enigmas.
Nat Rev Immunol. 2004; 4(5):360-70.

Mohan K, Cordeiro E, Vaci M, McMaster C, Issekutz TB.
CXCR3 is required for migration to dermal inflammation by normal and in vivo activated T cells: differential requirements by CD4 and CD8 memory subsets.
Eur J Immunol. 2005; 35(6):1702-11.

Nourshargh S, Hordijk PL, Sixt M.
Breaching multiple barriers: leukocyte motility through venular walls and the interstitium.
Nat Rev Mol Cell Biol. 2010; 11(5):366-78.

Odoardi F, Kawakami N, Li Z, Cordiglieri C, Streyl K, Nosov M, Klinkert WE, Ellwart JW, Bauer J, Lassmann H, Wekerle H, Flügel A.
Instant effect of soluble antigen on effector T cells in peripheral immune organs during immunotherapy of autoimmune encephalomyelitis.
Proc Natl Acad Sci U S A. 2007; 104(3):920-5.

Odoardi F, Sie C, Streyl K, Ulaganathan VK, Schläger C, Lodygin D, Heckelsmiller K, Nietfeld W, Ellwart J, Klinkert WE, Lottaz C, Nosov M, Brinkmann V, Spang R, Lehrach H, Vingron M, Wekerle H, Flügel-Koch C, Flügel A.
T cells become licensed in the lung to enter the central nervous system.
Nature. 2012; 488(7413):675-9.

Ousman SS, Kubes P.
Immune surveillance in the central nervous system.
Nat Neurosci. 2012; 15(8):1096-101.

Peled A, Grabovsky V, Habler L, Sandbank J, Arenzana-Seisdedos F, Petit I, Ben-Hur H, Lapidot T, Alon R.
The chemokine SDF-1 stimulates integrin-mediated arrest of CD34 (+) cells on vascular endothelium under shear flow.
J Clin Invest. 1999; 104(9):1199-211.

Pelletier AJ, van der Laan LJ, Hildbrand P, Siani MA, Thompson DA, Dawson PE, Torbett BE, Salomon DR.
Presentation of chemokine SDF-1 alpha by fibronectin mediates directed migration of T cells.
Blood. 2000; 96(8):2682-90.

Phillipson M, Heit B, Colarusso P, Liu L, Ballantyne CM, Kubes P.
Intraluminal crawling of neutrophils to emigration sites: a molecularly distinct process from adhesion in the recruitment cascade.
J Exp Med. 2006; 203(12):2569-75.

Pittman M.
Pertussis toxin: the cause of the harmful effects and prolonged immunity of whooping cough. A hypothesis.
Rev Infect Dis. 1979; 1(3):401-12.

Plaut RD, Carbonetti NH.
Retrograde transport of pertussis toxin in the mammalian cell.
Cell Microbiol. 2008; 10(5):1130-9.

Potter SM.
Vital imaging: two photons are better than one.
Curr Biol. 1996; 6(12):1595-8.

Proudfoot AE, Power CA, Hoogewerf AJ, Montjovent MO, Borlat F, Offord RE, Wells TN.
Extension of recombinant human RANTES by the retention of the initiating methionine produces a potent antagonist.
J Biol Chem. 1996; 271(5):2599-603.

Proudfoot AE.
The biological relevance of chemokine-proteoglycan interactions.
Biochem Soc Trans. 2006; 34(Pt 3):422-6.

Ransohoff RM, Kivisäkk P, Kidd G.
Three or more routes for leukocyte migration into the central nervous system.
Nat Rev Immunol. 2003; 3(7):569-81.

Ransohoff RM, Engelhardt B.
The anatomical and cellular basis of immune surveillance in the central nervous system.
Nat Rev Immunol. 2012; 12(9):623-35.

Ransohoff RM.
Immunology: Licensed in the lungs.
Nature. 2012; 488(7413):595-6.

Reboldi A, Coisne C, Baumjohann D, Benvenuto F, Bottinelli D, Lira S, Uccelli A, Lanzavecchia A, Engelhardt B, Sallusto F.
C-C chemokine receptor 6-regulated entry of TH-17 cells into the CNS through the choroid plexus is required for the initiation of EAE.
Nat Immunol. 2009; 10(5):514-23.

Ridley AJ, Schwartz MA, Burridge K, Firtel RA, Ginsberg MH, Borisy G, Parsons JT, Horwitz AR.
Cell migration: integrating signals from front to back.
Science. 2003; 302(5651):1704-9.

Rosenbaum DM, Rasmussen SG, Kobilka BK.
The structure and function of G-protein-coupled receptors.
Nature. 2009; 459(7245):356-63.

Rosenberg SA, Spiess PJ, Schwarz S.
In vitro growth of murine T cells. I. Production of factors necessary for T cell growth.
J. Immunol. 1978; 121: 1946–1950.

Rubart M.
Two-photon microscopy of cells and tissue.
Circ Res. 2004; 95(12):1154-66.

Rutka JT, Giblin J, Dougherty DV, McCulloch JR, DeArmond SJ, Rosenblum ML.
An ultrastructural and immunocytochemical analysis of leptomeningeal and meningioma cultures.
J Neuropathol Exp Neurol. 1986; 45(3):285-303.

Sawcer, S. et al.
Genetic risk and a primary role for cell-mediated immune mechanisms in multiple sclerosis.
Nature. 2011; 476(7359):214-9.

Schenkel AR, Mamdouh Z, Muller WA.
Locomotion of monocytes on endothelium is a critical step during extravasation.
Nat Immunol. 2004; 5(4):393-400.

Schmid-Schönbein,G.W., Usami,S., Skalak,R., & Chien,S.
The interaction of leukocytes and erythrocytes in capillary and postcapillary vessels.
Microvasc Res. 1980; 19, 45-70.

Schumann K, Lämmermann T, Bruckner M, Legler DF, Polleux J, Spatz JP, Schuler G, Förster R, Lutz MB, Sorokin L, Sixt M.
Immobilized chemokine fields and soluble chemokine gradients cooperatively shape migration patterns of dendritic cells.
Immunity. 2010; 32(5):703-13. 13.

Shamri R, Grabovsky V, Gauguet JM, Feigelson S, Manevich E, Kolanus W, Robinson MK, Staunton DE, von Andrian UH, Alon R.
Lymphocyte arrest requires instantaneous induction of an extended LFA-1 conformation mediated by endothelium-bound chemokines.
Nat Immunol. 2005; 6(5):497-506.

Shaw JP, Utz PJ, Durand DB, Toole JJ, Emmel EA, Crabtree GR.
Identification of a putative regulator of early T cell activation genes.
Science. 1988; 241(4862):202-5.

Shulman Z, Shinder V, Klein E, Grabovsky V, Yeger O, Geron E, Montresor A, Bolomini-Vittori M, Feigelson SW, Kirchhausen T, Laudanna C, Shakhar G, Alon R.
Lymphocyte crawling and transendothelial migration require chemokine triggering of high-affinity LFA-1 integrin.
Immunity. 2009; 30(3):384-96.

Sigal A, Bleijs DA, Grabovsky V, van Vliet SJ, Dwir O, Figdor CG, van Kooyk Y, Alon R.
The LFA-1 integrin supports rolling adhesions on ICAM-1 under physiological shear flow in a permissive cellular environment.
J Immunol. 2000; 165(1):442-52.

Silva AA, Roffê E, Lannes-Vieira J.
Expression of extracellular matrix components and their receptors in the central nervous system during experimental Toxoplasma gondii and Trypanosoma cruzi infection.
Braz J Med Biol Res. 1999; 32(5):593-600.

Sørensen TL, Tani M, Jensen J, Pierce V, Lucchinetti C, Folcik VA, Qin S, Rottman J, Sellebjerg F, Strieter RM, Frederiksen JL, Ransohoff RM.
Expression of specific chemokines and chemokine receptors in the central nervous system of multiple sclerosis patients.
J Clin Invest. 1999; 103(6):807-15.

Sporici R, Issekutz TB.
CXCR3 blockade inhibits T-cell migration into the CNS during EAE and prevents development of adoptively transferred, but not actively induced, disease.
Eur J Immunol. 2010; 40(10):2751-61.

Stein JV, Nombela-Arrieta C.
Chemokine control of lymphocyte trafficking: a general overview.
Immunology. 2005; 116(1):1-12.

Stein PE, Boodhoo A, Armstrong GD, Cockle SA, Klein MH, Read RJ.
The crystal structure of pertussis toxin.
Structure. 1994; 2(1):45-57.

Tamura M, Nogimori K, Murai S, Yajima M, Ito K, Katada T, Ui M, Ishii S.
Subunit structure of islet-activating protein, pertussis toxin, in conformity with the A-B model.
Biochemistry. 1982; 21(22):5516-22.

Trebst C, Ransohoff RM.
Investigating chemokines and chemokine receptors in patients with multiple sclerosis: opportunities and challenges.
Arch Neurol. 2001; 58(12):1975-80.

Vajkoczy P, Laschinger M, Engelhardt B.
Alpha4-integrin-VCAM-1 binding mediates G protein-independent capture of encephalitogenic T cell blasts to CNS white matter microvessels.
J Clin Invest. 2001; 108(4):557-65.

Wekerle H, Linington C, Lassmann H, Meyermann R.
Cellular immune reactivity within the CNS.
Trends Neurosci. 1986; 9, 271–277.

Wess J, Han SJ, Kim SK, Jacobson KA, Li JH.
Conformational changes involved in G-protein-coupled-receptor activation.
Trends Pharmacol Sci. 2008; 29(12):616-25.

Wilson EH, Harris TH, Mrass P, John B, Tait ED, Wu GF, Pepper M, Wherry EJ, Dzierzinski F, Roos D, Haydon PG, Laufer TM, Weninger W, Hunter CA.
Behavior of parasite-specific effector CD8+ T cells in the brain and visualization of a kinesis-associated system of reticular fibers.
Immunity. 2009; 30(2):300-11.

Witvliet MH, Burns DL, Brennan MJ, Poolman JT, Manclark CR.
Binding of pertussis toxin to eucaryotic cells and glycoproteins.
Infect Immun. 1989; 57(11):3324-30.

Woolf E, Grigorova I, Sagiv A, Grabovsky V, Feigelson SW, Shulman Z, Hartmann T, Sixt M, Cyster JG, Alon R.
Lymph node chemokines promote sustained T lymphocyte motility without triggering stable integrin adhesiveness in the absence of shear forces.
Nat Immunol. 2007; 8(10):1076-85.

Worbs T, Mempel TR, Bölter J, von Andrian UH, Förster R.
CCR7 ligands stimulate the intranodal motility of T lymphocytes in vivo.
J Exp Med. 2007; 204(3):489-95.

Wucherpfennig KW, Strominger JL.
Molecular mimicry in T cell-mediated autoimmunity: viral peptides activate human T cell clones specific for myelin basic protein.
Cell. 1995; 80(5):695-705.

Yang BG, Tanaka T, Jang MH, Bai Z, Hayasaka H, Miyasaka M.
Binding of lymphoid chemokines to collagen IV that accumulates in the basal lamina of high endothelial venules: its implications in lymphocyte trafficking.
J Immunol. 2007; 179(7):4376-82.

Zipfel WR, Williams RM, Webb WW.
Nonlinear magic: multiphoton microscopy in the biosciences.
Nat Biotechnol. 2003; 21(11):1369-77.

Zlotnik A, Yoshie O.
Chemokines: a new classification system and their role in immunity.
Immunity. 2000; 12(2):121-7.

7. Curriculum vitae

Personal data

Full name:	Christian Schläger
Date of birth:	01.02.1980
Address:	Institute for Multiple Sclerosis Research, Department of Neuroimmunology, University Medical Center of the Georg-August University Waldweg 33, 37073 Göttingen, Germany
Phone:	++49-(0)551-39 13332
Email:	christian.schlaeger@med.uni-goettingen.de
Marital status:	single
Nationality:	German

Education

02/2008 -	PhD studies. Topic: "Migratory cues for encephalitogenic effector T cells within the CNS during the different phases of EAE"
02/2010-	Institute for Multiple Sclerosis Research, Department of Neuroimmunology, University Medical Center of the Georg-August University, Göttingen, Germany (Director and supervisor: Prof. Alexander Flügel)
02/2008 - 02/2010	Max-Planck-Institute of Neurobiology, Department of Neuroimmunology, Martinsried, Germany (Director: Prof. Hartmut Wekerle; supervisor: Prof. Alexander Flügel)
08/2007-12/2007	Scientist in Prof. Martin Oppermann's research group Department of Cellular and Molecular Immunology, University Medical Center of the Georg-August University, Göttingen, Germany (Director: Prof. Jürgen Wienands)
07/2007	Degree: Diploma in Biology; Awarded grade: "sehr gut"
09/2006-07/2007	Completion of diploma thesis Department of Cellular and Molecular Immunology, University Medical Center of the Georg-August University, Göttingen, Germany (Director: Prof. Jürgen Wienands; supervisor: Prof. Martin Oppermann)
10/2001-07/2007	Study of biology Bavarian Julius-Maximilians University Würzburg, Germany